THE UNIVERSITY *of* LIVERPOOL

Maximum Power Control of Permanent Magnet Synchronous Generator Based Wind Power Generation Systems

Thesis submitted in accordance with the
requirements of the University of Liverpool
for the degree of Doctor of Philosophy

in

Electrical Engineering and Electronics

by

Liuying Li, B.Sc.(Eng.)

September 2016

Maximum Power Control of Permanent Magnet Synchronous Generator Based Wind Power Generation Systems

by

Liuying Li

Acknowledgements

I would like to give my heartfelt thanks to my supervisor, Dr. L. Jiang, whose encouragement, guidance and support enabled me to develop a deep understanding of my work. Without his consistent and illuminating instruction, my research work could not proceed to this stage. The research skill, writing skill and presenting skill he taught me will benefit me throughout my life.

I offer my regards and blessings to all of the members of smart grid control and renewable energy sub-group, the University of Liverpool. Special thanks also go to my friends, Dr Jian Chen, Dr. Yaxing Ren, for their support and friendship. My thanks also go to the Department of Electrical Engineering and Electronics at the University of Liverpool, for providing the research facilities that made it possible for me to carry out this research.

Last but not least, I am deeply grateful to my parents and my fiance Mr. Zhuo Chang, for their encourage, support and love, during the period of my postgraduate life.

Abstract

Wind power has been one of the fastest growing and most competitive renewable sources in the past decade. After the massive installation of new wind power generation systems (WPGSs), efficient and reliable operation of them has become one main concern of the wind power industry. This thesis focuses on improving the generation efficiency of WPGSs. The study is carried out based on permanent magnet synchronous generator (PMSG)-WPGS, which is one main stream WPGS due to the merits such as high reliability, high efficiency, low noise, fast dynamic response and self-excitation on the rotor. A PMSG based wind turbine connects to the power grid via back to back full-rate power electronic converters and can be controlled to rotate at a varying speed in variable wind power to achieve high efficiency.

Chapter 1 starts an overview of typical WPGSs, including different types of wind turbines, generators and power electronic devices. Then the three typical operation regions of a variable speed variable pitch wind turbine are presented, i.e. the first one variable speed operation region, the second one fixed rated rotation speed operation region, and the third one rated power operation region. In the first operation region, the control objective is achieving maximum power extraction from the wind, so called maximum power point tracking (MPPT). Methods for WPGSs to achieve MPPT are reviewed.

A reliable and efficient operation of a WPGS requires smooth switching between three operation regions when the wind speed changes between the cut-in and the cut-out speed. As different region has different control strategy, thus the switching between different operation regions is required. Non-smooth and excessive switching between different control strategies will introduce fatigue loads during the transitions period thus damage the mechanical part of a WPGS. Thus a smooth

region switching logic is proposed in Chapter 2 to minimise sudden changes during switching. The proposed method is verified via simulation on a 5th-order nonlinear variable-speed wind turbine model and by hardware-in-the-loop test based on Speedflo and dSPACE platform.

Among all the MPPT methods, perturbation&observation (P&O), also called hill-climb-search (HCS) method, is commonly used in industry for small-scale wind turbine as it does not require wind speed measurement and prior knowledge of the wind turbine characteristics. However, it may fail to track the optimal power points, or even lose its trackability in variable wind speed environment. To tackle this challenge, a wind speed variation detection method is proposed to improve performance of the HCS method. With the wind speed variation detection, the wind turbine can change its rotational speed according to the changes in wind speed. The proposed method is verified in simulation and hardware-in-the-loop tests with a PMSG based WPGS. The simulation results show the proposed method can detect the wind speed variation during the operation such that the misleading of HCS during variable wind speed can be avoided. Results of hardware-in-the-loop tests show that compared with the conventional HCS method, the developed method has higher MPPT efficiency. It can generate 4% more power than the conventional HCS method with the same wind speed input.

Besides HCS method, power signal feedback (PSF) is another feasible MPPT method. PSF method needs the wind turbine's optimal power-speed curve as the reference to control the rotational speed to track maximum power points. In industry, the wind turbine manufacturers need additional aerodynamic experiments to obtain the accurate optimal power-speed curve of wind turbines. However, the optimal power-speed curve of each type of wind turbines is different. Even for the same wind turbine, the optimal curve may change after installation, due to the change of operation environment such as temperature variation and dust pollution. To avoid those special tests, a method is proposed in Chapter 4 for wind turbines to on-site detect the optimal power-speed curve. With an accurate optimal power-speed curve, the WPGS can efficiently achieve MPPT by PSF control. Both simulation and hardware-in-the-loop tests show that the proposed method can detect the wind tur-

bine optimal power-speed curve in variable wind speed. It can be used to calibrate PSF reference and improve the MPPT efficiency.

To verify the proposed MPPT algorithm, in Chapter 5, a designed power electronics hardware is tested with a PMSG based WPGS and finally implemented in a small scale prototype WPGS. The small scale prototype implementation and field tests are given in Chapter 6. In Chapter 5, a diode rectifier with DC-DC boost converter is designed and implemented as the generator-side converter in a PMSG based WPGS. The operation and model of DC-DC boost converter are given. Due to the low cost and high reliability of diode rectifier, it is widely used in PMSG based WPGSs. A boost converter controls the dc-side voltage and current for MPPT and steps up the voltage for grid connection.

Declaration

The author hereby declares that this thesis is a record of work carried out in the Department of Electrical Engineering and Electronics at the University of Liverpool during the period from October 2012 to September 2016. The thesis is original in content except where otherwise indicated.

Contents

List of Figures

List of Abbreviations and Notations

Abbreviations

AC	Alternating Current
CCM	Continuous Conduction Mode
CT	Current Transducer
DC	Direct Current
DCM	Discontinuous Conduction Mode
DFIG	Doubly Fed Induction Generator
FLC	Fuzzy Logic Control
HCS	Hill Climb Searching
IGBT	Insulated-Gate Bipolar Transistor
MOSFET	Metal-Oxide-Semiconductor Field Effect Transistor
MPP	Maximum Power Points
MPPT	Maximum Power Point Tracking
MVPO	Multivariable Perturb and Observe
NN	Neural Network
OT	Optimal Torque
PDF	Pseudo-Derivative Feedback
PI	Proportional-Integral
PID	Proportional-Integral-Derivative
PMS	Permanent Magnet Synchronous
PMSG	Permanent Magnet Synchronous Generator
PSF	Power Signal Feedback
PWM	Pulse Width Modulation
P&O	Perturbation & Observation
TSR	Tip Speed Ratio
VC	Vector Control

VSC	Voltage Source Converter
VT	Voltage Transducer
WPGS	Wind Power Generation System
WT	Wind Turbine

Notations

P_{air}	Power in the air flow
ρ	Air density
V_w	Wind speed
A_r	Power coefficient
C_p	Pitch angle
P_r	Wind turbine rotor power
λ	Tip-speed ratio
ω_r	Rotor rotational speed
R_b	Radius to tip of rotor
E_g	Voltage magnitude of the sending source
P_g	Generator active power
X_g	Synchronous reactance of the generator
V_t	Voltage magnitude of the receiving source
α_g	Phase angle between the sending and receiving source
$P_{g_{ref}}$	Reference value of the generator active power
$Q_{g_{ref}}$	Reference value of the generator reactive power
T_e	Electromagnetic torque
T_m	Mechanical torque
J	Inertia constant
ω_m	Mechanical rotational speed
p	Number of poles
T_{sp}	Torque reference
i_{ds}, i_{qs}	Stator currents in d and q axis
v_{ds}, v_{qs}	Stator voltages in d and q axis
ω	Rotational speed of rotor
C_d	DC link capacitor
v_{dc}	DC link voltage
v_g	Voltage of the grid

i_g	Current of the grid
L_g	Grid-side line inductance
v_{ai}, v_{bi}, v_{ci}	Phase-a, b, c voltage of the inverter
i_{ag}, i_{bg}, i_{cg}	Phase-a, b, c current of the grid
v_{ag}, v_{bg}, v_{cg}	Phase-a, b, c voltage of the grid
ω_{m_opt}	Optimum mechanical rotation speed
λ_{opt}	Optimum tip-speed-ratio
P_{m_opt}	Optimum mechanical power
T_{m_opt}	Optimum mechanical torque
C_{p_max}	Maximum power coefficient
T_r	Torque transferred from rotor to the gear
J_r	Inertia of rotor
T_{sr}	Generator torque transferred to rotor
K_s	Spring constant of shaft
D_s	Shaft damping
N_g	Gear ratio
T_{sg}	Rotor torque transferred to gearbox
ω_g	Generator rotational speed
J_g	Inertia of generator
T_g	Generator load torque
P_r	Mechanical power absorbed from the wind
β_{ref}	Blade pitch angle reference
T_{g_ref}	Generator torque reference
P_e	Power generated by generator
β	Blade pitch angle
δ	Twist of rotor shaft
Ω_r	Shaft angle at the rotor
Ω_g	Shaft angle at the generator
ω_{r_rat}	Rated rotor rotational speed
η	Generator efficiency
Γ_T	Time constant of torque
Γ_β	Time constant of pitch angle
P_{opt}	Optimum power
k_{opt}	The key constant effect optimal power curve
$P_{threshold}$	Predefined power threshold

k_1	Predefined constant higher than k_{opt}
k_2	Predefined constant lower than k_{opt}
ω	Rotational speed calculated by k_{opt} and P
$A_{threshold}$	Predefined threshold for MPP detection
i_d, i_q	Currents in d and q axis
v_d, v_q	Voltages in d and q axis
L_d, L_q	Inductance of d and q axis
R	Resistance of the stator
p	Number of pole pairs
ϕ_f	Magnitude flux of the permanent magnet
T_e	Electrical rotating speed
ω_e	maximum power coefficient
B	Friction coefficient
θ	Rotor angular position
L	Inductance of d and q axis when $L_d = L_q$
ε_ω	Predefined constant for rotational speed rocording
ε_v	Predefined constant for wind speed rocording
ω_{ref_p}	Reference rotational speed of the previous step
K	A parameter of the control system
T	Period of the control system
ω_k	Rotational speed at step k
$P_{(k,i)}$	Power at rotational speed k and wind speed i
$P_{i,max}$	Maximum power in wind speed i
ω_{i_opt}	Optimum rotational speed in wind speed i
L_b	Boost inductor
C_o	Output capacitor
R_L	Resistive load
V_o	Output voltage
V_{dcg}	Output DC voltage of the diode rectifier
I_{dcg}	Output DC current of the diode rectifier
T_{sw}	Switching period
d, D	Duty cycle
V_{dcg_min}	Minimum input DC voltage
V_{dcg_max}	Maximum input DC voltage
V_{o_min}	Minimum output DC voltage

V_{o_max}	Maximum output DC voltage
V_{r_min}	Minimum output voltage ripple
I_{dcg_max}	Maximum input DC current
P_o	Output power
d_{max}	Maximum duty cycle
d_{min}	Minimum duty cycle
C_{o_max}	Maximum output capacitor
L_{b_min}	Minimum boost inductor
V_{in}	Input voltage
V_o	Output voltage
R_{ce}	IGBT external resistor for adjusting the steady-state threshold
C_{ce}	IGBT external resistor for adjusting the steady-state blanking time
R_{Gon}, R_{Goff}	IGBT external resistors for adjusting the turn-on and off speed
V_{ab}	Line voltage of phase a and b
V_{bc}	Line voltage of phase b and c
V_{ca}	Line voltage of phase c and a
V_a, V_b, V_c	Voltages of phase a, b, c

Chapter 1

Introduction and Literature Review

Wind is a clean and environmentally friendly renewable energy resource that can reduce our dependency on fossil fuels and has developed rapidly in recent years [1]. Over the past few years, wind power has shown the fastest rate of growth of any form of electricity generation with its development stimulated by concerns of national policy makers over climate change, energy diversity and security of supply [2]. Figure 1.1 shows the global wind power capacity installed between 2000 to 2015. It indicates that at the end of 2015, the world's wind energy installation capacity reached 63013 MW, a 22% increase over 2014 [3].

This research is sponsored by European Regional Development Fund. The project is supported by the Centre for Global Eco-Innovation and collaborated with Gencoa Ltd. This project aims to develop a controller to improve the efficiency of wind turbines. With literature review, models building, simulation and hardware experiments, an advanced wind turbine controller was designed and tested in prototype experiments.

This chapter presents a brief review of wind power generation system (WPGS). It contains the configuration of WPGSs, including wind turbines, generators and power electronics, and operation and control of WPGSs. A literature review of maximum power point tracking (MPPT) is given in Section 1.2. Motivations and objectives, thesis outline and contributions are given.

1.1 Wind Power Generation Systems

1.1.1 Typical configurations

A WPGS consists of a wind turbine, a generator and related power electronics. There are a large number of choices of architecture available to the designer of a wind power generation system [2, 4, 5]. Typically, there are two well-known types of WPGSs: fixed-speed and variable-speed wind power generation systems.

Fixed-speed wind power generation system

Fixed-speed wind turbines basically operate at constant speed. There are relatively simple devices in a fixed-speed wind power generation system. It normally consists of an aerodynamic rotor driving a low-speed shaft, a gearbox, a high-speed shaft and an induction generator. From the electrical system viewpoint, they are perhaps best considered as large fan drives with torque applied to the low-speed shaft from the wind flow [2].

Figure 1.2 illustrates the schematic of a fixed-speed wind power generation system. A fixed-speed wind power generation system consists of a squirrel-cage induction generator coupled to the power system through a turbine transformer [6]. The generator operating slip changes slightly as the operating power level changes and the rotational speed is therefore not entirely constant. Because the operating slip variation is generally less than 1%, this type of wind power generation system is normally referred to as fixed speed [7].

Squirrel-cage induction machines consume reactive power, and so it is conventional to provide power factor correction capacitors at each wind turbine. The function of the soft-starter unit is to build up the magnetic flux slowly and so minimise transient currents during energization of the generator. Also, by applying the network voltage slowly to the generator, once energised, it brings the drive train slowly to its operating rotational speed [8].

For fixed-speed wind power generation systems, connecting the induction generators to power system produces transients that are short duration with very high inrush currents, thus causing disturbances to both the grid and high torque spikes in

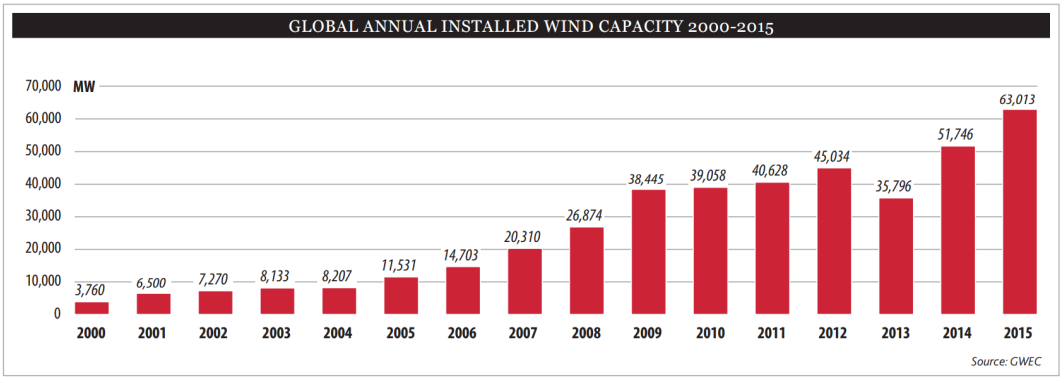

Figure 1.1: Global wind energy installation capacity [3]

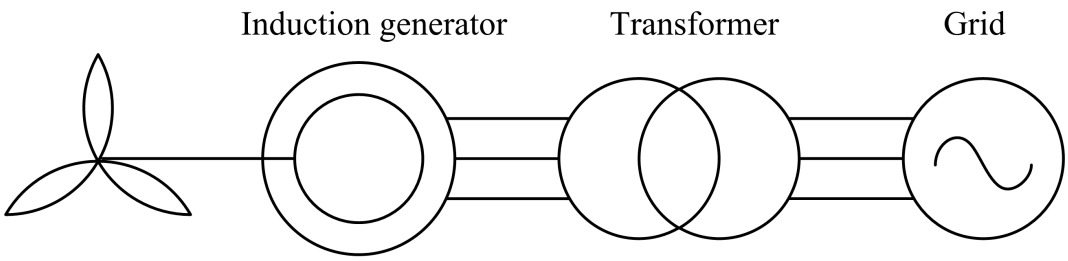

Figure 1.2: Schematic of a fixed-speed wind power generation system [2]

the drive train of wind turbines with a directly connected induction generator. Such a transient disturbs the grid and limits the acceptable number of wind turbines. The high starting currents of induction generators are usually limited by a thyristor soft-starter. The current limiter or soft-starter, based on thyristor technology, typically limits the RMS value of the inrush current to a level below two times of the generator rated current. The soft-starter has a limited thermal capacity and it is short-circuited by a contactor, which carries the full-load current when the connection to the grid has been completed. In addition to reducing the impact on the grid, the soft-starter also effectively dampens the torque peaks associated with the peak currents, and hence reduces the loads on the gearbox.

A fixed-speed wind power generation system, even though simple and reliable, severely limits the energy output of a wind turbine. Since there is no torque control loop, fluctuations in generated power are larger.

Variable-speed wind power generation system

Variable-speed technologies are widely used in wind power generation systems recently as the variable-speed operation of a wind turbine system has many advantages. For instance, the wind turbine can increase or decrease its speed if the wind speed and torque vary. This means less wear and tear on the tower, gearbox, and other components in the drive train. Also, variable-speed systems can increase the production of the energy and reduce the fluctuation of the power injected into the grid. In variable-speed systems, the generator is normally connected to the grid through a power electronic system [9]. Currently, the most common variable-speed wind power generation systems configurations are doubly fed induction generator (DFIG) based WPGS and fully rated converter WPGS based on a synchronous or induction generator.

A typical configuration of a DFIG based wind power generation system consists of a wound rotor induction generator, a power converter and a crowbar as shown in Figure 1.3. The wound-rotor induction generator has slip rings to take current into or out of the rotor winding, and the variable-speed operation is obtained by injecting a controllable voltage into the rotor at slip frequency [8, 10].

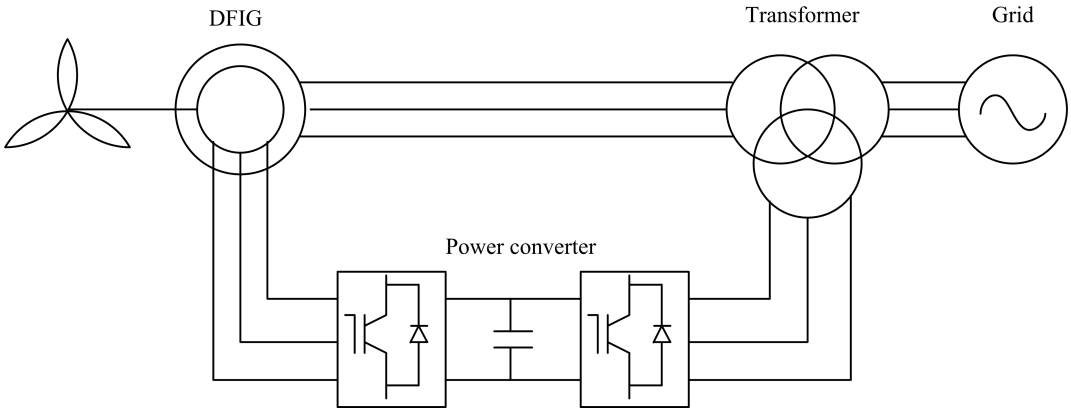

Figure 1.3: Schematic of a DFIG WPGS with a back-to-back power converter [2]

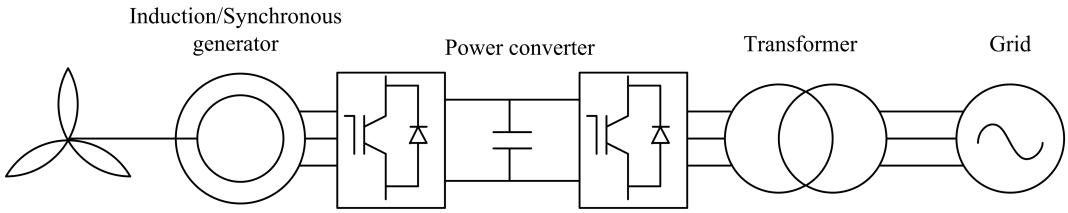

Figure 1.4: Schematic of WPGS with a fully rated back-to-back converter [2]

The typical configuration of a fully rated converter WPGS is shown in Figure 1.4. This type of wind power generation system may or may not include a gearbox. A wide range of electrical generator types can be employed, for example, induction, wound-rotor synchronous or permanent magnet synchronous.

Generators

Doubly fed induction generator (DFIG)

The DFIG based WPGS use a wound-rotor induction generator whose stator winding connected to the grid through a transformer and rotor winding fed through a variable-frequency power converter [11]. The power converter decouples the grid electrical frequency from the rotor mechanical frequency, enabling variable-speed operation of the wind turbine. The generator and converters are protected by voltage limits and an over-current 'crowbar' [2].

A DFIG based WPGS can deliver power to grid through the stator and rotor, while the rotor can also absorb power. This depends on the rotational speed of the generator. If the generator operates above synchronous speed, power will be delivered from the rotor through the converters to the grid, and if the generator operates below synchronous speed, then the rotor will absorb power from the grid through the converters. By controlling the active power of the converter, it is possible to vary the rotational speed of the generator, and thus the speed of the rotor of the wind turbine [9].

Permanent magnetic synchronous generator (PMSG)

PMSG has the property of self-excitation, which allows an operation at a high power and a high efficiency. This makes it widely employed in WPGSs [4]. PMSG avoids the field current supply or reactive power compensation facilities needed by wound-rotor synchronous generators and induction generators and it also removes the need for slip rings [2]. The efficiency of PMSG is higher than in the induction generator, as the excitation is provided without any energy supply.

The synchronous machine can provide its own excitation on the rotor. Such excitation may be obtained using either a current-carrying winding or permanent magnets. The wound-rotor synchronous machine has a very desirable feature compared with its permanent magnets counterpart, namely an adjustable excitation current and, consequently, control of its output voltage independent of load current. This feature explains why most constant-speed generators use wound rotors instead of permanent magnets excited rotors. The synchronous generator in wind turbines is in most cases connected to the network via an electronic converter. Therefore, the advantage of controllable no-load voltage is not as critical.

Wound rotors are heavier than permanent magnet rotors and typically bulkier (particularly in short pole-pitch synchronous generators). Also, electrically excited synchronous generators have higher losses in the rotor windings. Although there will be some losses in the magnets caused by the circulation of eddy currents in the permanent magnets volume, they will usually be much lower than the copper losses of electrically excited rotors. This increase in copper losses will also increase on increasing the number of poles [2].

In a conventional wind turbine, a gearbox is used between the turbine and the generator as the turbine speed is much lower than the generator speed. An alternative is to use a generator for very low speed. The generator can then be directly connected to the turbine shaft.There are two main reasons for using direct-driven generators in wind turbine systems. Direct-driven generators are favoured for some applications due to the reduction in losses in the drive train and less noise [2]. The most important difference between conventional and direct-driven wind turbine generators is that the low speed of the direct-driven generator makes a very high-rated torque necessary. This is an important difference because the size and the losses of a low-speed generator depend on the rated torque rather than on the rated power. A direct-driven generator for a 500 kW, 30 RPM wind turbine has the same rated torque as a 50 MW, 3000 RPM steam-turbine generator [2].

Wind turbines

A wind turbine is a device for extracting kinetic energy from the wind. There is a variety of wind turbine types. It can be divided by structure into horizontal and vertical wind turbine types. Practical horizontal axis wind turbine designs use airfoils to transform the kinetic energy in the wind into mechanical energy. Depending on the design of the pitch in wind turbines, there are fixed pitch and variable pitch blades wind turbines. And also there are different types of wind turbines depends on the yaw systems [5].

Wind turbine characteristics

Wind turbines produce electricity by using the power of the wind to drive an electrical generator. The wind passes over the blades, generating lift and exerting a turning force. The rotating blades turn a shaft inside the nacelle, which goes into a gearbox. The gearbox increases the rotational speed to that which is appropriate for the generator, which uses magnetic fields to convert the rotational energy into electrical energy. The power output goes to a transformer, which converts the electricity from the generator to the appropriate voltage level for the power collection system.

A wind turbine extracts kinetic energy from the swept area of the blades. The power in the airflow is given by [12, 13]:

$$P_{air} = \frac{1}{2}\rho A_r V_w^3 \tag{1.1.1}$$

where ρ = air density (approximately 1.225 kg·m^{-3})

A_r = swept area of rotor, m^2

V_w = upwind free wind speed, m/s.

Although Equation 1.1.1 gives the power available in the wind. The power transferred to the wind turbine rotor is reduced by the power coefficient, C_p:

$$C_p = \frac{P_r}{P_{air}} \tag{1.1.2}$$

$$P_r = C_p P_{air} = C_p \times \frac{1}{2}\rho A_r V_w^3 \tag{1.1.3}$$

A maximum value of C_p is defined by the Betz limit [5, 12], which states that a turbine can never extract more than 59.3% of the power from an air stream. In reality, wind turbine rotors have maximum C_p values in the range 25-45%.

λ is a defined tip-speed ratio, as

$$\lambda = \frac{\omega_r R_b}{V_w} \tag{1.1.4}$$

where

ω_r = rotational speed of rotor, rad/s

R_b = radius to tip of rotor, m

The tip-speed ratio, λ and the power coefficient, C_p, are dimensionless and so can be used to describe the performance of any size of wind turbine rotor. The maximum power coefficient is only achieved at a single tip-speed ratio. For a fixed rotational speed of the wind turbine, this only occurs at a single wind speed. Hence, one argument for operating a wind turbine at variable rotational speed is that it is possible to operate at maximum C_p over a range of wind speeds.

The power output of a wind turbine at various wind speeds is conventionally described by its power curve. The power curve gives the steady-state electrical power output as a function of the wind speed at the hub height. An example of a power curve is given in Figure 1.5.

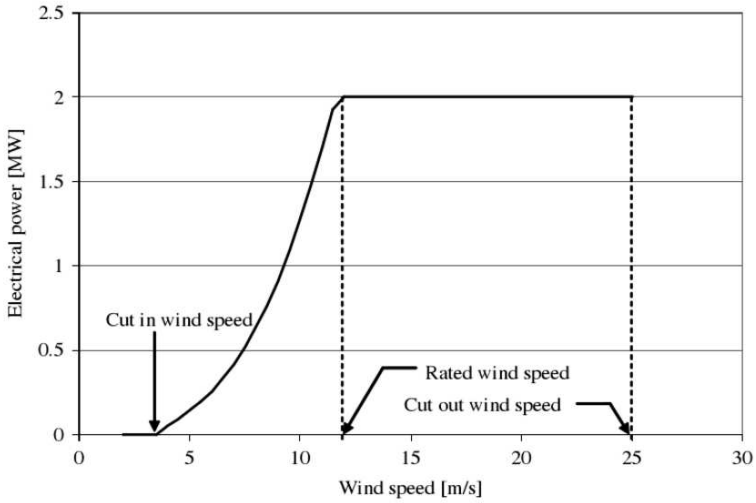

Figure 1.5: Power curve for a 2MW wind turbine

The power curve has three key points on the velocity scale:

- Cut-in wind speed - the minimum wind speed at which the machine will deliver useful power.
- Rated wind speed - the wind speed at which rated power is obtained (rated power is generally the maximum power output of the electrical generator).
- Cut-out wind speed - the maximum wind speed at which the turbine is allowed to deliver power (usually limited by engineering loads and safety constraints).

Below the cut-in wind speed speed, the wind turbine remains shut down as the speed of the wind is too low for useful energy production. Then, once in operation, the power output increases following a broadly cubic relationship with wind speed until rated wind speed is reached. Above rated wind speed the aerodynamic rotor is arranged to limit the mechanical power extracted from the wind and so reduce the mechanical loads on the drive train. Then at very high wind speeds the turbine is shut down.

Power electronics

Power electronics is a key component of a wind power generation system. Within the wind turbine generator, power electronics converters are used to control the steady-state and dynamic active and reactive power flow to and from the electrical generator.

As all of the power from the turbine goes through the power converters, the dynamic operation of the electrical generator is effectively isolated from the power grid [14]. The electrical frequency of the generator may vary as the wind speed changes, while the grid frequency remains unchanged, thus allowing variable-speed operation of the wind turbine [15].

The power converters can be arranged in various ways. Whereas the generator-side converter can be a diode rectifier or a PMW voltage source converter (VSC), the grid-side converter is typically a PWM-VSC. The strategy to control the operation of the generator and the power flows to the network depends very much on the type of power converter arrangement employed. The grid-side converter can be controlled to maintain the DC bus voltage constant. Active power is transmitted through the converters with very little energy stored in the DC link capacitor. Hence the torque applied to the generator can be controlled by the network-side converter. Each converter can generate or absorb reactive power independently [16, 17].

The variable-speed operation can be achieved by using any suitable combination of generator, synchronous or asynchronous, and a power electronic interface. Table 1.1 summarizes the application of VSCs for different generator configurations [2].

Diode bridge-VSC with DC-DC boost converter

Figure 1.6 shows an arrangement of a diode bridge-VSC with a DC-DC boost converter. In this configuration, power can only flow from the generator to the grid. The generated AC voltage and current are converted into DC using the diode bridge and then inverted back to AC using the PWM-VSC. This arrangement decouples the wind turbine from the AC grid, thus allowing variable-speed operation of the wind turbine. The PWM-VSC is generally controlled to maintain the DC link capacitor at a constant voltage. This will ensure the power transfer between the DC link and the grid. The active power of the generator is controlled by adjusting the duty cycle

Generator	Power electronic conversion used
DFIG	Back-to-back VSCs connected to the rotor
PMSG	Diode bridge-VSC and back-to-back VSCs connected to the armature
Wound rotor synchronous generator	Diode bridge-VSC and back-to-back VSCs connected to the armature and field

Table 1.1: Generated energy comparison of power transfer to charge the batteries

D of the DC-DC boost converter through a controller, whereas the reactive power is adjusted by the grid side inverter.

A DC/DC boost converter with a three-phase diode rectifier used in a wind power generation system could simplify the control and potentially reduce the cost of the system. There are two distinctive characteristics of this type of wind energy system [18]:

1. The rotor flux of the synchronous generator is produced by permanent magnets or rotor field winding, and, therefore, the generator does not require the rectifier to provide magnetization as it does for the induction generators.

2. The output DC voltage of the boost converter can be regulated (increased) to a level required by the inverter. This is especially important at low wind speeds, when the output voltage of the diode rectifier is too low for the inverter to operate properly.

Back-to-back VSCs

The back-to-back VSC is a bi-direction power converter consisting of two voltage source converters as shown in Figure 1.7.

The IGBTs on the generator-side VSC are controlled using a PWM technique. The classical PWM is carrier-based PWM where a reference signal, V_{ref}, which varies sinusoidally, is compared with a fixed-frequency triangular carrier waveform, V_{tri}, to create a switching pattern. If a single-phase two-level VSC is considered with the waveforms shown in Figure 1.8, then signal of one IGBT is 1 when

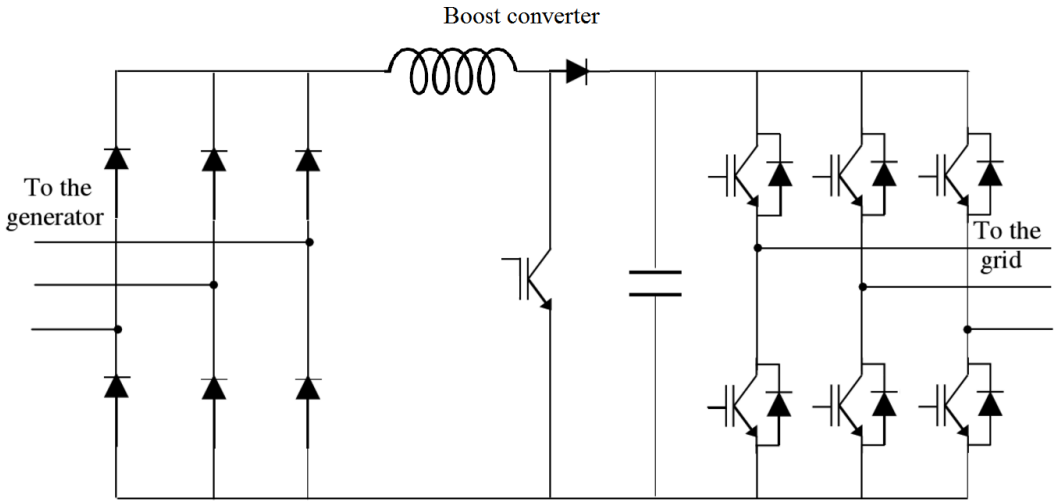

Figure 1.6: VSC with a three-phase diode bridge and DC/DC boost converter [2]

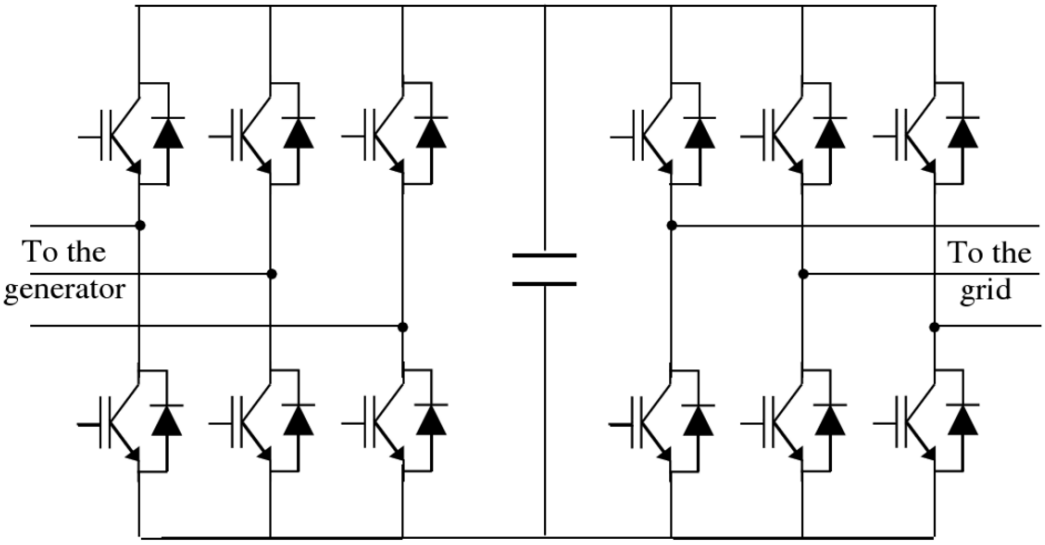

Figure 1.7: Back-to-back VSCs [2]

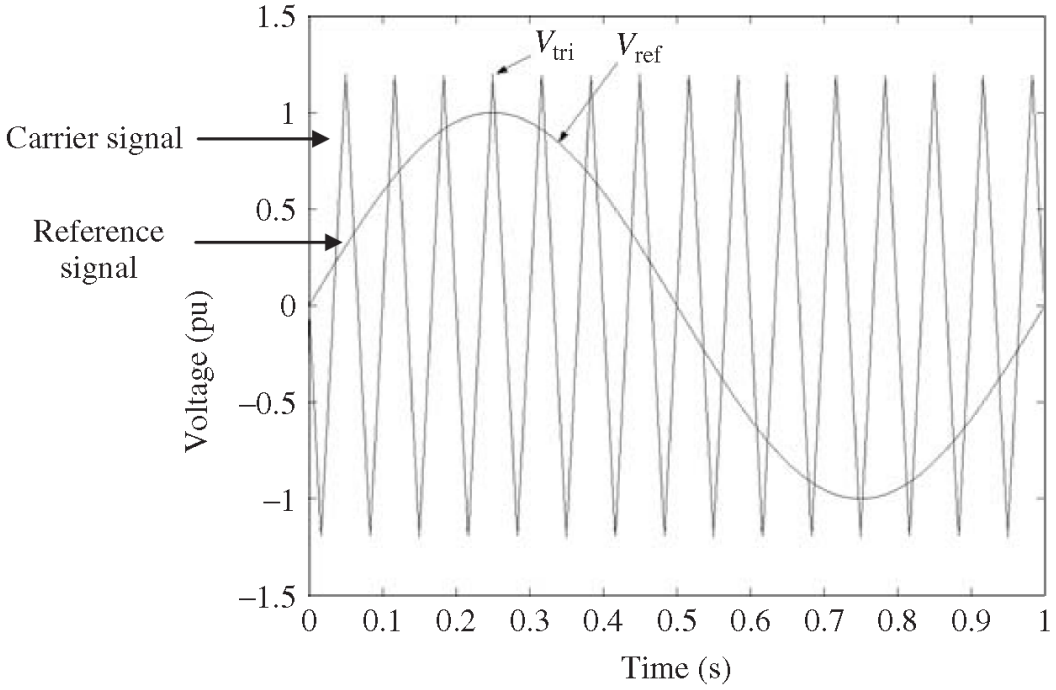

Figure 1.8: Reference voltage, V_{ref}, and the carrier waveform, V_{tri} [2]

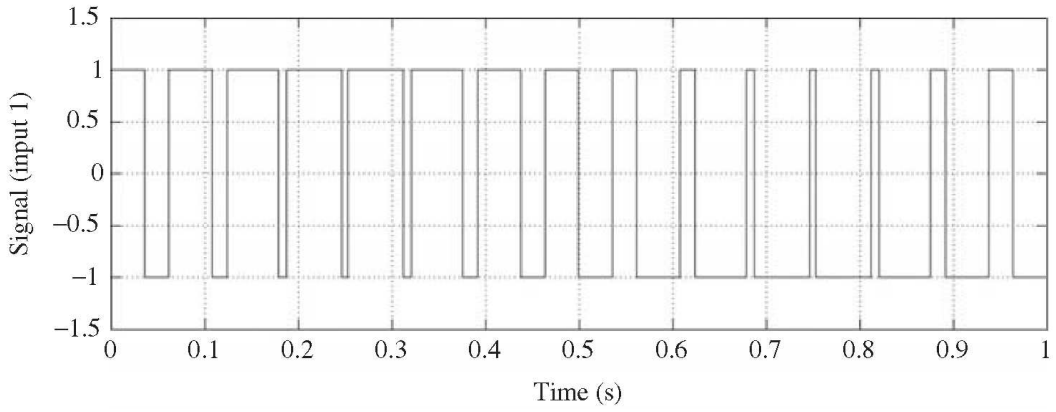

Figure 1.9: Output PWM waveform of a single-phase, two-level VSC [2]

$V_{ref} > V_{tri}$. The signal is -1 when $V_{ref} < V_{tri}$. The PWM switching pattern is shown in Figure 1.9. In variable-speed wind turbines, the frequency of the sinusoidal reference waveform (V_{ref} in Figure 1.8) is locked to the frequency of the generated voltage. Therefore, the frequency of the output voltage of the VSC contains a component at the frequency of the generated voltage, referred to as the fundamental and also higher-order harmonics. The magnitude of the VSC output voltage can be controlled by changing the amplitude modulation index and the phase angle can be controlled by controlling the phase angle of V_{ref} with respect to the generated voltage [2].

The main advantages of using back-back VSCs include the following: (a) it has been applied in industry for many years; (b) many manufacturers produce components specially designed for this type of converter; and (c) the decoupling of the two VSCs through a capacitor allows separate control of the two converters [17].

1.1.2 Operation and control

A wind turbine is essentially a device that captures part of the wind energy and converts it into useful work. In particular, WPGS connected to the grid must be designed to minimise the cost of supplied energy ensuring safe operation as well as acoustic emission and power quality standards [19].

The minimisation of the energy cost involves a series of partial objectives. These objectives are actually closely related and sometimes conflicting. Therefore, they should not be pursued separately. Conversely, the question is to find a well-balanced compromise among them. These partial goals can be arranged in the following topics [19]:

- Energy capture: Maximization of energy capture taking account of safe operation restrictions such as rated power, rated speed and cut-out wind speed, etc.

- Mechanical loads: Preventing the WECS from excessive dynamic mechanical loads. This general goal encompasses transient loads alleviation, high frequency loads mitigation and resonance avoidance.

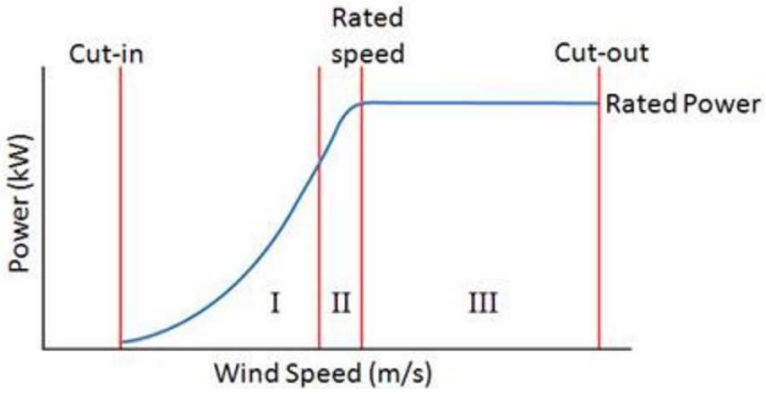

Figure 1.10: Wind turbine operation regions division

- Power quality: Conditioning the generated power to comply with interconnection standards.

Operation regions

The ideal power curve exhibits three different regions with distinctive generation objectives (Figure 1.10). At low wind speeds (Region 1), the available power is lower than rated power. The available power is defined as the power in the wind passing through the rotor area multiplied by the maximum power coefficient C_{p_max}.

So, the generation objective in region 1 is to extract all the available power. Therefore, the ideal power curve in this region follows a cubic parabola defined by Equation 1.1.1 [19].

On the other side, the generation goal in the high wind speed region (Region 3) is to limit the generated power below its rated value to avoid overloading. In this region the available power exceeds rated power, therefore the turbine must be operated with efficiency lower than C_{p_max}. Finally, there is region 2, which is actually a transition between the optimum power curve of Region 1 and the constant power line of region 3. In this region, the rotational speed is limited to maintain acoustic noise emission within admissible levels and to keep centrifugal forces below values tolerated by the rotor. Eventually, in the case that such a speed limit is not reached, Region 2 may not exist, and the optimum power curve (i.e. Region 1) may continue until getting to rated power [19].

Mechanical load

To minimise of the energy cost, the control system should not merely be designed to track as tightly as possible the ideal power curve. In fact, the other control objectives must not be ignored. For instance, the mechanical loads of wind turbines are exposed to must also be considered [20] [21]. Mechanical loads may cause fatigue damage on several devices, thereby reducing the useful life of the system. Since the overall cost of the WPGS is spread over a shorter period of time, the cost of energy will rise.

There are basically two types of mechanical loads, namely static and dynamic ones. Static loads result from the interaction of the turbine with the mean wind speed. Much more important from the control viewpoint are the dynamic loads, which are induced by the spatial and temporal distribution of the wind speed field over the area swept by the rotor. Dynamic loads comprise variations in the net aerodynamic torque that propagate down the drive-train and variations in the aerodynamic loads that impact on the mechanical structure. They are the so-called drive-train and structural loads, respectively.

There is also another common classification of dynamic loads. On the one hand, there are the transient loads, which are induced by turbulence and gusts. They are predominantly of low frequency. Transient loads have very important implications in high wind speeds, particularly for the determination of the components rating. The transition between maximum power tracking (Region 1) and power regulation (Region 3) and the way power is limited in above rated wind speeds have a direct impact on transient loads. Unsuitable control strategies may inevitably lead to strong transient loads. Therefore, the planning of the control strategy must also take them into consideration. In addition, controller setup and design also influence the transient loads. In fact, the tighter the closed-loop system follows the steady-state control strategy curve after a wind gust, the heavier the transient loads will be [19].

On the other hand, rotational sampling induces high-frequency cyclic loads concentrated around spectral peaks at multiples of rotor speed. For an N-bladed wind turbine, the spectral peak at NP predominates in cyclic drive-train loads whereas the energy of cyclic structural loads is mainly concentrated around 1P and NP. When

propagated down the drive-train and structure, cyclic loads may excite some of the poorly damped vibration modes of the system. In this respect, control systems are increasingly important as the wind turbines are larger and their components more flexible [22]. Cyclic loads are highly influenced by the control strategy as well as by the controller setup and design. For instance, the control of the electric generator affects the propagation of drive-train loads whereas the pitch control impacts directly on the structural loads. Therefore, inappropriate control designs might accentuate the vibration modes, potentially leading to the destruction of some mechanical devices such as gearbox or blades. The controller must provide damping at the vibration modes whenever possible in order to mitigate high frequency loads and reduce the risk of fatigue breakdown. On the other hand, the control strategy must avoid operation at points where those vibration modes that cannot be damped by the controller are likely to be excited [23].

Wind turbines control

Stall control

Many turbines are stall-regulated, which means that the blades are designed to stall in high winds without any pitch action being required. This means that pitch actuators are not required, although some means of aerodynamic braking is likely to be required, if only for emergencies [13].

In order to achieve stall-regulation at reasonable wind speeds, the turbine must operate closer to stall than its pitch-regulated counterpart, resulting in lower aerodynamic efficiency below rated. This disadvantage may be mitigated in a variable-speed turbine when the rotor speed can be varied below rated in order to maintain peak power coefficient.

For the turbine to stall rather than accelerate in high winds, the rotor speed must be restrained. In a fixed speed turbine, the rotor speed is restrained by the generator, which is governed by the network frequency, as long as the torque remains below the pull-out torque. In a variable speed turbine, the speed is maintained by ensuring that the generator torque is varied to match the aerodynamic torque. A variable-speed turbine offers the possibility to slow the rotor down in high winds in order to bring

it into stall. This means that the turbine can operate further from the stall point in low winds, resulting in higher aerodynamic efficiency. However, this strategy means that when a gust hits the turbine, the load torque not only has to rise to match the wind torque but also has to increase further in order to slow the rotor down into stall. This removes one of the main advantaged of variable-speed operation, namely that it allows very smooth control of torque and power above rated.

Yaw control

Horizontal axis wind turbines need some means to direct the turbine towards the wind. The entire nacelle is rotated about the tower to yaw the rotor out of the wind [7]. Usually, this is accomplished actively with an electrical or hydraulic servo. A wind vane placed on top of the nacelle senses the wind direction. However, the nacelle is mechanically parked most of the time. The servo is activated only when the mean relative wind direction exceeds some predefined limits [24].

If the yaw parking mechanism is stiff, then large dynamic loads appear in its components and the tower. It may be better to make it flexible, for instance, with mechanical suspension devices. An alternative is to use the yaw motor continuously, instead of parking the nacelle. The same dynamic behaviour as with a spring and damper suspension can theoretically be obtained with feedback of the yaw angle [24].

The disadvantage of this concept is the increased demands on the yaw servo. Continuous operation leads to increased wear. The ratings of the motor, for example, the maximum torque and speed, may have to be improved. Furthermore, additional or improved measurements may be required [24].

Pitch control

Pitch angle regulation is required in conditions above the rated wind speed when the rotational speed is kept constant. The blades are physically rotated about their longitudinal axis. Small changes in pitch angle can have a dramatic effect on the power output. The purpose of the pitch angle control might be [25]:

1. Optimizing the power output of the wind turbine. Below rated wind speed, the pitch setting should be at its optimum value to give maximum power.

2. Preventing input mechanical power to exceed the design limits. Above rated

wind speed, pitch angle control provides a very effective means of regulating the aerodynamic power and loads produced by the rotor.

3. Minimizing fatigue loads of the turbine mechanical component. It is clear that the action of the control system can have a major impact on the loads experienced by the turbine. The design of the controller must take into account the effect on loads, and the controller should ensure that excessive loads will not result from the control action. It is possible to go further than this, and explicitly design the controller with the reduction of certain fatigue loads as an additional objective.

One advantage of blade pitch control is that aerodynamic loads are controlled directly without undesirable transmission through the drive train and turbine structure [26].

In some commercial wind turbines, pitch control in Region 3 is performed using the proportional-integral-derivative (PID) collective pitch control law [27]. The output signal of the pitch angle controller can be either blade pitch angle or rate of change. While collective blade pitch requires only a single-input, single-output controller, many utility-scale turbines allow the blades to be pitched independently. If additional sensors and measurements, such as strain gauges measuring tower or blade bending moments, are available for feedback, then multi-input, multi-output individual blade pitch controllers can be designed for improved performance [27, 28].

Generation and power electronics control

The power converter can be arranged in various ways. While the generator-side converter can be a diode-based rectifier or a PWM voltage source converter, the strategy to control the operation of the generator and power flows to the network depends very much on the type of power converter arrangement employed.

Control of the generator side converter

The operation of the generator and the power transferred from the generator to the DC link are controlled by adjusting the magnitude and angle of the voltage at the

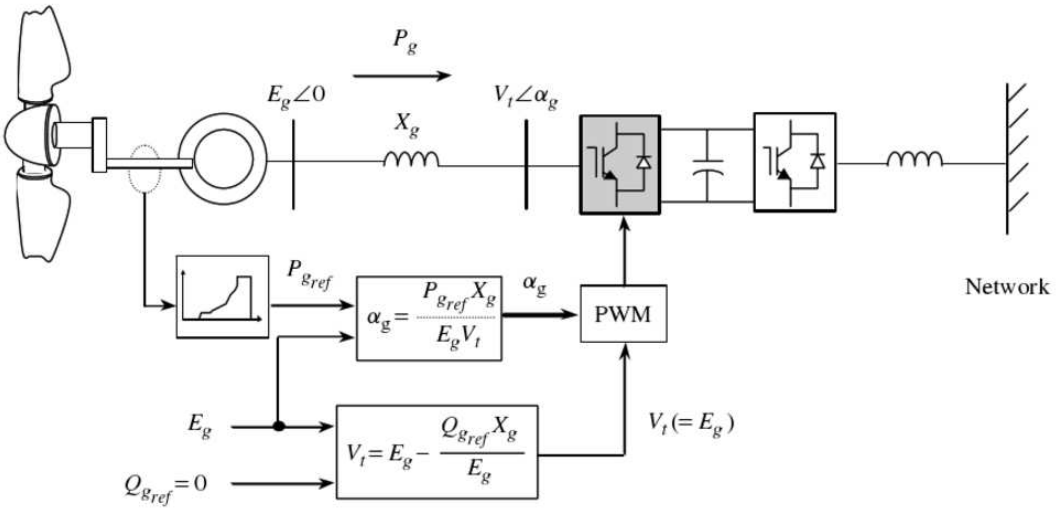

Figure 1.11: Load angle control of the generator-side converter

AC terminals of the generator-side converter. This can be achieved using the load angle control technique or vector control techniques.

Load angle control

The load angle control strategy employs steady-state power flow equations to determine the transfer of active and reactive power between the generator and the DC link. The implementation of the load angle control scheme is shown in Figure 1.11. The major advantage of the load angle control is its simplicity. However, as in this technique, the dynamics of the generator are not considered, it may not be very effective in controlling the generator during a transient operating condition [7]. Hence an alternative way to control the generator is to employ vector control techniques.

In Figure 1.11, E_g is the magnitude of the generator internal voltage, X_g the synchronous reactance, V_t the voltage at the converter terminals, α_g the phase difference between the voltages E_g and V_t, $P_{g_{ref}}$ and $Q_{g_{ref}}$ are the reference value of the active and reactive power.

Vector control

Vector control techniques are implemented based on the dynamic model of the synchronous generator expressed in the dq frame. The dq frame is defined as the d

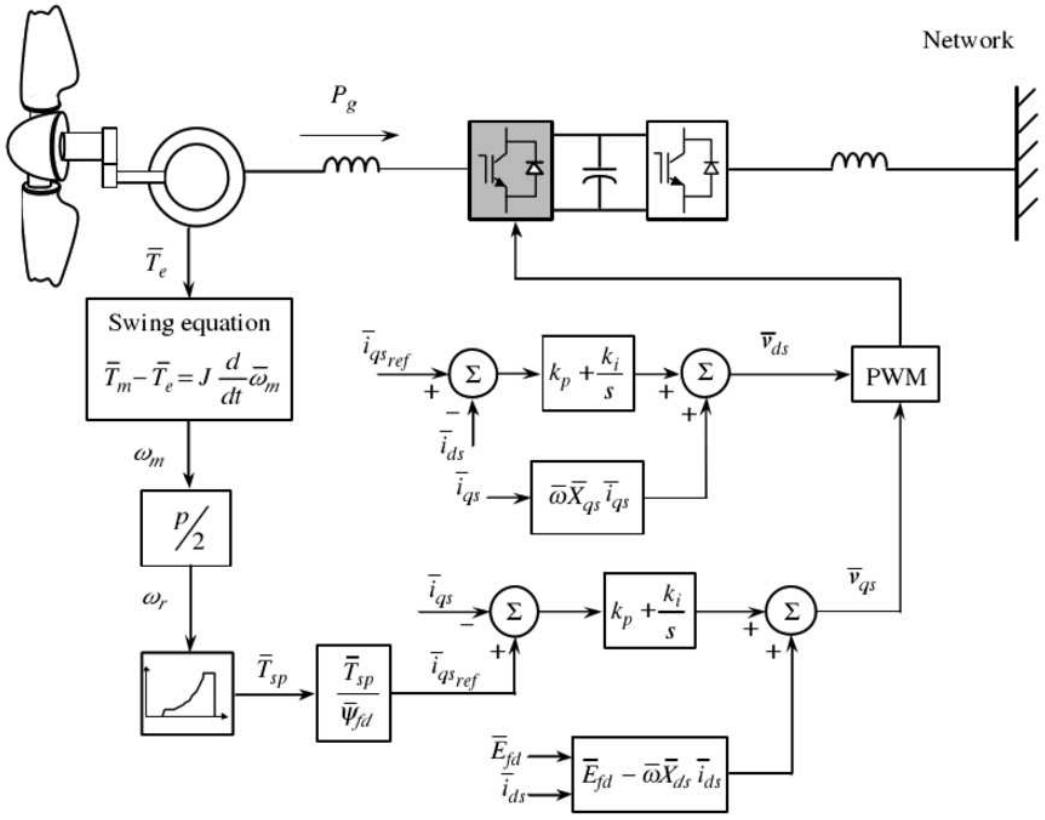

Figure 1.12: Vector control of the generator-side converter

axis aligned with the magnetic axis of the rotor (field). A PI controller is used to regulate the error between the reference and actual current values. The implementation of the vector control technique is shown in Figure 1.12 [2].

In Figure 1.12, T_e and T_m are electromagnetic and mechanical torque, ψ_f is field flux linkage, $X_{qs} = \omega_s L_{qs}$, $X_{ds} = \omega_s L_{ds}$ and $E_{fd} = \omega_s L_{md} i_f$ where L_{ds} and L_{qs} are the d and q axis inductance, L_{md} is mutual inductance in d axis, i_f is field current. For the vector control, the reference stator current on d axis $i_{ds_{ref}}$ is set to zero. The current reference $i_{qs_{ref}}$ which is the reference stator current on q axis is determined from the torque equation.

The torque control is exercised in the q axis and the magnetization of the generators is controlled in the d axis.

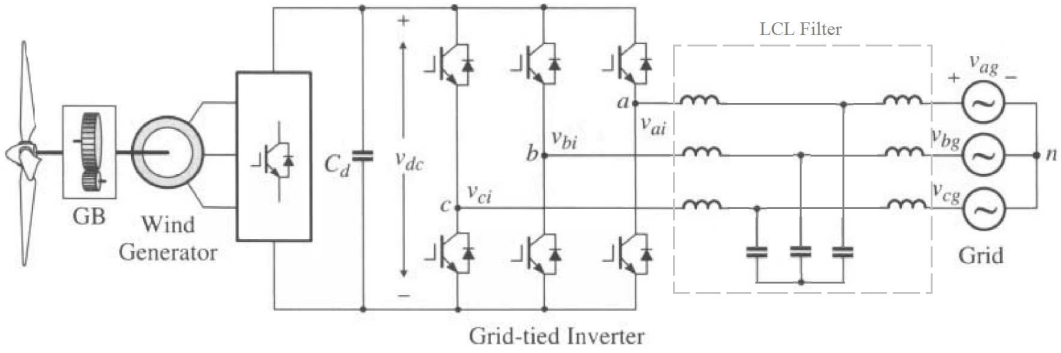

Figure 1.13: Grid side converter in a wind power generation system

Control of the grid side converter

Wind turbines deliver the generated power to the electric grid through power converters. A typical grid-side converter for wind power generation systems is shown in Figure 1.13, where a PWM-VSC is used as an example. The converter is connected to the grid through a line inductance L_g, which represents the leakage inductance of the transformer [18].

The objective of the grid-side converter is to maintain the DC link voltage at the reference value and export active power to the grid. In addition, the controller is designed to enable the exchange of reactive power between the converter and the grid as required by the application specifications [2, 7]. The grid side converter is modulated by the PWM schemes. Both load angle control technique and vector control technique can be used to control the grid side converter to achieve its control objectives.

1.2 Literature Review of Maximum Power Point Tracking Methods

From Figure 1.10, there are three different operational regions. Region1 is bounded by the cut-in speed and the rated rotational speed. Although the speed of the wind turbine could be fixed or variable, maximisation of the extracted energy

is achievable with variable speed wind turbines only. These turbines can change their rotational speed to follow instantaneous changes in wind speed.

In order to determine the optimal operating point of the wind turbine, inclusion of an MPPT algorithm in the system is essential. Much has been written on the topic of MPPT algorithms, especially of wind energy systems. Dipesh Kumar et al. [29] presented a comprehensive review and discussion of the different MPPT algorithm used in the WPGS, with three categories: indirect power controller, direct power controller and hybrid controller. Studies [30] reviewed many published wind MPPT algorithms and compared some of the wind MPPT algorithms, particularly for PMSG driven wind turbines. The authors in [31] reported that there is an increasing trend of MPPT algorithm use among researchers over the past decade.

This section summaries the main methods for PMSG based wind power generation system to achieve MPPT.

1.2.1 Tip speed ratio (TSR) MPPT algorithm

In the TSR MPPT algorithm, it is required to keep up the TSR to an optimum value at which extracted energy is maximised by regulating the rotational speed of the generator. The block diagram of this method is shown in Figure 1.14 [29,32]. In this method, the optimum rotational speed is compared with the actual value and the difference is then given to the controller, which changes the speed of the generator to reduce this error. Thus the mechanical power of the generator is controlled to track its maximum value. The optimum rotational speed in Equation 1.2.1 is determined from Equation 1.1.4 as:

$$\omega_{m\_opt} = \lambda_{opt} V_w / R_b \tag{1.2.1}$$

where ω_{m_opt} is the optimum mechanical rotation speed, λ_{opt} is the optimum tip-speed-ratio, V_w is wind speed and R_b is rotor radius.

This method requires an anemometer for the wind speed measurement and also the pre-known value of the optimal TSR to convert the wind speed measurement into the corresponding reference for optimal rotational speed. Although TSR algorithm is simple and efficient, additional experiments are required for getting the optimal

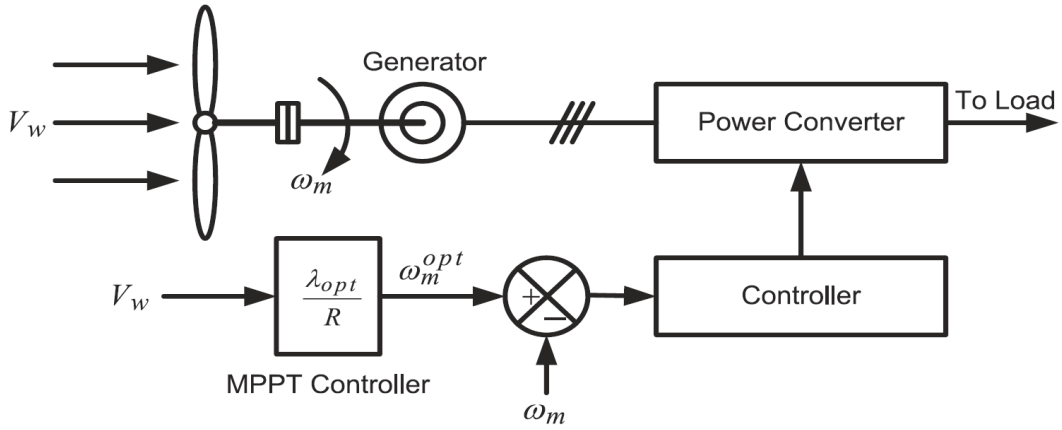

Figure 1.14: The block diagram of TSR MPPT algorithm [29]

TSR value and a precise measurement of wind speed cause the system more costly [30–32].

1.2.2 Optimal torque (OT) MPPT algorithm

The principle of this method is to adjust the mechanical torque according to a maximum power reference torque of the wind turbine at a given wind speed [33,34]. The generator torque is determined as a function of λ and ω_m. If the turbine's rotor is running at $\lambda = \lambda_{opt}$, it will also run at $C_p = C_{p\_max}$. Thus from Equation 1.1.1, it can be obtained:

$$P_{m\_opt} = \frac{1}{2}\rho\pi R^5 \frac{C_{p\_max}}{\lambda_{opt}^3}\omega_m^3 \tag{1.2.2}$$

In the OT algorithm, the torque of the generator is controlled to obtain optimum torque reference curve according to the maximum power of the wind turbine at a given wind speed. As $P_m = \omega_m T_m$, the expression for optimum mechanical torque of the turbine can be written as:

$$T_{m\_opt} = \frac{1}{2}\rho\pi R^5 \frac{C_{p\_max}}{\lambda_{opt}^3}\omega_m^2 \tag{1.2.3}$$

The block diagram of OT algorithm is shown in Figure 1.15. It is a torque-control-based algorithm, where the analytical expression of the optimum torque

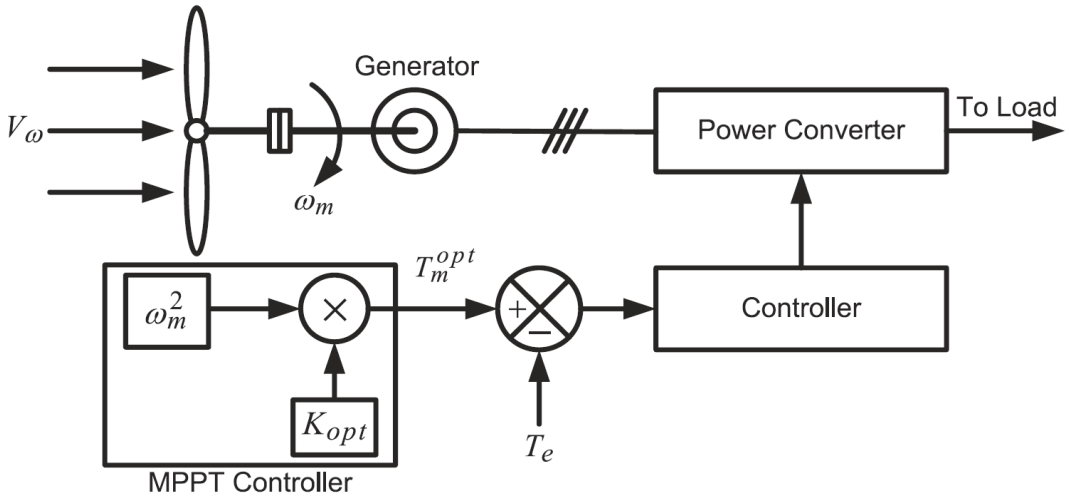

Figure 1.15: The block diagram of OT MPPT algorithm [29]

curve, represented by Equation 1.2.3 and Figure 1.16, is given as a reference torque for the controller that is connected to the wind turbine. This optimum reference torque is subtracted with actual torque to give the control signal to the controller, which then minimises the difference between them.

This MPPT algorithm has the advantage of simple and fast. However, it needs the actual torque value for feedback. Besides, the OT curve, which affects the MPPT efficiency, need to be obtained via experimental tests [35–37].

1.2.3 Power signal feedback (PSF) MPPT algorithm

Classically the most popular approach of MPPT is PSF algorithm [32]. The block diagram of PSF algorithm is shown in Figure 1.17. In the PSF algorithm, the controller reduces the error between optimum power P_{m_opt} and actual power. The optimum power P_{m_opt} is generated either using a pre-obtained power-speed curve or using the expression of turbine output power as shown in Equation 1.2.2.

In this method, the reference optimum power curve of the wind turbine should be obtained before. Then the data points for maximum output power and the corresponding wind turbine speed in a lookup table or a function employing the product of the cube of measured rotational speed with the optimum proportionality constan-

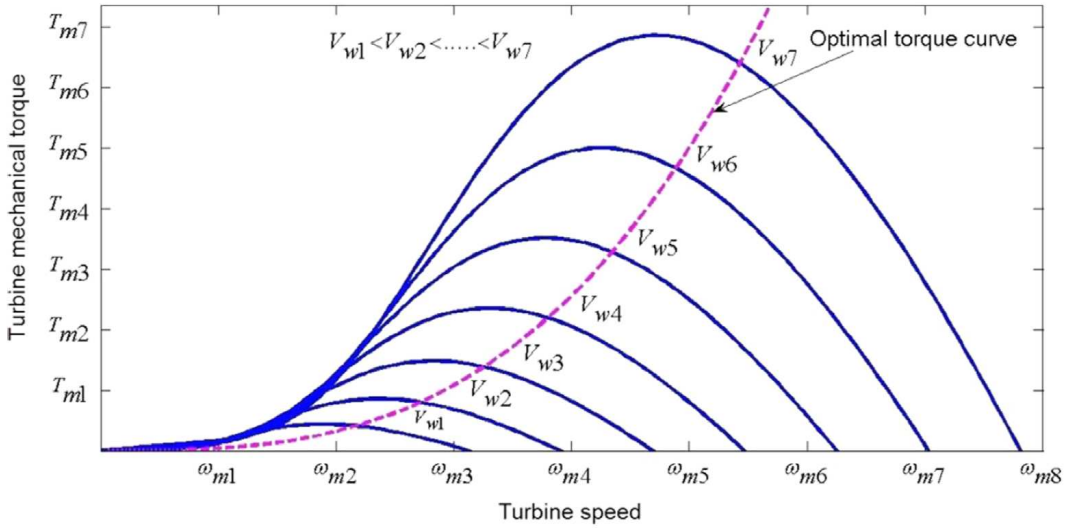

Figure 1.16: The torque-speed characteristic curve for a series of different wind speeds [29]

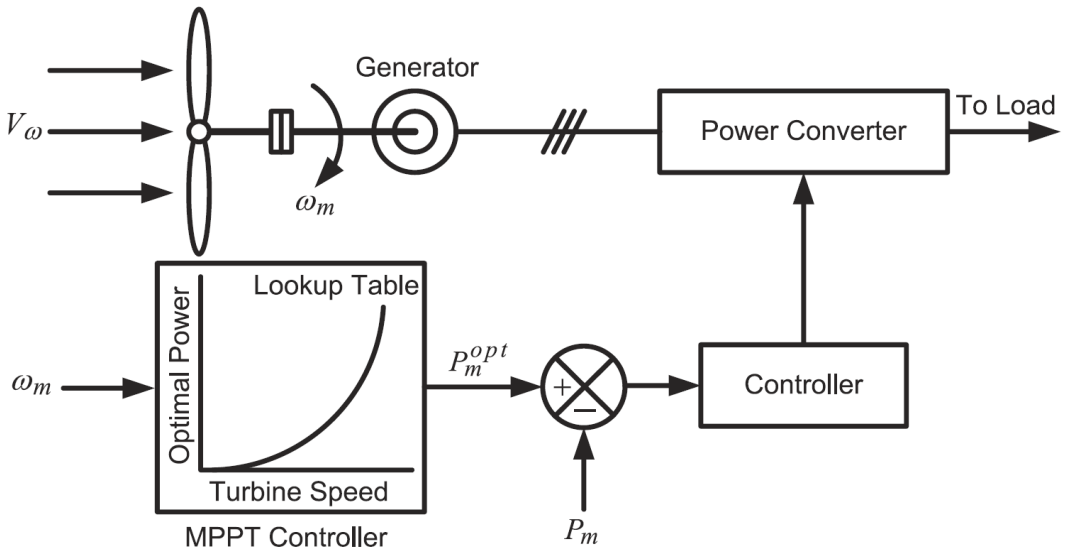

Figure 1.17: The block diagram of PSF MPPT algorithm [29]

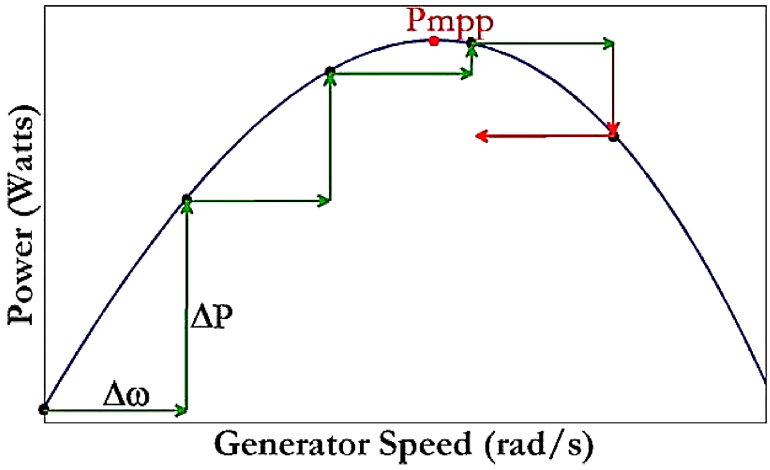

Figure 1.18: HCS control principle with a fixed step size [29]

t [38–40].

According to Raza Kazmi et al. [41], there is no difference between the PSF and the OT methods in performance and complexity of implementation in wind power generation systems. Although this algorithm is widely used in wind power generation systems, it requires the optimal power-speed curve which requires aerodynamic tests. Moreover, these characteristics can dramatically change with time and factors such as dirt and ice on the turbine blades [39, 42].

1.2.4 Perturbation and observation (P&O) or called hill climb search (HCS) MPPT algorithm

The perturbation and observation (P&O) or called hill climb search (HCS) MPPT algorithm is a mathematical optimisation strategy used to search for the local optimum point of a given function [29, 30, 43]. This algorithm involves a perturbation in the reference signal, generally the generator rotor speed or the terminal voltage or current and observing the change in the power. In this algorithm, if the operating point is on the left side of the peak point, the controller must move it to the right to be nearer to the peak point, and vice versa if it is on the other side [44–46]. The principle is shown in Figure 1.18.

The P&O or HCS algorithm is widely used in wind power generation systems as it is independent, simple and flexible. Besides, it does not require prior knowledge of the wind turbine's characteristic curve. However, it fails to reach the maximum power points under rapid wind variations if used for large and medium inertia wind turbines. Additionally, one major drawback that can lead to the failure of the tracking process is the lack of distinction between the power differences resulting from the change in the wind with those resulting from the change in the previous perturbation [47].

1.2.5 Other MPPT algorithm

Hybrid MPPT algorithm

One simple and effective solution to overcome the drawbacks of the conventional MPPT algorithms is by hybridization of two or more MPPT algorithms [41, 48–51]. An example of these methods was proposed in [49]. There are two modes of operation: the first one is a P&O mode, in which the conventional fixed step P&O MPPT algorithm is initially activated to search for an MPP at any local wind speed. Once the MPP is detected and the voltage and current are measured, the unknown parameter (k) is easily calculated. Once the k is extracted, it will be used to calculate the optimal current curve, and at that time the hybrid MPPT algorithm current curve, and at that time the hybrid MPPT algorithm switches to the second mode, which can track the MPP based on the equation with k. Another example was the combining of PSF control and HCS by Quincy and Liuchen [48] to develop a sensorless and flexible method that is applicable to all wind turbine levels.

Fuzzy-based MPPT algorithm

Many control strategies [52–56] have been proposed that use the Fuzzy Logic Control (FLC) for MPPT applications either independently or along with other methods. Fuzzy logic control generally consists of three stages: fuzzification, rule base table lookup, and defuzzification [31]. In the fuzzification stage, input variables are converted into linguistic variables based on a membership function. The

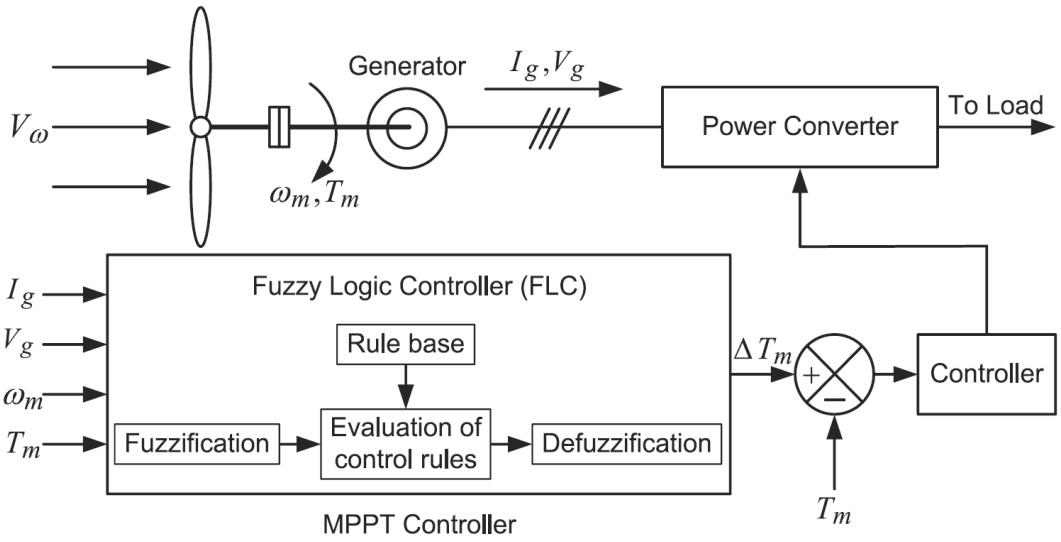

Figure 1.19: The block diagram of fuzzy-based MPPT algorithm [29]

commonly used inputs to an FLC are error and change in error. Based on the input, a rule base lookup table obtained by prior knowledge of the system's response to various errors, the FLC generates output, which is typically a change in duty ratio or rotor speed. In the defuzzification stage, the FLC output is converted from a linguistic variable to a numerical variable using another membership function. An example of fuzzy-based MPPT algorithm is shown in Figure 1.19 [57].

Although fuzzy-based MPPT algorithms have been shown to perform well under varying atmospheric conditions, their effectiveness depends on a lot on the knowledge of the user in choosing the right error, levels of membership functions, and selection of rule base table. The memory requirement also poses limitations in its implementation [29, 31].

Neural network (NN)-based MPPT algorithm

Both fuzzy logic controller and neural network (NN) have become popular and expanded with the development of soft computing technology [52, 58–63]. A neural network consists of three layers: input, hidden and output layers. The number of nodes in each layer vary and are user dependent [64].In wind power generation

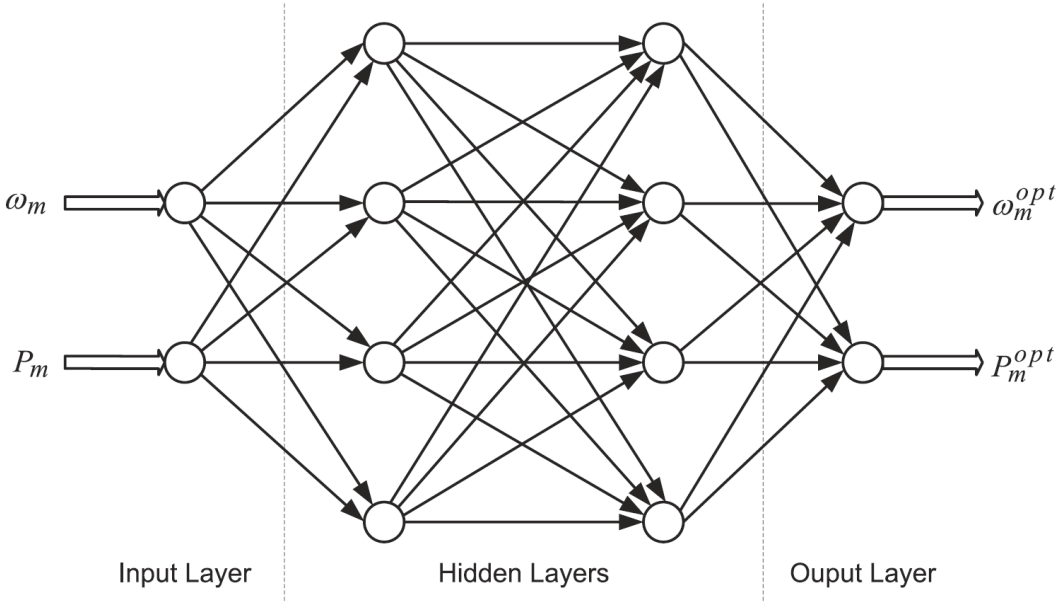

Figure 1.20: The structure of a NN used for estimation of optimal turbine power and speed [29]

systems, the input variables of NN based MPPT algorithm can be wind speed, pitch angle, rotor speed, output torque, terminal voltage, etc. or any combination of these. The output is generally a reference signal like duty cycle, reference rotor speed, reference torque, etc. that is used to drive the power converter close to the MPP. An example of NN used for estimation of optimal turbine power and speed are given in Figure 1.20.

The convergence of operating point to the peak point depends on the weights assigned to the layers, the type of algorithm used by the hidden layer and the training given to the neural network for a particular system for different input-output patterns [29, 31]. NN-based control can be quite effective and robust only after it is sufficiently trained for all kinds of operating conditions. This is quite a tough requirement and requires a long offline training. This long offline training makes NN quite unattractive for the real time practical applications [32].

Adaptive MPPT algorithm

Adaptive MPPT algorithm provides optimal response and can measure the uncertain system parameters. The flow chart of the adaptive MPPT algorithm is shown in Figure 1.21. It is based on the vector control algorithm which switches between multi-operational modes based on the detection of variable wind speed [65]. With these specially-designed modes, this method is specifically adapted to environmental changes and presents a significantly enhanced tracking performance. There are three operating modes for each control period, as classified in [41]. The MPPT block inputs are measured rotational speed and mechanical power. The output is the rotor rotational speed reference [65].

This kind of algorithms usually use HCS to seek for a parameter and then use the adaptive parameter in TSR, OT or PSF MPPT algorithm. Thus the limitation of the adaptive MPPT algorithm is that in variable wind speed environment, it takes time to seek for the parameter value and the found value may not be very accurate [66].

Multivariable perturb and observe (MVPO) MPPT algorithm

The aim of this algorithm is to maximise the generated power output of the wind farm, reducing the requirements of control units and sensors [67,68]. Such a solution causes the wind power systems economically strong, because the extracted power is same as compared with power classical wind farms, but the number of components required is reduced in MVPO algorithm. To maximise the wind farm output power, an extension of the P&O algorithm is adopted to optimise currents of all generators present in wind farm [29, 67]. Such a multivariable P&O algorithm, named MVPO, is designed to optimize each generator operating point by using the P&O principle as shown in Figure 1.22 [29].

In this algorithm the current of the first generator is perturbed meanwhile the aggregated output power increases, then, when the power is decreased, the current of the second generator is perturbed in the opposite direction with respect to the last perturbation performed to that generator. The procedure is iteratively performed to cover all the generators available in the wind farm [29].

Table 1.2 shows a comparison of the described MPPT algorithms in terms of

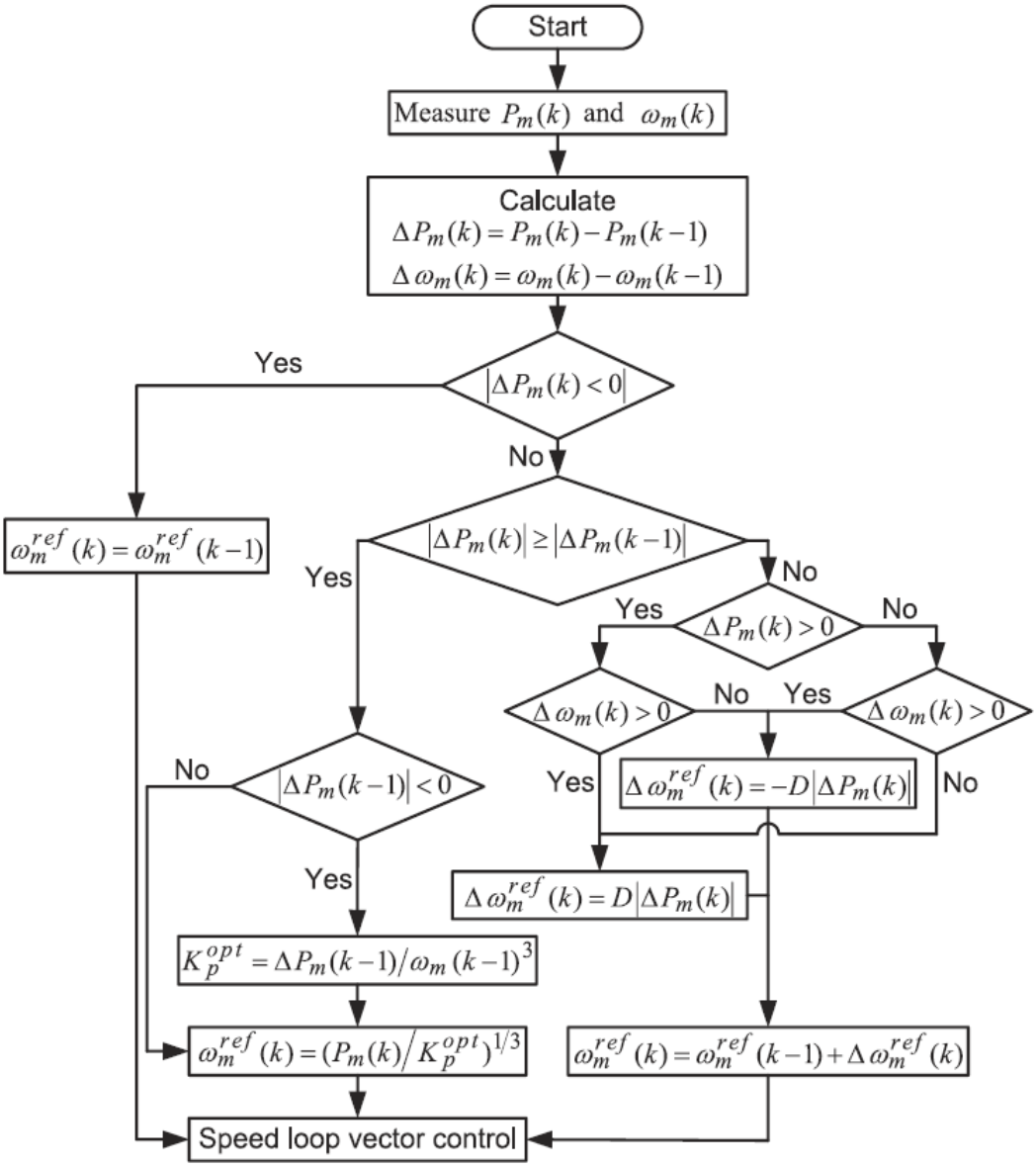

Figure 1.21: Flowchart of adaptive MPPT algorithm [29]

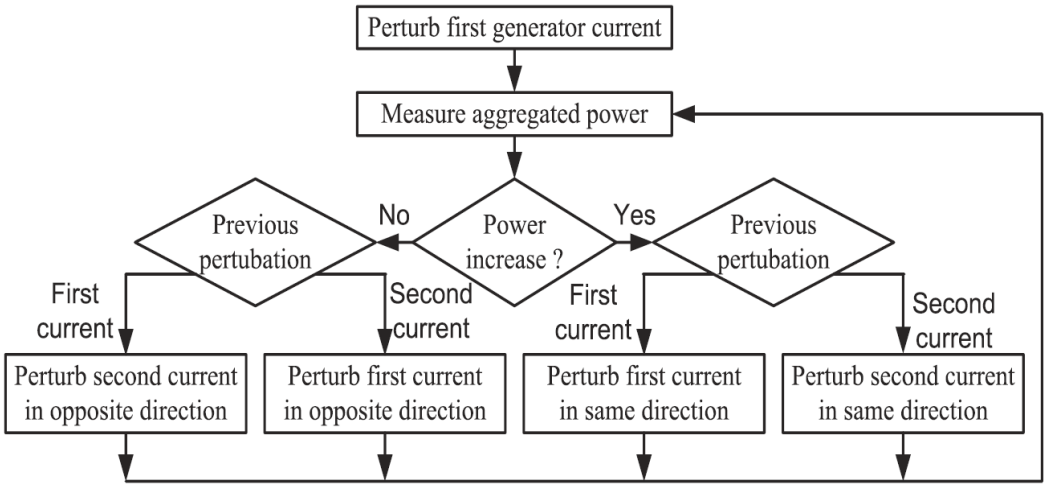

Figure 1.22: Flowchart of MVPO MPPT algorithm [29]

complexity, convergence speed, wind speed measurement, performance, memory requirement and prior training. The main aim of the MPPT algorithm is to track the optimum power point of variable speed wind turbine. Choosing an appropriate MPPT technique is a tough task and should consider different situations and conditions.

1.3 Motivation and Objectives

As mentioned previously, WPGS has many advantages and has a rapid growing and development in the past decade. With the increased penetration into the power grid and the large number of installation and operation of large-scale WPGS and wind farms, high reliability and high efficiency have become two main concerns of the operation and maintenance of WPGSs. Although lots of technologies advancement and achievement have been devoted to wind power industry, there are still some challenges in the context of the reliable and efficient operation and control of WPGSs. Firstly, the transition between wind turbine operation regions can be problematic. In fact, for some turbines, significant structural damage occurs due to extreme fatigue loads during this transition. Secondly, MPPT methods have

Algorithm	Comple -xity	Converg -ence speed	Memo -ry require -ment	Wind speed measu - rement	Perfor -mance under varying wind speed	Prior train- ing/ knowledge
TSR	Simple	Fast	No	Yes	Moderate	Not required
OT	Simple	Fast	No	No	Moderate	Required
PSF	Simple	Fast	Yes	Yes	Moderate	Required
HCS	Simple	Low	No	No	Moderate	Not required
Hybrid	Medium	Fast	No	No	Good	Not required
Fuzzy-based	High	Medium	Yes	Depends	Very good	Required
NN-based	High	Medium	Yes	Depends	Very good	Required
Adaptive	High	Medium	Yes	Depends	Very good	Required
MVPO	High	Low	No	No	Good	Not required

Table 1.2: Comparison of described MPPT algorithms

some limitation in applications, e.g. HCS algorithm may loose its trackability in variable wind speed; OT and PSF algorithm need optimal torque or power curve in advance. Thirdly, power generation efficiency decreases during the wind turbine lifetime. The wind power industries prefer reliable, simple and advanced control methods to improve the efficiency of WPGSs, adapt different wind turbine characteristics and extend the wind turbines life cycle. Finally, the design of simple power electronics converter (e.g. diode rectifier and DC-DC boost converter) and control methods is still challenging tasks to obtain cost-effectively and high efficiency.

To tackle those challenges, this thesis aims to achieving the following objectives:

- Develop a new algorithm to improve the switching of a WPGS between different operation regions with a reduced mechanical load.
- Investigate new MPPT methods for wind turbines with different characteristics and parameter, to maximise the output power of a WPGS.
- Investigate hardware implementation and verification for implementing the proposed algorithm and build up prototype experiment platform, for monitoring and control system implementation and verification.

1.4 Contributions and Thesis Outline

This thesis is structured as follows:

Chapter 2 presents a method for smoothly switching of controllers between wind turbine operating regions. As control systems for wind turbines will operate with different objectives throughout its complete wind speed regions: from cut-in speed to cut-out speed. The controllers designed are based on Pseudo Derivative Feedback (PDF), which provides smoother dynamic and simpler tuning of parameters than general PI controllers. Simulations of the presented method are performed with a non-linear wind turbine model at first, followed by preliminary results of hardware-in-the-loop simulation. The simulation and hardware implementation results present a smooth performance of region switching between different controllers and verify the effectiveness of the controller proposed.

In Chapter 3, an advanced hybrid hill climb search (HCS) algorithm is proposed via combining the conventional HCS and power signal feedback (PSF) control with a novel algorithm to detect the wind speed variation. During the period that the wind speed is detected as constant, the controller optimise the parameter of the power curve. The proposed method is verified in simulation on a permanent magnet synchronous generator (PMSG) based wind turbine. Wind speed sensorless control methods for wind turbine MPPT are beneficial as they do not require knowledge of wind speed or wind turbine characteristics. Simulation results show that this algorithm has better performance in tracking the maximum power coefficient than the conventional HCS algorithms, particularly in variable wind speed.

In Chapter 4, a new detection method is proposed to obtain the wind turbine's optimal power-speed curve under natural variable wind speed conditions and then used for maximum power point tracking (MPPT). The curve of maximum power versus wind turbine rotational speed is detected, which is then used in the power signal feedback control of a wind power generation system. The proposed detection method does not require any previous knowledge of the wind turbine, and the environment. The curve detection process can be undertaken in natural variable wind speed environment, without requiring additional wind turbine tests using wind tunnels. The proposed method is verified by MATLAB/Simulink simulations and experiment tests of a WPGS with a permanent magnet synchronous generator (PMSG) with a VSC.

In industry, diode bridge rectifier with DC-DC boost converter is widely used on PMSG based wind power generation systems. As it is low cost and easy control, in Chapter 5, the operation and design of DC-DC boost converter in PMSG based WPGS is presented. Chapter 5 contains the model of DC-DC boost converter and the hardware implementation progress. Field test results are given to for the built hardware. And the hardware is used in prototype experiments in Chapter 6. The hardware platform implemented can be used for designed methods and control system verification.

In Chapter 6, a prototype wind power generation system is presented. As there are two small scale wind turbines installed on the department roof and cable con-

nected to the laboratory for experiments. It is a used to build a micro-smart network platform to demonstrate renewable energy generation, monitoring and coordination system. With this prototype, the further green energy conversion ideas are enabling to be developed, tested and validated. Further comparison experiments can be done with the implemented prototype wind power generation system. This chapter describes the prototype settings, experiment design, field test and experiments results with the roof turbines.

Chapter 7 concludes the findings of this thesis and suggests future research work that can be extended based on results.

Publications list

Liuying Li, Yaxing Ren, Yang Liu, Mohammed Alsumiri & Lin Jiang, Wind Turbine Optimal Power-Speed Curve Detection under Natural Variable Wind Speed, *IET Renewable Power Generation* (Under review)

Liuying Li, Yaxing Ren, Lin Jiang, Joseph Brindley & Victor Bellido-Gonzalez, Hardware Implementation of Smooth Region Switching for Wind Turbine Control using PDF Controller, *The 2nd International Conference on Renewable Energy Research and Applications (ICRERA)*, pp. 115-120, IEEE, 2013.

Liuying. Li, Yaxing. Ren, Mohammed. Alsumiri, Joseph. Brindley & Lin. Jiang, Maximum Power Point Tracking of Wind Turbine Based on Optimal Power Curve Detection under Variable Wind Speed, *International Conference on Renewable Power Generation (RPG 2015)*, IET, 2015.

Liuying. Li, Bing. Han, Yaxing. Ren, Joseph. Brindley & Lin. Jiang, An Improved Hybrid Hill Climb Searching Control for MPPT of Wind Power Generation Systems under Fast Varying Wind Speed, *International Conference on Renewable Power Generation (RPG 2015)*, IET, 2015.

Yaxing Ren, Liuying Li, Lin Jiang & Joseph Brindley, Nonlinear PID Control of Variable Pitch Wind Turbine, *Control Engineering Practice*, vol. 50, pp. 84-94, May 2016.

W. Zhang, J. Chen, Y. Ren, L. Li, W. Yao & L. Jiang, Nonlinear Adaptive Control of Induction Motor with Sliding Mode Flux Observer, *The 17th International*

Conference on Electrical Machines and Systems (ICEMS), pp. 2738-2742, Oct. 2014.

Chapter 2

Wind Turbine Smooth Region Switching

Control system for wind turbine will operate with different objectives throughout its complete wind speed regions: from cut-in speed to cut-out speed. This chapter presents a method for smoothly switching of controllers between these operating regions. The controllers designed in this chapter are based on Pseudo Derivative Feedback (PDF), which provides smoother dynamic and simpler tuning of parameters than general PI controllers. Simulations of the presented method are performed with a non-linear wind turbine model at first, followed by preliminary results of hardware-in-the-loop simulation. The simulation and hardware implementation results present a smooth performance of region switching between different controllers and verify the effectiveness of the controller proposed.

2.1 Introduction

Torque control and pitch angle control are widely used in the wind power generation systems. For variable-speed wind turbines, generator torque control is used to capture the maximum energy from wind when rotational speed is below the rated value. The pitch angle control for blades is used to limit the generator power when the power is above the rated power, and to keep the wind turbine within its designed limits [69, 70]. Because wind turbine control is often achieved by using these two different controllers, the transition between different operating regions can be problematic. In fact, for some wind turbines, significant structural damage occurs due to extreme fatigue loads during these transitions [71, 72]. One technique is to arrange switchings which can ensure that only one of the control loops is activated at any one time. However, there always be occasions when the controller is caught briefly in the wrong mode. Another approach is to run both control loops together. But they can be made to interfere constructively when close to the rated point [22].

This chapter presents a strategy of smooth region switching between operating regions. It can minimise sudden changes in control actions and mechanical loads. A switching logic is given and simulated on a 5th-order nonlinear variable speed wind turbine model. Besides, practical considerations for implementing the switching logic will be discussed in this chapter.

2.2 Variable-Speed Wind Turbine Model

The main components of a wind energy conversion system are the rotor, the transmission system and the generator. The scheme of a two-mass wind turbine model is given in Figure 2.1 [73]. As an example, for a horizontal-axis wind turbine, the rotor comprises the blades where the aerodynamic conversion takes place. The transmission system transmits the mechanical power captured by the rotor to the electric machine. The gearbox in the transmission system increases the rotor speed to values more suitable for driving the generator. The electric generator is the device that converts mechanical power into electric power. In the case of variable-speed wind power generation systems, electronic converters are used as interface between

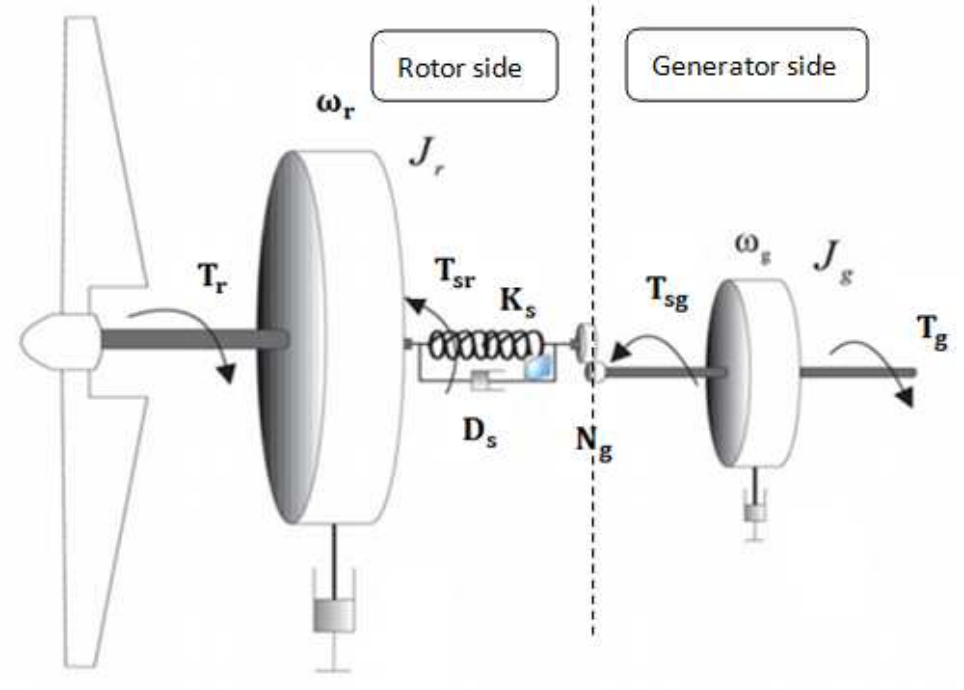

Figure 2.1: The scheme of a 5th-order two-mass state-space wind turbine model [73]

the AC grid and the stator or rotor windings [19].

In Figure 2.1, T_r is the torque transferred from rotor to the gear, ω_r the rotor speed, J_r inertia of rotor, K_s spring constant of shaft, D_s shaft damping, T_{sr} generator torque transferred to rotor, N_g gear ratio, T_{sg} generator torque transferred to gear box, ω_g the generator speed, J_g inertia generator and T_g is generator load torque.

A model for the entire wind turbine can be structured as several interconnected subsystem models as shown in Figure 2.2. The aerodynamic subsystem describes the transformation of the wind speed into forces on the blades that originate the rotational movement. The drive-train in the mechanical subsystem transfers the aerodynamic torque on the blades to the generator shaft. It encompasses the rotor, the transmission and the mechanical parts of the generator. The electrical subsystem describes the conversion of mechanical power at the generator shaft into electricity. Besides, for a variable-pitch wind turbine, there is an actuator subsystem that models the pitch servo behavior [19].

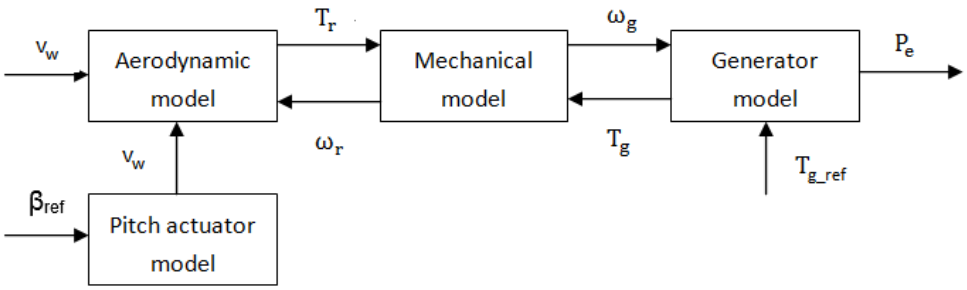

Figure 2.2: Interconnection of sub-models describing the characteristics of the wind turbine

2.2.1 Aerodynamics

The aerodynamics considers the rotating parts of the wind turbine, including the rotors and blades, which converts the kinetic energy of the wind into mechanical energy. When there is a thrust force from wind to blades, generated torque on the rotor is:

$$T_r = \frac{P_r}{\omega_r} \tag{2.2.1}$$

where the mechanical power absorbed from the wind P_r is given by the following equation:

$$P_r = \frac{1}{2}\rho A_r v_w^3 C_p(\lambda, \beta) \tag{2.2.2}$$

where ρ is the air density; A_r is the area swept by the blades; v_w is the wind speed; C_p is the turbine power coefficient which is determined by the blade pitch angle β and the tip speed ratio λ. Groups of $C_p - \lambda$ curves obtained by measurement or by computation can also be approximated in closed form by non-linear function. Following [74], a model can be derived in the form:

$$C_p(\lambda, \beta) = 0.22(\frac{116}{\lambda_t} - 0.6\beta - 5)exp(-\frac{12.5}{\lambda_t}) \tag{2.2.3}$$

where

$$\lambda_t = \frac{1}{\lambda^{-1} + 0.12\beta} - \frac{0.035}{(1.5\beta)^3 + 1} \tag{2.2.4}$$

The tip-speed ratio λ is given in Equation 1.1.4. For a certain wind speed, there is a unique optimal power which exhibits a cubic function of the generator speed [75].

2.2.2 Mechanics

Figure 2.1 shows the schematic of the two-mass wind turbine mechanics model which separates the mechanics into two parts: the rotor side and the generator side.

J_r and J_g are the inertia on the rotor side and generator side respectively. The shaft which is modeled as a damped spring connecting the rotor to the transmission system is subject to immense torques that cause it to twist. The damping constant D_s and the spring constant K_s can illustrate the dynamic nature of the shaft. The torques at each side of the transmission have the relationship:

$$T_{sg} = \frac{T_{sr}}{N_g} \tag{2.2.5}$$

where N_g is the gear ratio which is determined by the discs in the middle. T_r and T_g are rotor torque and generator torque respectively. From Newton's second law for rotating bodies, the following two equations can be captured:

$$\dot{\omega_r} J_r = T_r - T_{sr} \tag{2.2.6}$$

$$\dot{\omega_g} J_g = T_{sg} - T_g \tag{2.2.7}$$

The torque at the rotor side of the transmission can be described by the twist of the flexible shaft δ:

$$T_{sr} = D_s\dot{\delta} + K_s\delta \tag{2.2.8}$$

where the twist of the flexible shaft is determined by:

$$\delta = \Omega_r - \frac{\Omega_g}{N_g} \tag{2.2.9}$$

$$\dot{\delta} = \omega_r - \frac{\omega_g}{N_g} \tag{2.2.10}$$

Ω_r and Ω_g are the shaft angles at the rotor and the generator.

From Equation (2.2.5) to (2.2.10), the mechanical model can be constructed based on the following two equations:

$$\omega_r = \frac{1}{J_r}\int\left[T_r - D_s\left(\omega_r - \frac{\omega_g}{N_g}\right) - K_s\int\left(\omega_r - \frac{\omega_g}{N_g}\right)\right] \tag{2.2.11}$$

$$\omega_g = \frac{1}{J_g}\int\frac{1}{N_g}\left[D_s\left(\omega_r - \frac{\omega_g}{N_g}\right) - K_s\int\left(\omega_r - \frac{\omega_g}{N_g}\right)\right] - T_g \tag{2.2.12}$$

2.2.3 Generator dynamics

It is assumed that the generator in the model is an asynchronous lossless generator. Hence the generator power P_e can be calculated by:

$$P_e = T_g\omega_g \tag{2.2.13}$$

The generator torque T_g can be controlled and the dynamic response of the generator is modeled by a first order linear model with a time constant τ_T:

$$\dot{T_g} = -\frac{1}{\tau_T}T_g + \frac{1}{\tau_T}T_{g\_ref} \tag{2.2.14}$$

T_{g_ref} is the generator torque reference. Combing Equation (2.2.13) and (2.2.14), there comes:

$$P_e = \omega_g\int[\frac{1}{\tau_T}(T_{g\_ref} - T_g)] \tag{2.2.15}$$

2.2.4 Pitch actuator

The pitch angle of the blades is adjusted by a mechanical actuator. Its physical meaning is that there is a time delay when the controller changes the pitch angle

with a time constant τ_β. The following first order linear model is a simplified model with β_{ref} representing pitch angle reference:

$$\dot{\beta} = -\frac{1}{\tau_\beta}\beta + \frac{1}{\tau_\beta}\beta_{ref} \tag{2.2.16}$$

2.2.5 5th-order wind turbine state-space model

From Equation (2.2.1) to Equation (2.2.16), a combined 5th-order two-mass state-space model of the wind turbine is System (2.2.17).

$$\begin{aligned} \dot{x} &= f(x) + Bu \\ &= \begin{bmatrix} \frac{P_r(x_1,x_4,v)}{x_1 J_r} - \frac{x_1 D_s}{J_r} + \frac{x_2 D_s}{N_g J_r} - \frac{x_3 K_s}{J_r} \\ \frac{x_1 D_s}{N_g J_g} - \frac{x_2 D_s}{N_g^2 J_g} + \frac{x_3 K_s}{N_g J_g} - \frac{x_5}{J_g} \\ x_1 - \frac{x_2}{N_g} \\ -\frac{1}{\tau_\beta} x_4 \\ -\frac{1}{\tau_T} x_5 \end{bmatrix} + \begin{bmatrix} 0 & 0 \\ 0 & 0 \\ 0 & 0 \\ \frac{1}{\tau_\beta} & 0 \\ 0 & \frac{1}{\tau_T} \end{bmatrix} u \end{aligned} \tag{2.2.17}$$

where

$$x = [\omega_r \quad \omega_g \quad \delta \quad \beta \quad T_g]^\intercal$$

$$u = [\beta_{ref} \quad T_{g\_ref}]^\intercal$$

$$P_r = \tfrac{1}{2}\pi\rho R_b^2 v_w^3 C_p(x_4, \lambda)$$

$$\lambda = \frac{x_1 R_b}{v_w}$$

The wind turbine dynamic model is given in Equation (2.2.17). x and u in Equation (2.2.17) represent the states vector and the control inputs respectively. The five states of x are: the rotor speed ω_r, the generator speed ω_g, the twist angle δ, the pitch angle β, and the generator torque T_g. The two control inputs of u are pitch angle reference β_r, and generator torque reference T_{g_ref}.

2.2.6 Control objectives

Operating regions

To control a wind turbine in a varying wind speed, the wind turbine operation range can be divided into three regions shown in Figure 2.3 [76, 77].

The solid curve in Figure 2.3(a) illustrates the desired power (P_e) versus wind speed (v_w) relationship for a specified power coefficient, C_p. Once the wind speed is sufficient to rotate the rotor and to generate the electrical power output, the turbine is operating in Region 1. When the wind turbine reaches the rated rotational speed, it enters Region 2, which is a transition region. Comparing between Figure 2.3(a) and Figure 2.3(b), it shows that the turbines rotational speed is at its rated value in Region 2, but it is operating below its rated power. The objective of Region 2 is to have a smooth transition between the controllers used in Region 1 and Region 3. When the wind turbine is operating at both the rated rotational speed and rated power, it is in Region 3. Once the wind speed achieves the cutoff speed, the turbine will be stopped to protect the generator from over current and other components in the wind power generation system.

Control methods in different regions

1) Region 1:Maximum Power Point Tracking Control

When the wind speed is sufficient to make the wind turbine rotating but not enough to reach the rated rotational speed, the control objective in this region is to maximise the energy captured from the wind. So the controller in this region is to make the turbine operating at the peak point of its efficiency coefficient C_p curve. The blade pitch angle is a fixed value in this region. One method for tracking the maximum C_p is to vary the rotor rotational speed and keep the tip-speed-ratio at the optimum value. The tip-speed-ratio λ is defined as Equation (1.1.4).

If the optimum tip speed ratio, λ_{opt}, is to be maintained, the rotor speed reference can be set as follows

$$\omega_{r\_opt} = \frac{\lambda_{opt} v_w}{R_b} \tag{2.2.18}$$

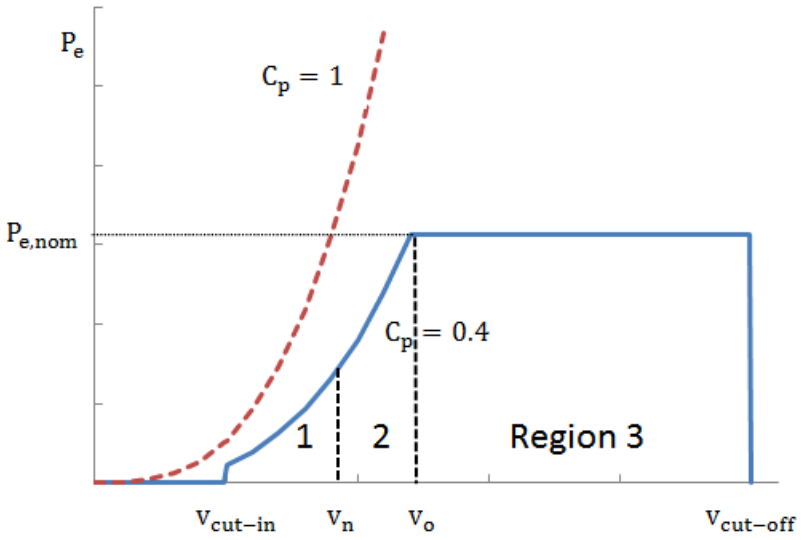

(a)

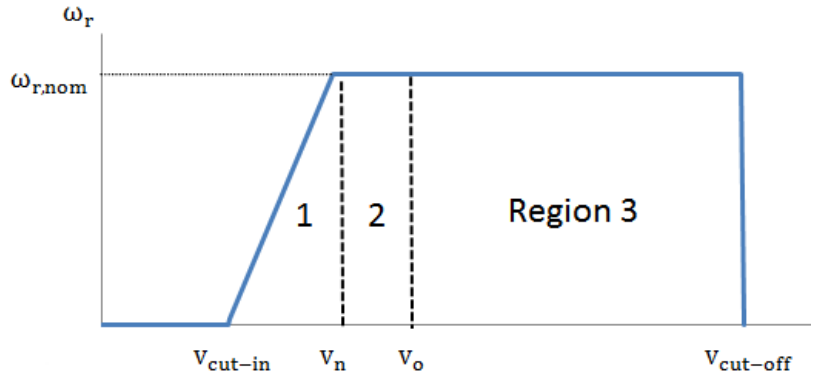

(b)

Figure 2.3: Illustrative curves in three regions. (a) Steady-state power curves. (b) Rotor angular speed curve.

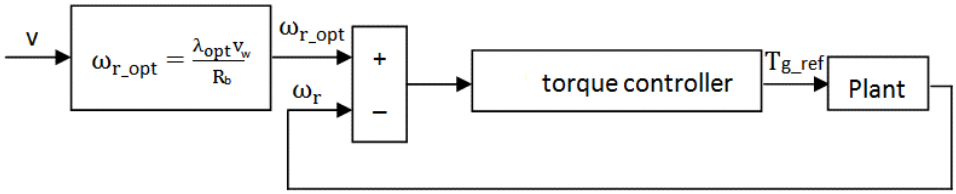

Figure 2.4: Torque control in low wind speed region

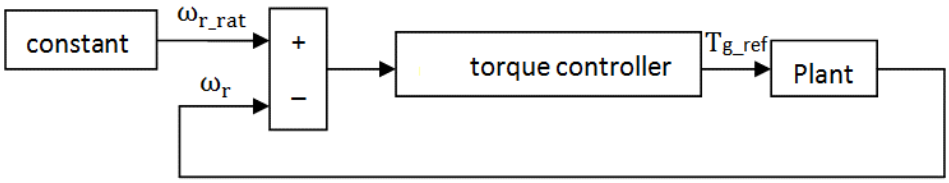

Figure 2.5: Torque control in middle wind speed region

The control scheme in Region 1 is shown in Figure 2.4. The reference rotor speed is tracked by control the generator torque.

2) Region 2: Rated Rotational Speed Torque Control

In Region 2, the control objective is to keep the rotational speed constant at its rated value for a smooth transition to Region 3 when the rated power is reached. This is usually achieved by varying the generator torque. The control loop can be similar to that in Region 1, as shown in Figure 2.5.

3) Region 3: Rated Generated Power Pitch Control

When wind speed is sufficiently high that the wind turbine reaches its rated power output then it is in Region 3. The control objective in this region is to keep the rotor rotational speed constant and produce a constant power output. In this region, the generator torque is constant at its rated value T_{g_rat}. Blade pitch angle control is used to limit the rotational speed and the generated power to keep the power output constant at its rated value. The control scheme is in Figure 2.6.

In Region 3 the torque controller can be regarded as inactive because the generator torque reference, T_{g_ref}, is held at its rated value.

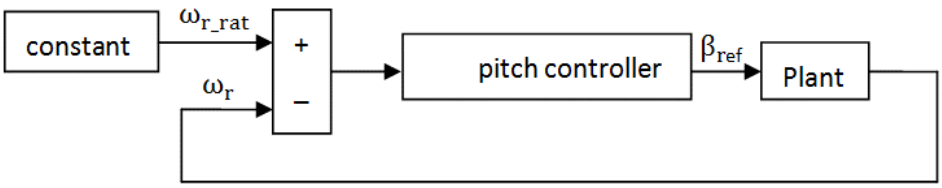

Figure 2.6: Pitch control in high wind speed region

2.3 Switching Design

2.3.1 Switching between different regions

To smoothly switch the controller between the three regions while minimising any sudden control actions and loads on the system, a set of trigger criteria are initiated.

(1) Region 1 to Region 2: $\omega_{r\_ref} \geq \omega_{r\_rat}$

In Region 1 the rotor speed is below its rated value. When wind speed increases, rotor speed will increase to capture the maximum energy from the wind. When rotor speed, ω_r, reaches ω_{r_rat}, it will switch from Region 1 to Region 2. However, this may cause a significant jump in generator torque as the controller attempts to bring the rotor speed back down after it passes ω_{r_rat}. A smoother transition is to switch the present control loop based on the value of ω_{r_ref} instead of ω_r. Since there is a lag between ω_{r_ref} and ω_r, there is a degree of prediction built into the switching. In this way, any overshoot of the rated rotor speed and subsequent aggressive control actions should be minimised. When the rotor speed reference, ω_{r_ref}, reaches the rated value, ω_{r_rat}, it is simply held at that value and the region switches from Region 1 to Region 2.

(2) Region 2 to Region 3: $T_g \geq T_{g\_rat}$

The relationship between generator power P_e and generator torque T_g is in E-quation (2.2.13). When consider about the losses in the generator, it becomes:

$$P_e = \omega_g \times T_g \times \eta \tag{2.3.1}$$

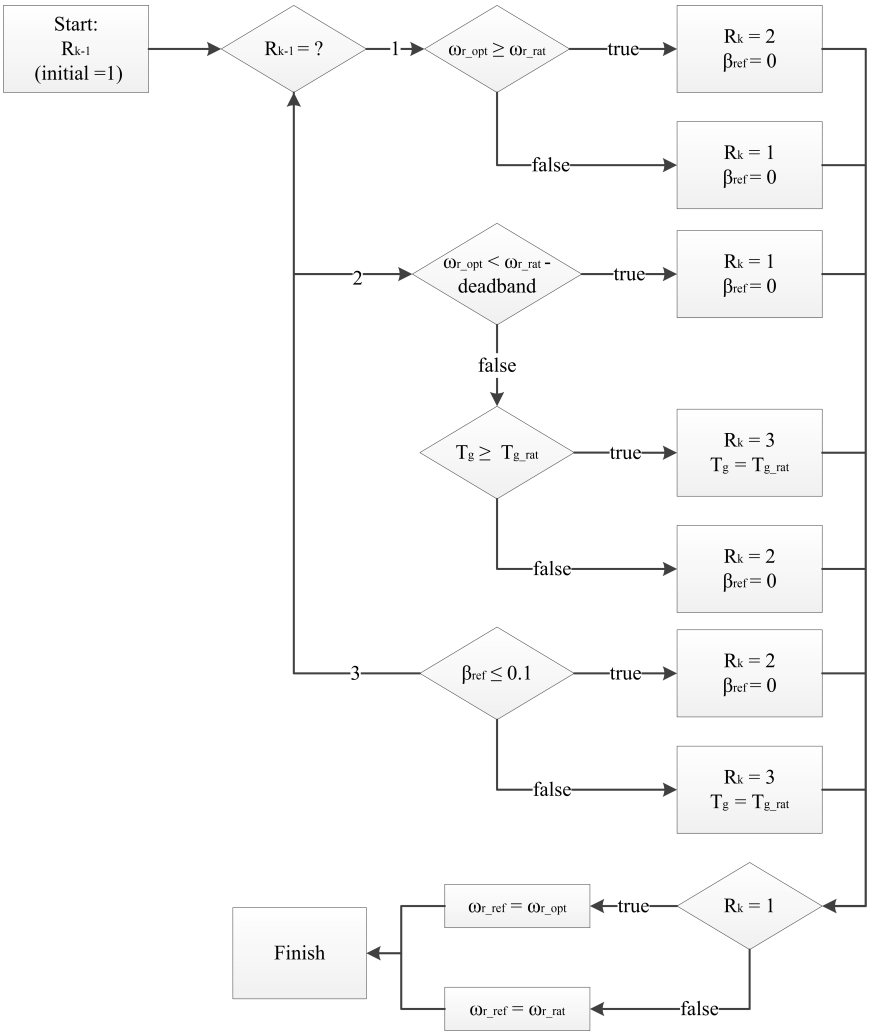

Figure 2.7: Flowchart of the regions switching logic

where η is the generator efficiency.

In Region 2, the rotational speed ω_r is controlled to track its rated value ω_{r_rat}. When wind speed rises, to restrict increasing of rotational speed, generator torque will increase and lead to the increasing in generator power. When the generator power reaches its rated value, the generator torque will be controlled to keep in its rated value T_{g_rat}. Thus, when $T_g \geq T_{g\_rat}$, T_{g_ref} is controlled in constant T_{g_rat}. The region switches from Region 2 to Region 3.

(3) Region 3 to Region 2: β_{ref} = 0

Essentially, when the region switches from Region 2 to Region 3, the torque controller has reached the limit of its ability to keep the rotor speed at the rated value and the pitch controller then takes over. The transition from Region 3 to Region 2 is the opposite of this, i.e. the pitch controller is no longer required in order to keep the rotor speed at the rated value and the torque controller can take over. This can be summarized as switching from Region 3 to 2 when the pitch angle, β, equals zero. However, due to mechanical and electrical limitations the measured pitch angle may never reach absolute zero, therefore, it is better practice to switch regions when the pitch angle reference, β_{ref}, reaches zero.

(4) Region 2 to Region 1: $\omega_{r\_ref} < \omega_{r\_rat} - dead\_band$

A dead band must be considered for the switching from Region 2 to Region 1 in order to prevent rapid cycling between these two regions. Rapid changes in wind speed could cause the rotor speed reference rapidly go above and below the rated value, causing rapid cycling between the regions. Introducing a dead band to act as a buffer will decrease the switching frequency in this situation. The value of this dead band is a trade-off between switching frequency and power extraction.

The flowchart shown in Figure 2.7 illustrates the region switching logic, as described above. In this flowchart, R_{k-1} is the region in the last sample, R_k is the region in the current sample, β_{ref} is the pitch angle reference, ω_{r_opt} is the rotational speed required to achieve optimum tip speed ratio, ω_{r_ref} is the rotational speed reference.

2.3.2 Control algorithm

The control algorithm used in this chapter is PDF (Pseudo Derivative Feedback) control method. The PDF controller appears similar to that of PI (Proportional Integral) but a subtle change in the controller structure means that PDF performs in a manner more similar to PID (Proportional Integral Derivative). This is advantageous as improved damping and a smoother controller performance can be achieved without noisy derivation and only two parameters to tune. Although not as popular as PID, the PDF controller has been proposed and used in some applications and has demonstrated a good regulation performance. According to [78], the PDF controller

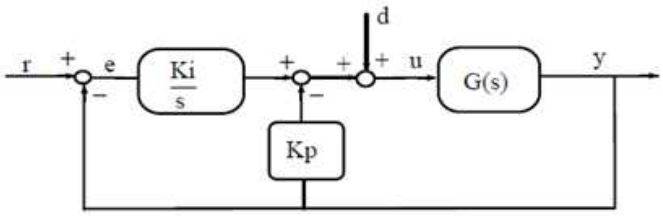

Figure 2.8: PDF controller configurations [78]

can be expressed in the time domain form as:

$$u(t) = z(t)K_i - K_p y(t) \tag{2.3.2}$$

$$\dot{z}(t) = r(t) - y(t) \tag{2.3.3}$$

Or alternatively in the Laplace domain as:

$$u(s) = \frac{K_i}{s}e(s) - K_p y(s) + d \tag{2.3.4}$$

$$e(s) = r(s) - y(s) \tag{2.3.5}$$

where u is the control signal (either the demanded torque or pitch angle), y is the feedback (rotor speed), e is the error, r is the set-point (rotor speed reference), d is the system disturbance (typically the wind), K_i and K_p are controller gains and $G(s)$ is the system to be controlled (in this case the wind turbine). Figure 2.8 shows the s-domain block diagram of the controller [78].

From the block diagram, the PI and PDF controller can be expressed in the form:

$$PI : u(s) = (\frac{K_i}{s})e(s) + K_p e(s) \tag{2.3.6}$$

$$PDF : u(s) = (\frac{K_i}{s})e(s) - K_p y(s) \tag{2.3.7}$$

Assume $G(s) = \frac{b}{(s+a)}$, thus the transfer functions of the PI and PDF controllers become:

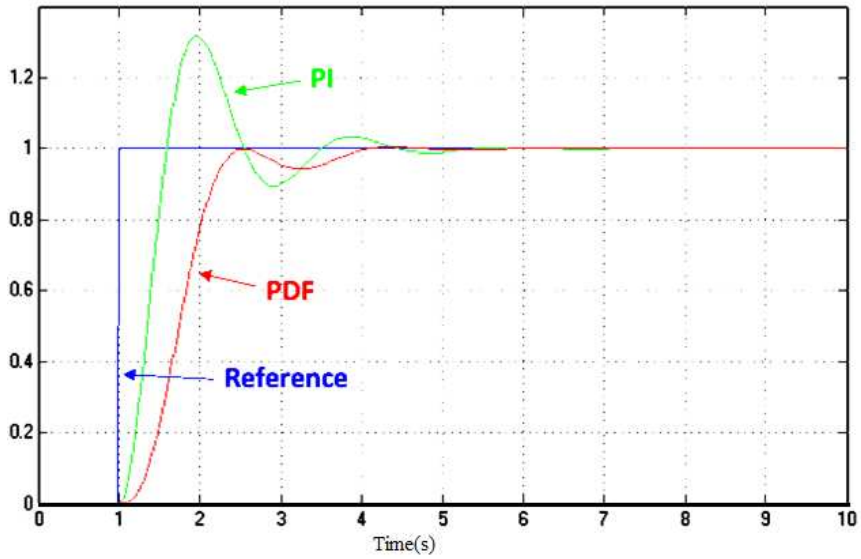

Figure 2.9: Step response comparison of PI and PDF

$$PI : TF = \frac{b(K_p s + K_i)}{s^2 + (a + bK_p)s + bK_i} \tag{2.3.8}$$

$$PDF : TF = \frac{bK_i}{s^2 + (a + bK_p)s + bK_i} \tag{2.3.9}$$

Following the block diagram set up the controllers in Simulink with a step source as input. The performance of PI and PDF step response is presented in Figure 2.9. It shows the PI controller has faster response but has higher overshoot while PDF avoids overshooting but slower dynamic response. For the purpose of the smooth switching between different operation regions with variation of wind speed, the PDF can be more qualified to this target.

2.4 Simulation Results

The described full wind speed range control system was simulated with a 5th-order nonlinear variable speed wind turbine model [79, 80] in Simulink. The parameters used in the model are taken from a Vestas v29 225 kW wind turbine. The rotor Radius R_b is 29 m; rated rotor speed ω_{r_rat} is 4.3 rad/s; rated generator torque

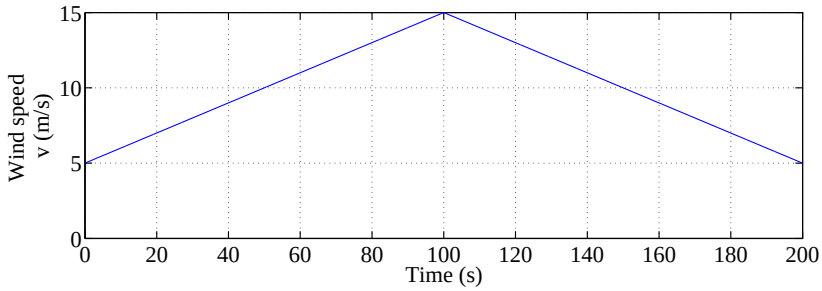

Figure 2.10: A slope changing wind speed between the cut-in and cut-out wind speed of the wind turbine.

T_{g_rat} is 2130 N·m; rated generator power P_{e_rat} is 225 kW (generator efficiency η was regard as 100% in the simulation).

The simulation test uses a slope changing wind speed between the cut-in and cut-out wind speed (Figure 2.10) as the input to the WPGS. The simulation results are shown in Figure 2.11 and 2.12. Figure 2.12(c) shows the Regions. At $t = 52$ s, it switches from Region 1 to Region 2. In Figure 2.11(a), it can be found that at this time rotational speed changes smoothly from increasing to a constant value which is the wind turbine's rated rotational speed. As the wind speed increasing, at $t = 58$ s, the region switches from Region 2 to Region 3. The generator torque shown in Figure 2.12(a) changes smoothly to a constant value. And the pitch angle $beta$ shown in Figure 2.11(b) starts increasing. After this switching, the generated power P_e shown in Figure 2.12(b) is controlled to at its rated value. After the wind speed decreases, at $t = 145$ s, region switches from Region 3 to Region 2; and at $t = 157$, region switches from 2 to 1. The progress reverses. From the generator torque results shown in Figure 2.12(a), it can be seen that there is no sudden change during every switching. This indicates the proposed method can smoothly switch the WPGS between different control objectives over a large wind speed range.

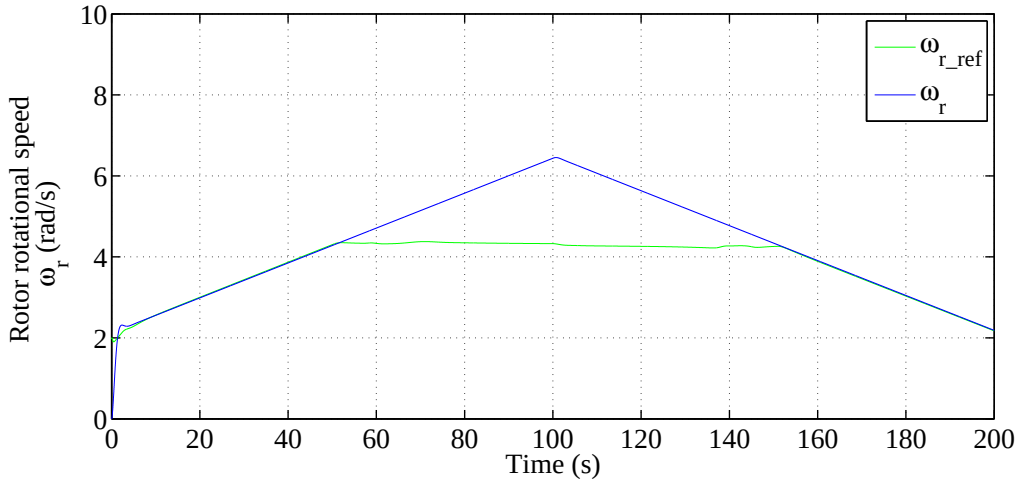

(a)

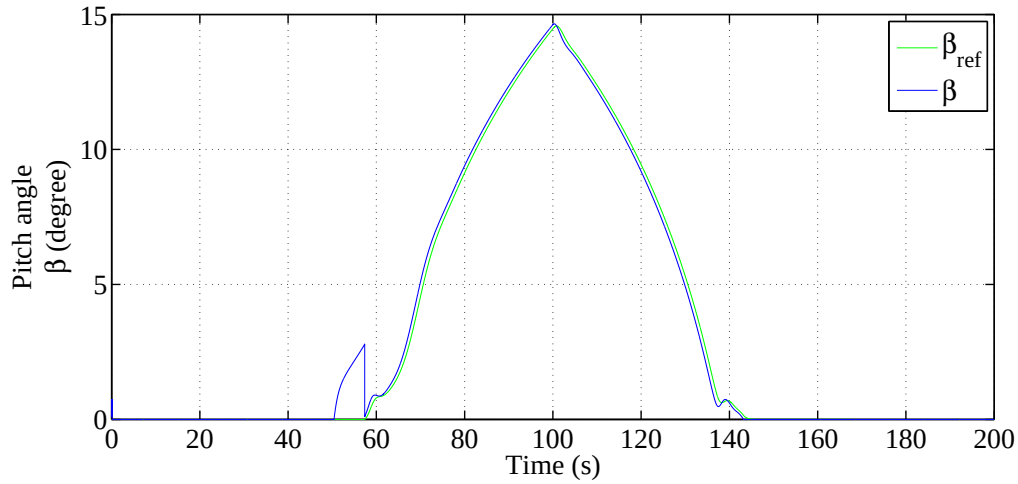

(b)

Figure 2.11: Wind speed, rotational speed and pitch angle in the simulation of the wind turbine switching in the whole operating wind speed range. (a) Rotor rotational speed and reference rotational speed.(b) Pitch angle and reference pitch angle.

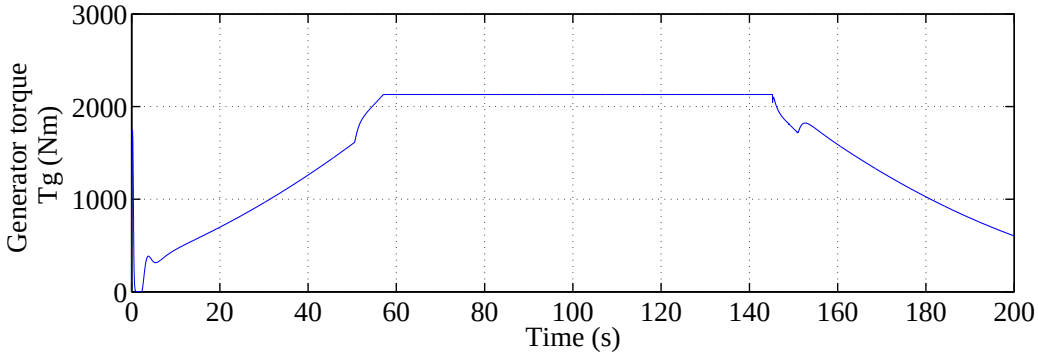

(a)

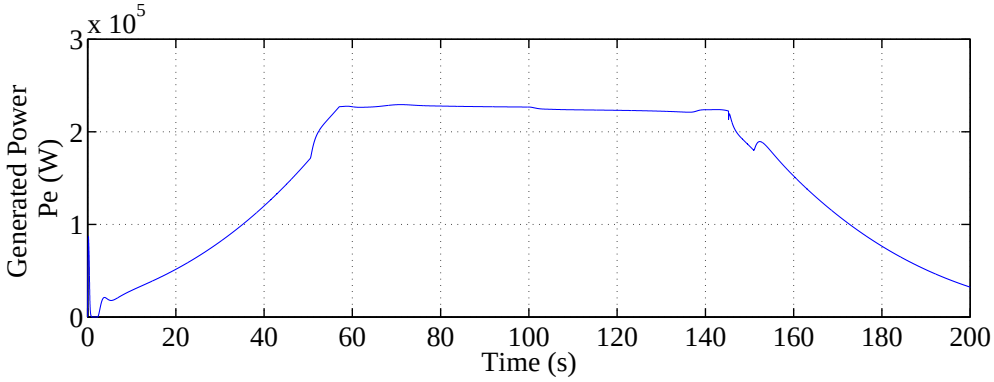

(b)

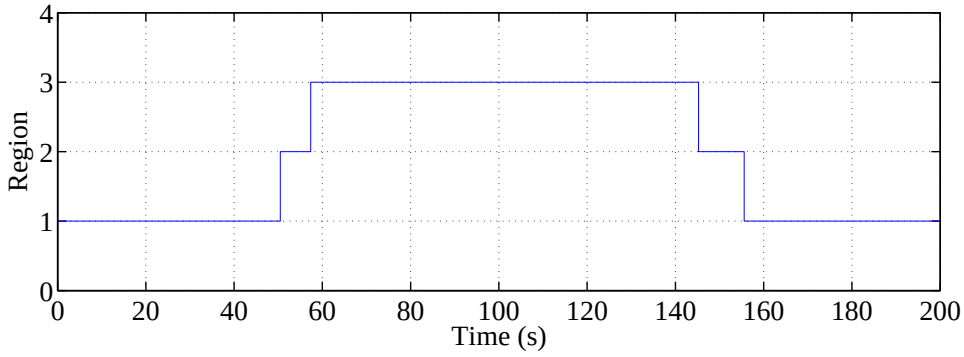

(c)

Figure 2.12: Generator torque, power and regions in the simulation of the wind turbine switching in the whole operating wind speed range. (a) Generator torque.(b) Generated power.(c) Region.

2.5 Hardware Implementation

2.5.1 Experiments with Speedflo

The wind turbine controllers with the designed region switching logic were coded onto an industrial controller named Speedflo. Speedflo is a multi-channel feedback controller product. It was used for high speed adjustment of a reactive gas during magnetron sputter processes. Its advanced digital control system automatically regulates gas flow to meet reactive sputtering requirements. Speedflo's advanced variable structure control algorithm offers significant performance improvements over conventional PID control techniques during magnetron sputter processes, both in terms of speed and robustness.

Speedflo has both hardware and software evolved based on demands of real processes and it comes with a range of current and voltage transducers, inputs and outputs, and communication options to meet the demands. Besides, simultaneous control of multiple inputs can be achieved with Speedflo. Further more, several sensor and monitoring options give a complete picture of the process when using Speedflo. These make Speedflo a robust and reliable controller and suitable for being developed into wind power generation system control [81].

2.5.2 Hardware-in-the-loop test results

Hardware-in-the-loop is carried out when the controller, intended for use in the real system, is implemented in hardware controller via microprocessor based system and interacts in real-time with other parts of WPGS in the simulation, replacing the controller simulation block in the original simulation. This is illustrated in Figure 2.13.

For this study the torque and pitch controllers, along with the region switching logic, were coded onto the Speedflo industrial controller. A dSPACE controller board was used to interface the Speedflo voltage inputs and outputs with Simulink wind turbine simulation. The simulation was then run in real time with an step of 0.001 seconds and a turbulent wind profile. The experimental setup is shown in

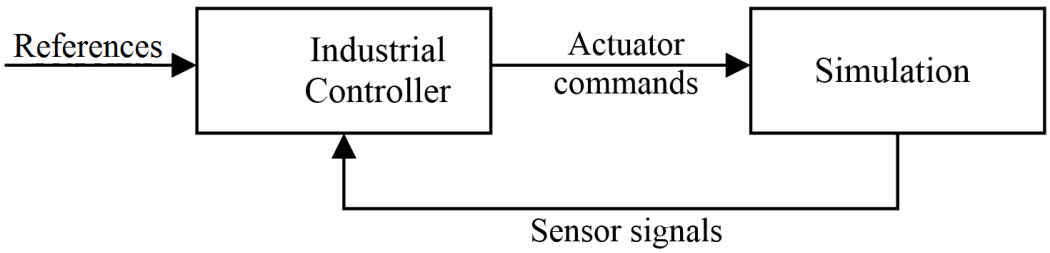

Figure 2.13: The schematic diagram of hardware-in-the-loop test

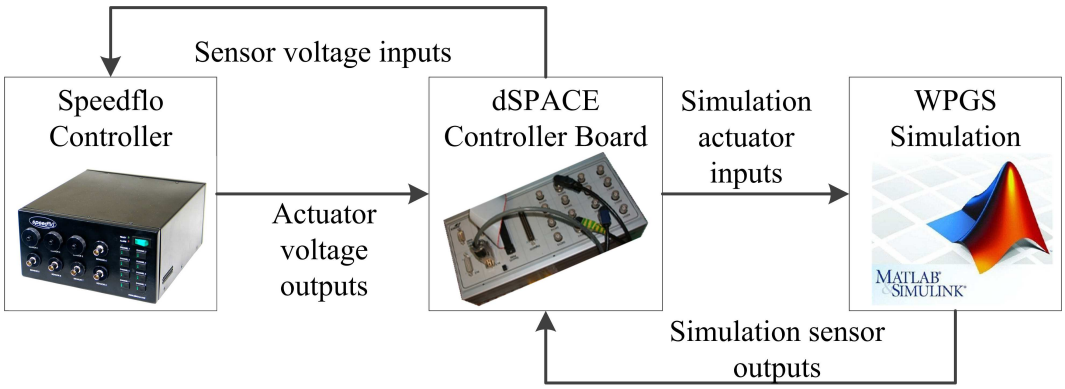

Figure 2.14: Experimental setup of hardware-in-the-loop test

Figure 2.14.

And the test results are shown in Figure 2.15. Figure 2.15(a) shows the wind speed profile which is generated using Turbsim [82].

As the wind speed changes, the rotor speed is shown on Figure 2.15(b) blue line. The initial rotor speed is 4 rad/s in this simulation. The green line in Figure 2.15(b) is the rotor speed reference which is calculated by the optimal tip speed ratio and wind speed. From the figure, the rotor speed ω_r is tracking ω_{r_ref} in Region 1 while tracking ω_{r_rat} in Region 2 and Region 3. Figure 2.15(c) is the pitch angle which is controlled only in Region3. As shown in Figure 2.15(d), for high wind speeds, the generator torque is set to be constant. The electrical power output is shown in Figure 2.15(e) and it roughly matches the rated power in Region 3. Figure 2.15(f) shows the Region.

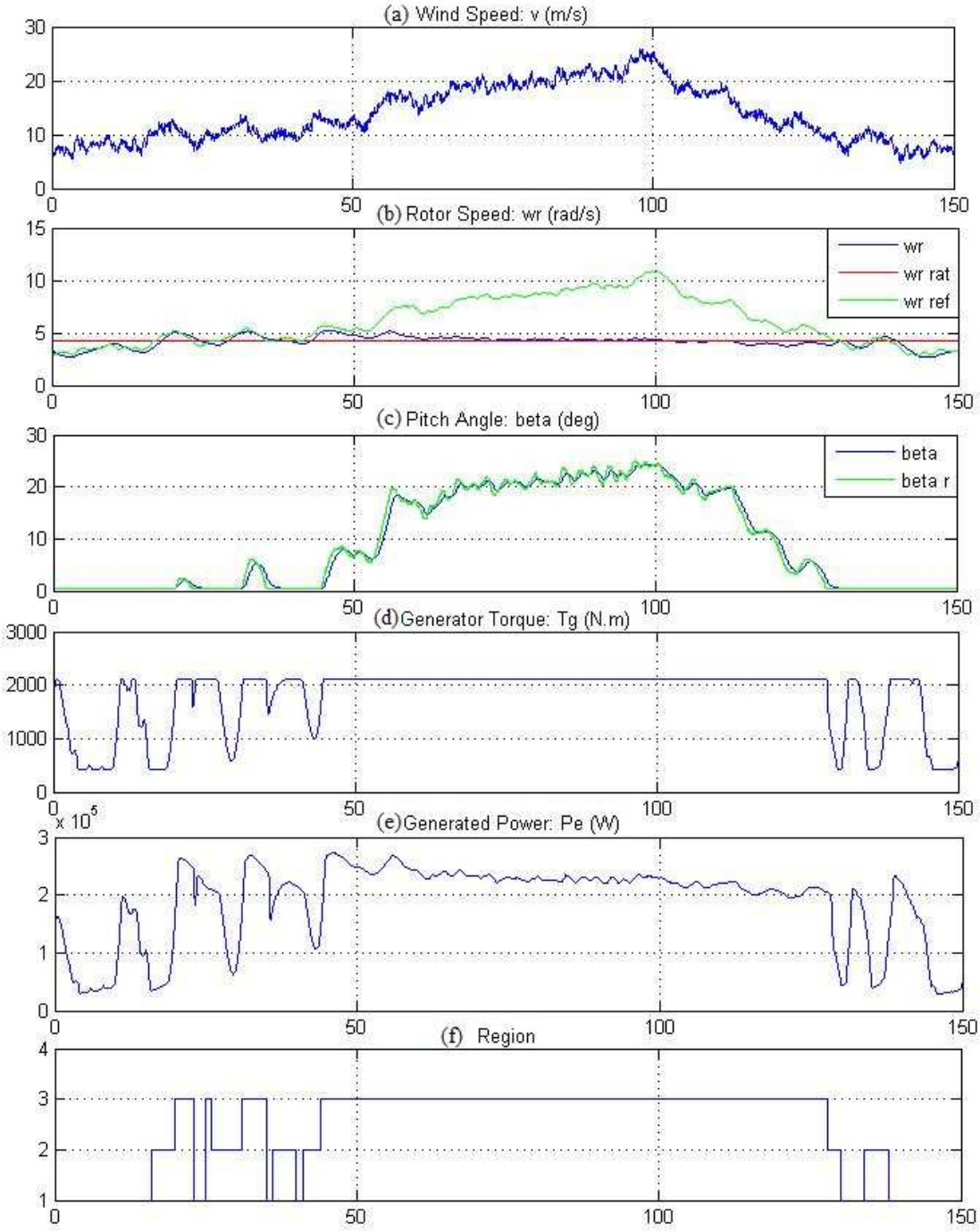

Figure 2.15: Hardware-in-the-loop test results of the wind turbine operating in turbulent wind peed between cut-in and cut-out wind speed of the wind turbine

As shown in Figure 2.15, the wind turbine controller operation is generally good over a large wind speed range. There are, however, some small overshoots in rotor speed. This is due to rapid changes in wind speed at the switching boundary, where because of the system inertia, the pitch controller cannot respond rapidly enough to keep the rotor speed at its rated value. Overall, the employed switching logic works to make smoothly transfer between different regions.

2.6 Conclusions

This chapter has presented a method for controlling a variable speed wind turbine over its complete operating wind speed regions. The control method attempts to minimize structure and mechanical loading whilst maximizing energy conversion from the wind. This involved designing a switching logic to enable smooth switching between different control objectives of torque controllers and pitch controllers. All these controllers used PDF control algorithm for smoothing performance and simplifying parameter tuning process. The simulation of a wind turbine with a hardware-in-the-loop industrial controller, that uses the presented switching logic, demonstrates good results; the switching is smooth between different control objectives over a large wind speed range.

Chapter 3

An Improved Hybrid Hill Climb Searching Algorithm for MPPT of Wind Power Generation Systems

Hill climb searching (HCS) or called perturbation and observation (P&O) control methods are beneficial for wind turbine maximum power point tracking as they do not require measurement of wind speed and in fact, it is difficult to measure wind speed in a real wind farm due to the fast changing and turbulent feature of the wind. In this chapter, an improved hybrid HCS algorithm is proposed based on the conventional HCS and power signal feedback (PSF) algorithm, with an additional algorithm to detect the wind speed variation. During the period that the wind speed is detected constant, the controller optimizes the parameter of the power curve. The proposed method is verified in simulation on a permanent magnet synchronous generator (PMSG) based wind turbine. Simulation results show that this algorithm has better performance in tracking the maximum power coefficient than the conventional algorithms, particularly during variable wind speeds. At the same wind speed, the proposed method can generate 4% more energy thatn the conventional HCS method.

3.1 Introduction

Maximum power point tracking (MPPT) control is designed for wind turbines operated below the rate rotor speed [83, 84]. In the review of MPPT algorithms, there are several methods in wind turbine generation systems, such as optimal torque control algorithm, perturbation and observation algorithm and power signal feedback algorithm.

The optimal torque control (OTC) has been found to be the most popular MPPT method for wind energy systems due to its simplicity [30]. According to [32], there is no difference between the power signal feedback (PSF) control and the OTC in terms of performance and the complexity of implementation. These two methods are both lookup table based. They require a cubic mapping function to provide reference signal for optimal turbine power (torque) at the operating generator speed and wind speed. Reference [85] gives a method to estimate the power characteristic with a Kalman-like estimator and the adjustment of the power curve polynomial with a Recursive Least-Square Algorithm. In reference [86], there is a method based on a dual Kalman filter to estimate wind turbine states and parameters. References [87] and [88] are about estimation of turbines power coefficient (C_p) curve.

In these methods, the perturbation and observation (P&O) method, or the so-called hill climb searching (HCS) method, is flexible and simple in implementation due to not requiring wind speed sensors and prior knowledge of the wind turbine's characteristics [30]. However, conventional HCS algorithms have problems with a speed vs. efficiency trade-off and wrong directionality under rapid wind change [41]. Being unable to sense wind speed, the HCS algorithm can be misleading as the sign at the next iteration might be dictated by the change in wind speed rather than the applied rotor speed perturbation. This wrong decision leads to the failure in keeping track of MPP and the HCS control moves downhill [32]. By combining HCS and PSF, performance can be improved and some of the obstacles found in the current methods can be overcome [30]. There are several researches on modified or hybrid HCS algorithm, such as references [32, 41], and [65].A method of combined the advantages of the PSF method and HCS method is proposed with optimal current given MPPT control in [89].According to [90], Hybrid HCS algorithm shows its

advantages in terms of efficiency and response speed.

This chapter presents a method to combine HCS and PSF methods and proposes a simple method to estimate the power curve parameter during the HCS progress. In this chapter, section 2 describes the wind turbine power capture system and the conventional HCS algorithm. Section 3 describes the methodology of the hybrid control method. Algorithms for judging the wind speed variation and optimizing the power curve parameter are presented. Results from simulations of the hybrid control algorithm with a wind turbine generation system model are given in section 4. Finally, this chapter concludes in Section 5.

3.2 Introduction of Conventional Hill-Climb-Search Algorithm

In a wind energy conversion system (WECS), MPPT optimizes the generator speed relative to the wind speed intercepted by the wind turbine such that the power output is maximized [32]. The wind turbine model is the same as Section 2.2. As shown in Figure 3.1, the power output for a certain wind speed is maximum at a certain value of generator speed. Combining Equation (2.2.2) and (1.1.4), the optimal power output of the generator can be given by

$$P_{opt} = \frac{1}{2}\rho A_r C_{p\_max}\left(\frac{R_b}{\lambda_{opt}}\right)^3 \omega^3 \tag{3.2.1}$$

$$P_{opt} = k_{opt}\omega^3 \tag{3.2.2}$$

where P_{opt} is the optimal power output of the generator; C_{p_max} is the power coefficient maximum value; λ_{opt} is the tip-speed ratio when power output is maximum; k_{opt} is a unique constant of one type of wind turbine which depends on the aerodynamics of the wind turbine.

A simple discrete time HCS control is to perturb the control variable (generator speed or control of duty cycle) and observe the results (power output) in terms of increase or decrease. If it results in a power increase, the same perturbation will

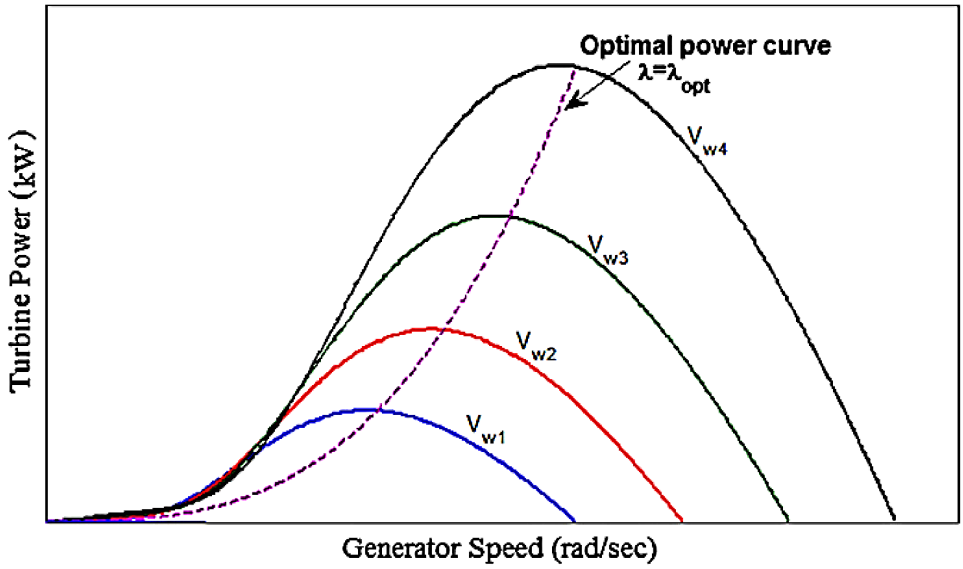

Figure 3.1: Characteristics of turbine power as a function of the rotor speed for a series of wind speeds

be applied for the next step. Otherwise the perturbation with a reversed sign will be applied to increase the power output. The perturbing control variable will be applied in the same direction until the output power is decreased. Principle of the HCS is shown in Figure 3.2.

HCS algorithms with fixed step-size exhibit a tracking speed versus control efficiency trade-off [41]. Variable step-size based HCS algorithms are designed to give a larger step-size when the operating point is far away from the MPP and will takes to a smaller step-size when it approaches very near the MPP. It can be achieved by setting the variable step-size proportional to the slope of the power-speed curve shown in Figure 3.2 as:

$$\Delta\omega_{(n+1)} = \beta\frac{\Delta P_{(n)}}{\Delta\omega_{(n)}} \tag{3.2.3}$$

where β is a positive coefficient in order to have appropriate step size and achieve steady tracking. Through Equation (3.2.3) it can be known the magnitude of $\Delta P/\Delta\omega$ is much large when the turbine is far from optimum point which means it could track the wind rapidly, and the value is near 0 when achieve steady state. Thus, the HCS

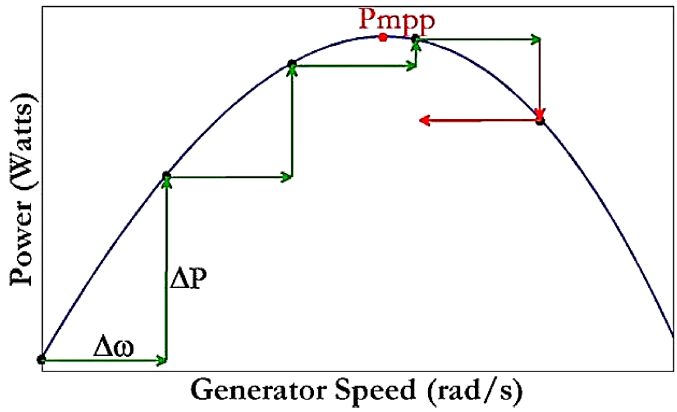

Figure 3.2: Principle of conventional HCS method

step size is variable and updated according to the operating point position. If the system is working on a certain point that is far from the peak, the step size should be increased to speed up the tracking process. Conversely, the action is reversed to decrease the step-size when the operating point nears the MPP. The coefficient β obtained by experiment can accelerates the speed to reach the maximum, and lowers the time needed for tracking. A large value of coefficient β can enlarge the step size. A small value of β will take less perturbation and not miss the MPP. An appropriate value of β can be obtained by experiment.

3.3 Proposed Hybrid Hill-Climb-Search

The conversional HCS only works well under a constant or slowly changing wind condition [41]. As it will lose the tractability of the MPP under a rapidly changing wind speed conditions as the $\frac{\Delta P}{\Delta \omega}$ used in Equation (3.2.3) will not give a correct measurement of the distance from the current point to the MPP. The proposed control method in this chapter is formulated by identifying conditions when the wind speed is rapidly changing. If it is detected the wind speed changing rapidly then the wind turbine will track its optimal power curve. When the wind is deemed constant, the control strategy changes to optimise the value of k_{opt}.

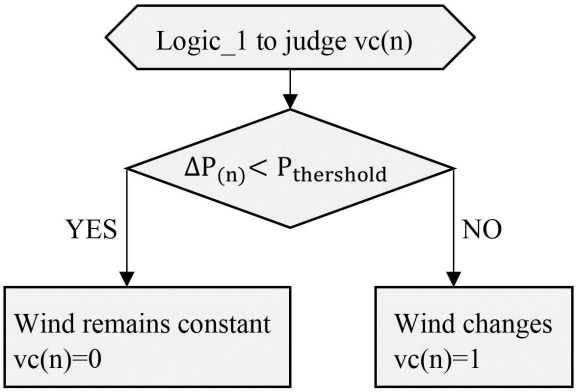

Figure 3.3: Logic flowchart of wind speed variation when the previous step is HCS method

3.3.1 Wind speed variation detection algorithm

This chapter proposes a new wind speed variation detection algorithm for the PSF method. For different operation modes, the wind speed variation is judged via different logic, Logic 0 for mode 0 and Logic 1 for mode 1, respectively. For Logic 1, at previous step, the optimal speed reference ω_{ref} is calculated based on PSF. If the incremental of power output in response to the perturbation in rotor speed is smaller than a predefined threshold $P_{threshold}$, then wind speed is not changed ($vc(n) = 0$), otherwise it is changed ($vc(n) = 1$). The flow chart Logic 1 is shown in in Figure 3.3.

If at the previous step, the optimal speed reference is obtained by the HCS , the way to judging wind speed variation is dependent on the relative distance between the operating point position at $(n-1)^{th}$ step and the peak. This logic is defined as Logic 0. Two regions are defined based on the relative distance, as shown in Figure 3.4.

Region ① is the region at the left side of curve k_1 and the right side of the curve k_2, in which the points are far away from the peak point. Within this region, if the wind speed does not change, wind turbine will operate at the same power-rotor speed curve and the value of $|\Delta P_{(n)}/\Delta\omega_{(n)}|$ will decrease. If this value increases, then there is a wind speed change. Region ② is the region between two curves k_1 and k_2, in which the operation point is close to the MPP. If wind remains constant,

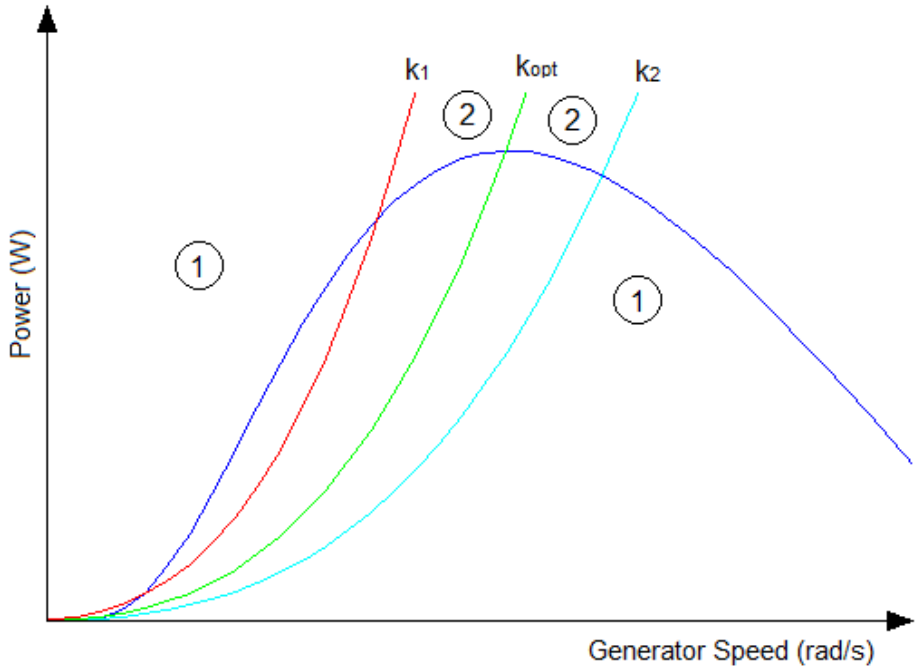

Figure 3.4: Division of the operation region

then the following-on operation point should be close to the MPP. The flow chart of Logic 1 is shown in Figure 3.5.

3.3.2 Hybrid hill-climb-search design

The proposed hybrid HCS control method is based on the detection of the wind speed variation. If wind speed is not changed, conventional variable step-size HCS method will be applied to obtain the reference speed at the next step to seek for the MPP. If wind speed has changed, the optimal rotor speed reference will be calculated from Equation (3.2.2) as:

$$\omega^* = \sqrt[3]{\frac{P_{(n)}}{k_{opt(n)}}} \tag{3.3.1}$$

where $k_{opt(n)}$ is the last step value. This method is a kind of power signal feedback control (PSF).

The flowchart of operation modes is shown in Figure 3.6. Two operation modes

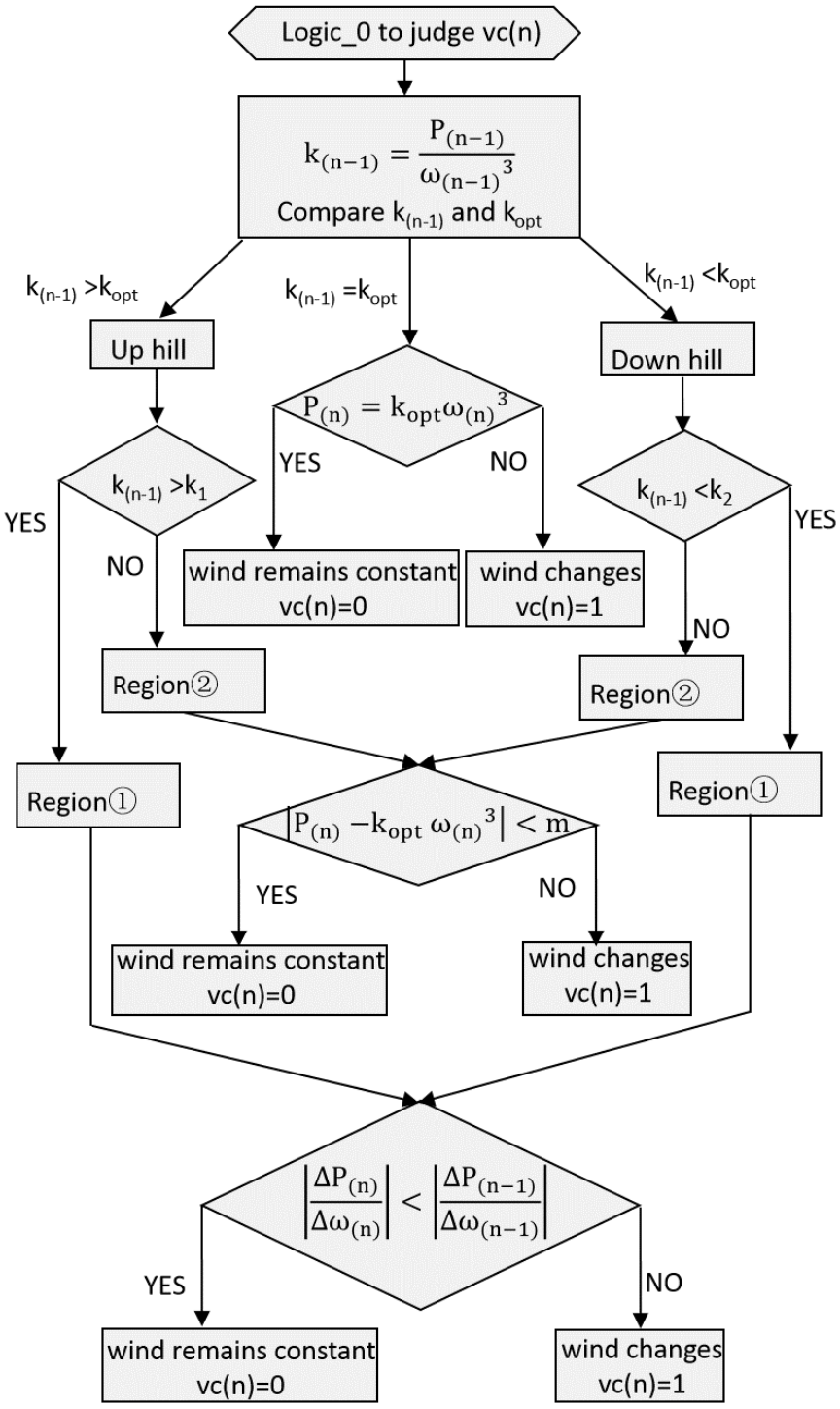

Figure 3.5: Logic flowchart of wind speed variation when the previous step is PSF method

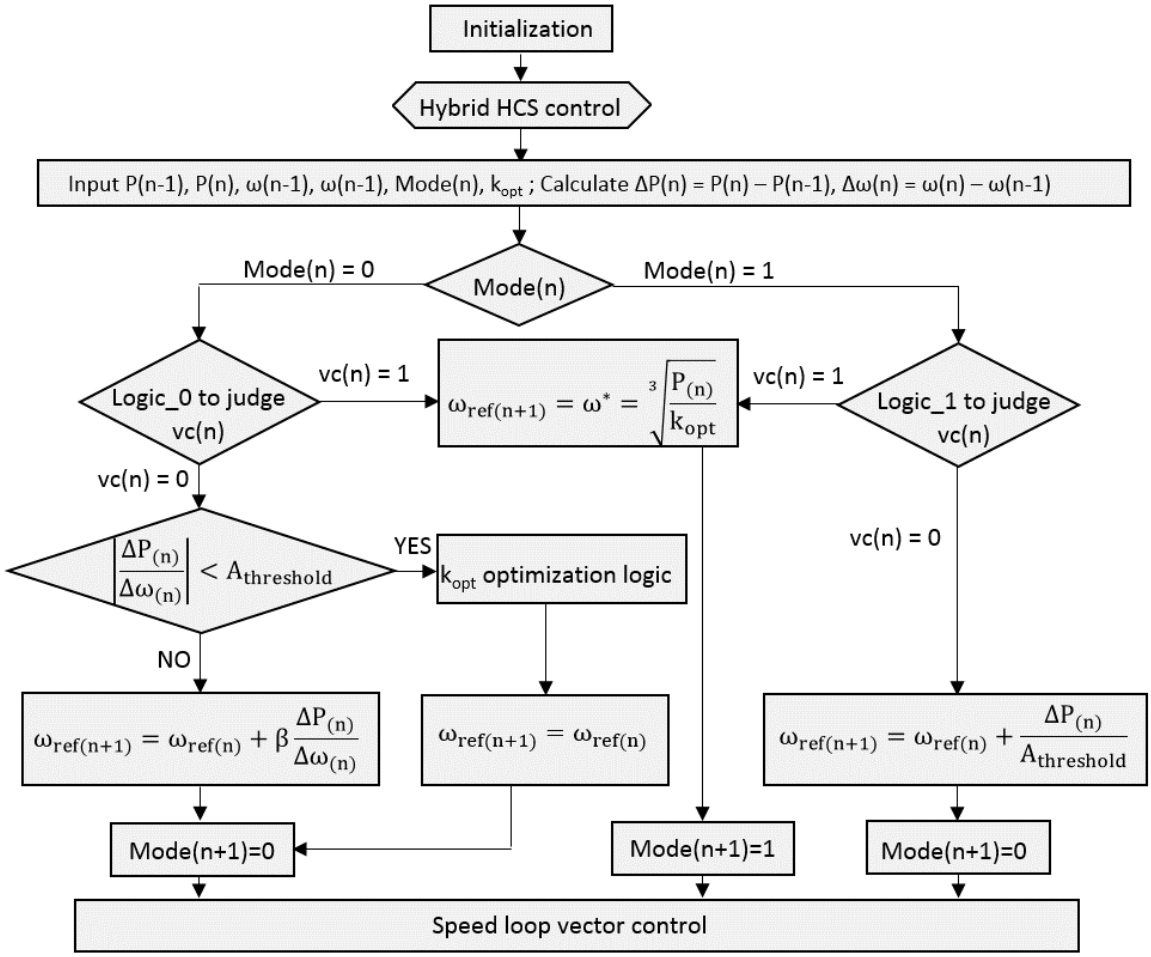

Figure 3.6: Logic flowchart of the proposed developed HCS method

are defined based on the previous step's method, $mode(n)$= 0 when the previous step uses HCS and $mode(n)$=1 when the previous uses the PSF. Two different speed variation logics are proposed for $mode$ 0 and $mode$ 1 and will be described in Section 3.2.

For $mode$ 0, when wind speed is detected as unchanged, i.e. $vc(n)$=0, the optimal speed reference value will be calculated based on HCS via Equation (3.2.3). If $\left|\Delta P_(n)/\Delta\omega_(n)\right| \leq A_{threshold}$, in which $A_{threshold}$ is a small slope threshold, the wind turbine reaches the MPP and the system has reached the optimal power point. Then the optimal rotation speed reference keeps unchanged and the rotor speed reaches its optimal value. Moreover, the maximum generator output power

obtained is used to calculate a real-time optimised $k_{opt(n)}$ which does not require the wind turbine characteristics and remove the impact of parameter uncertainties.

For $mode$ 0, when wind speed changes has been detected, i.e. $vc(n)$=1, the speed reference value is calculated by PSF via Equation (3.3.1) and the current optimised $k_{opt(n)}$. For $mode$ 1, if the wind speed is changed, i.e. $vc(n)$=1,the optimal speed reference is calculated as the same as $mode$ 0, based on the PSF. For $mode$ 1, when wind speed is judged as un-changed, i.e. $vc(n)$=0, the control method will switch back to HCS method. As the previous step the wind speed is changed, the wind turbine operates at a different power/generator speed curve for the new wind speed and has a different slope of the power/generator speed. Thus a relative bigger step size is calculated by using the threshold slope value

$$\Delta\omega_{ref(n+1)} = \frac{\Delta P_{(n)}}{A_{threshold}} \tag{3.3.2}$$

3.4 Simulation Results

The wind power generation system was simulated in MATLAB/Simulink. Figure 3.7 shows the advanced hybrid HCS control method under the step and slope change wind speed.

In reality, the changes in wind speed in a short time, can be regard as a step change or a slope change. Thus, in the HCS step period, the wind speed variation degree can be quantified as $\Delta V_w/\Delta t$ which is the variation gradient. To test the wind speed variation algorithm, wind speed changes in step and slope are used in the simulation test as shown in Figure 3.7(a).

In Figure 3.7(a), there is a step increase in wind speed at $t = 10$s and a step decrease in wind speed at $t = 20$s. Figure 3.7(c) shows the controller mode, which in 1 means the wind speed changed and PSF control is used and 2 means the wind speed is not changed and the HCS control is used. It can be seen that, when the wind speed suddenly increase or decrease, the proposed algorithm can successfully detect the changing in wind speed and give an appropriate rotational speed reference to the controller (Figure 3.7(b)).

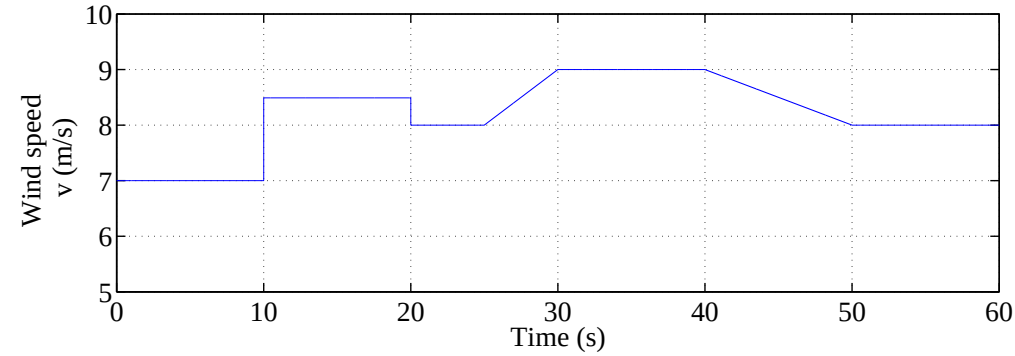

(a)

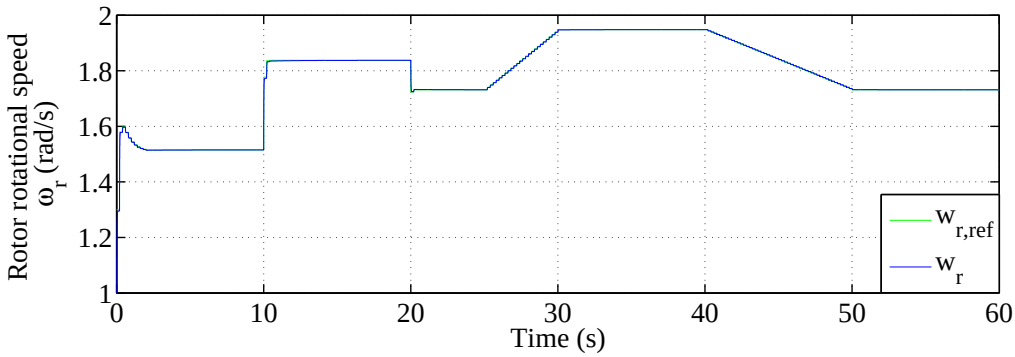

(b)

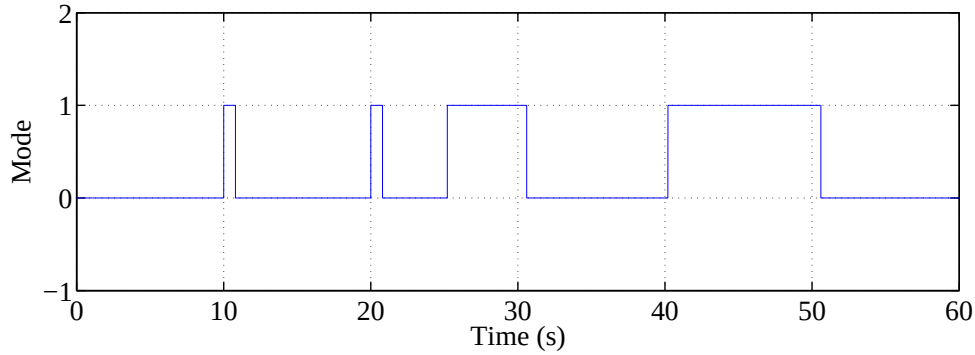

(c)

Figure 3.7: Wind speed, rotational speed and operation mode in the simulation of the proposed hybrid HCS control. (a) Wind speed. (b) Rotational speed controlled by the conventional HCS method. (c) Operation mode of the controller.

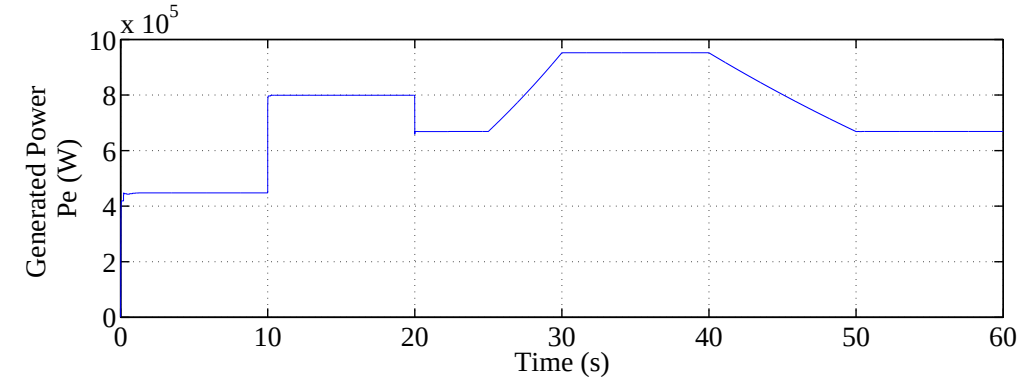

(a)

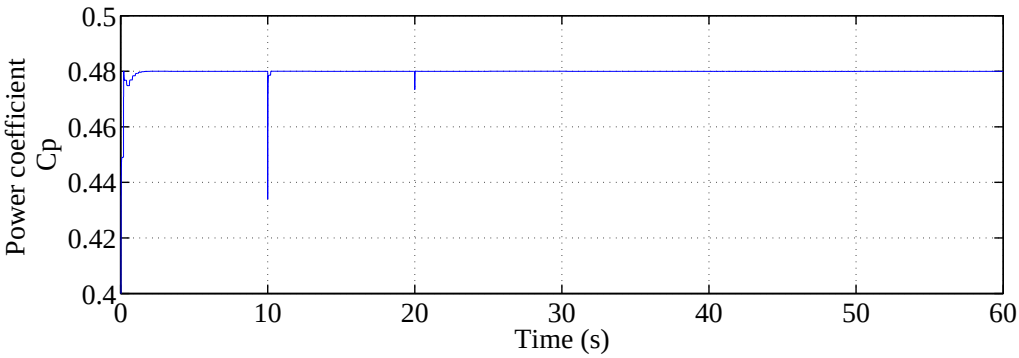

(b)

Figure 3.8: Generator power and power coefficient in the simulation of the proposed hybrid HCS control. (a) Generator power. (b) Power coefficient.

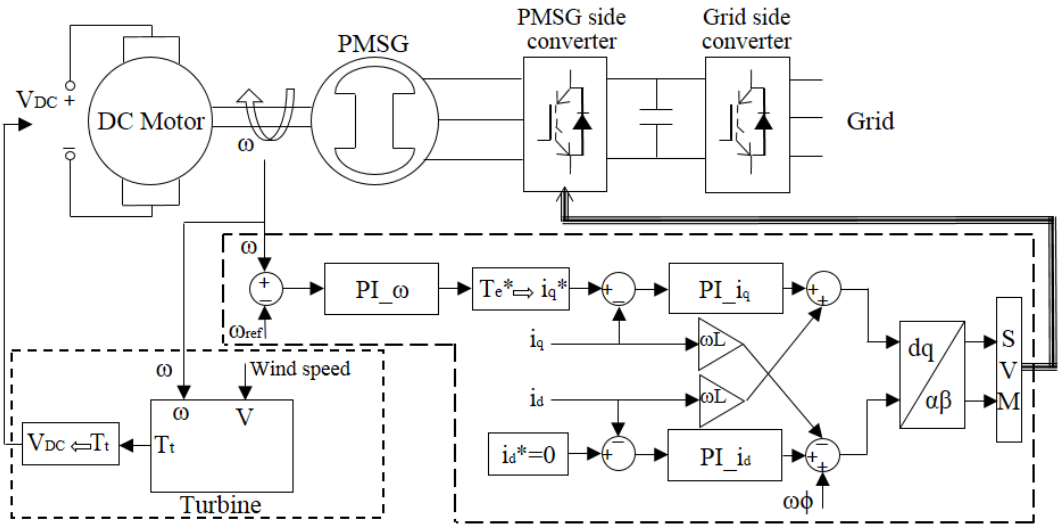

Figure 3.9: Schematic block diagram of the experimental setup and controller

From $t = 25$s to $t = 30$s and from $t = 40$s to $t = 50$s, the wind speed changes in a ramp as shown in Figure 3.7(a). In this situation, the judgement of the wind variation determined by the variation gradient and can be adjusted by changing the parameter m in Section 3.3. When it is judged the wind speed changed, then the controller will set to mode 1. Appropriate rotational speed reference will be given as shown in Figure 3.7(b). This makes the generator output maximum power (Figure 3.8(a)) and make the power coefficient C_p remains high (Figure 3.8(b)).

3.5 Hardware-In-The-Loop Test

The schematics of the WPGS controller and the experimental test rig is illustrated in Figure 3.9 and Figure 3.10 respectively. The experiment is implemented in the dSPACE 1104 environment. A DC motor is controlled as a wind turbine to produce a mechanical torque corresponding to the turbine model under variable wind conditions. A PMSG is driven by the DC motor to provide output electrical power. An IGBT based power electronics board is used as the PMSG side converter to control the WPGS with the PWM signals from the dSPACE control board.

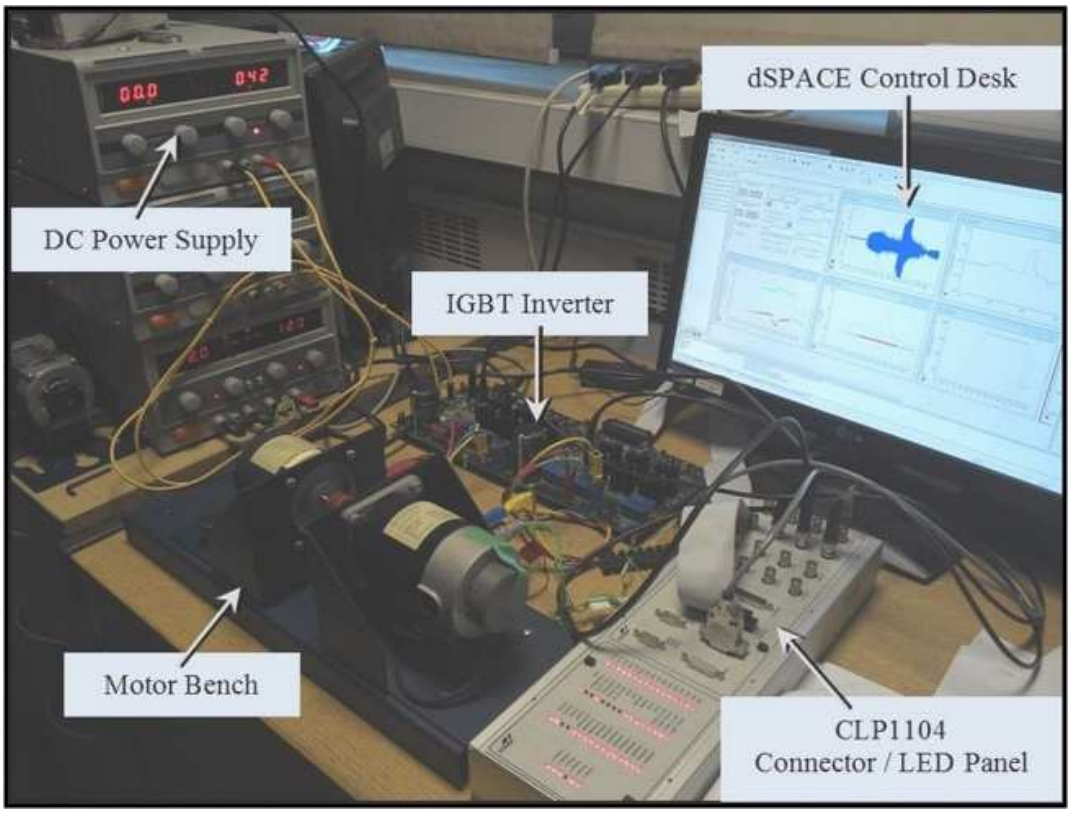

Figure 3.10: Experiment platform of the hard-ware-in-the-loop test

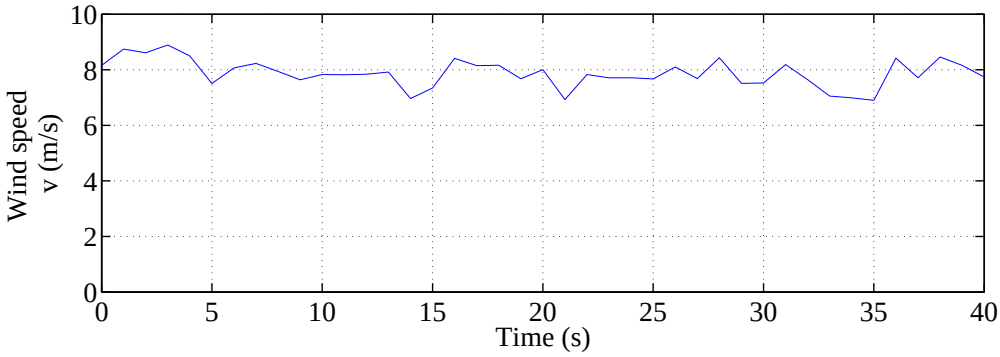

Figure 3.11: Variable wind speed used in hard-ware-in-the-loop test

3.5.1 Results and discussion

Under the variable wind speed as shown in Figure 3.11, the rotational speed controlled by the conventional HCS and the proposed advanced hybrid HCS are given in Figure 3.12(a) and 3.12(b). The two results are got with the same WPGS and in the same wind speed, only changed MPPT method. Comparing the two rotational speed results, it can be found that, the proposed HCS method can always tracking up the MPPs even during variable wind speed as it can detect the variation in wind speed. The rotor power curves of the wind turbine controlled by the two control methods are given in Figure 3.13(a). It can be concluded that the generated power by using the hybrid HCS can generate more power than the conventional HCS method. And by comparing the total energy captured from wind between using the two methods, it is found that the proposed method increase 4% generated energy than the conventional method. The power coefficient comparison in Figure 3.13(b) illustrates the better performance of the proposed method as well.

Therefore, these results confirm that the proposed method has better performance in tracking the maximum power coefficient as compared with the conventional HCS method.

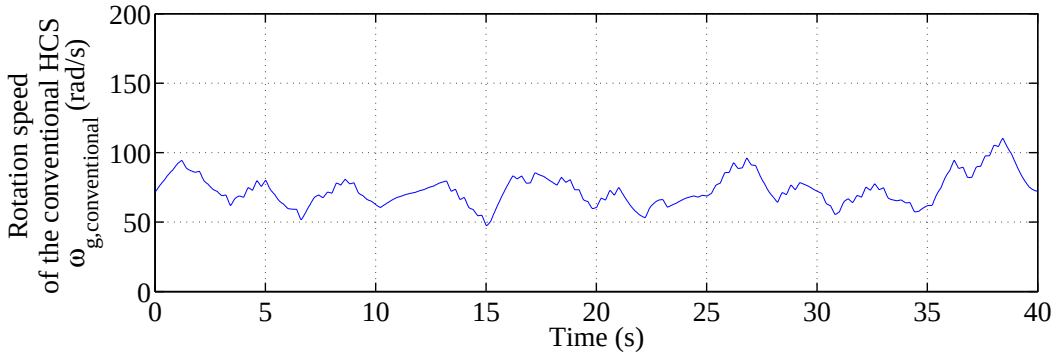

(a)

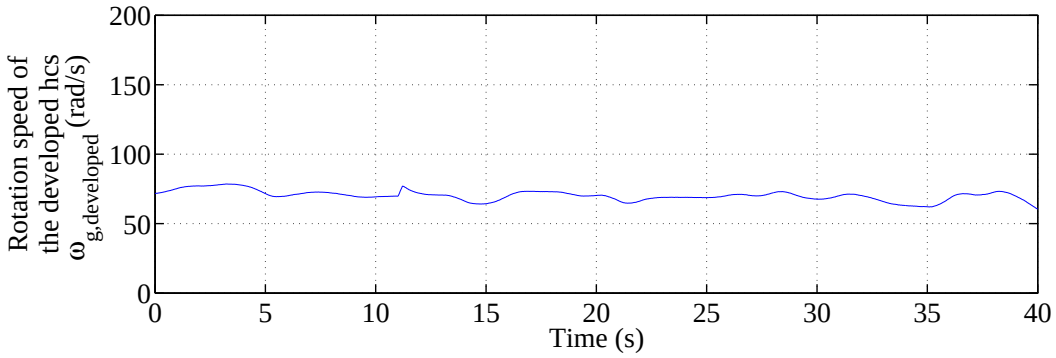

(b)

Figure 3.12: The comparison of wind turbine rotational speed controlled by the conventional HCS method and the developed HCS method in hardware-in-the-loop test. (a) Generator speed controlled by conventional HCS method. (b) Generator speed controlled by advanced HCS method.

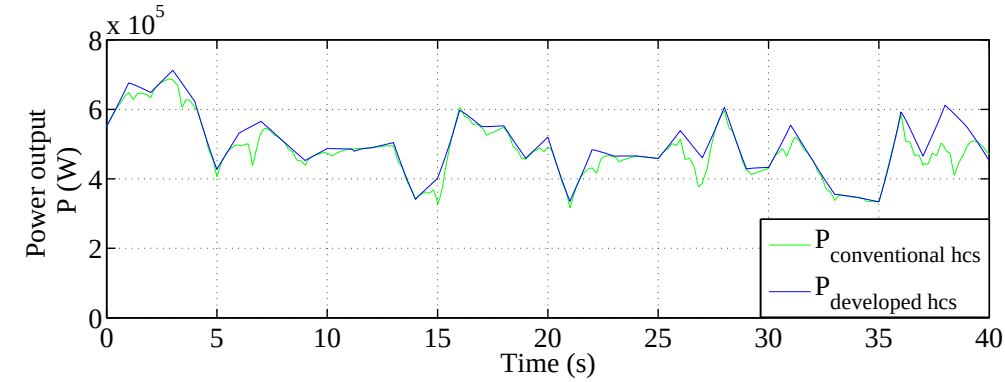

(a)

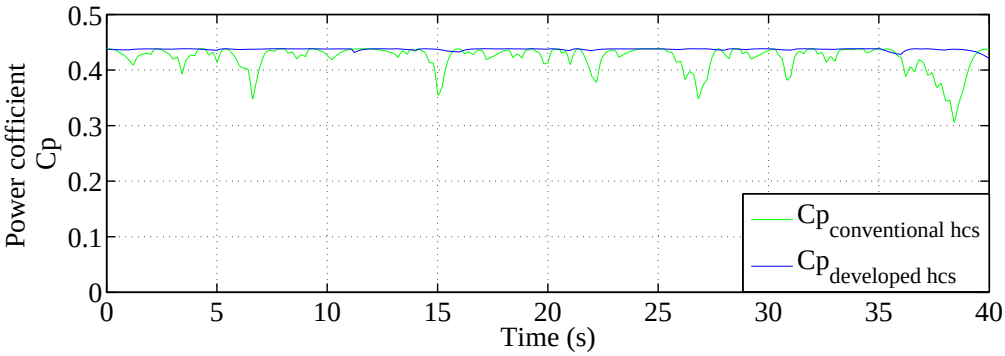

(b)

Figure 3.13: The comparison of output power and power coefficient in hard-ware-in-the-loop test. (a) Output power comparison between two control methods. (b) Power coefficient comparison.

3.6 Conclusion

This chapter proposed a new hybrid HCS algorithm for wind speed sensorless maximum power point tracking of wind turbine generation systems under varying wind speeds. The proposed algorithm introduces a new detection method of wind speed variation and combine it with the conventional HCS algorithm. It can obtain a real-time optimal power curve coefficient based on the optimal power under constant wind condition. The simulation compares the proposed hybrid HCS algorithm and the conventional HCS algorithm method on a PMSG based wind turbine. Under rapidly changing wind speeds, the proposed hybrid HCS algorithm performs much better in tracking the maximum power coefficient without the requirement of directly sensing wind speed and knowing wind turbine characteristics.

Chapter 4

Wind Turbine Optimal Power-Speed Curve Detection under Natural Variable Wind Speed

A new detection method is proposed to obtain the wind turbine's optimal power-speed curve under natural variable wind speed conditions and then used for maximum power point tracking (MPPT). The curve of power versus wind turbine rotational speed is detected, which is then used in the power signal feedback control of a wind power generation system. The proposed detection method does not require any previous knowledge of the wind turbine, and the curve detection process is undertaken in natural variable wind speed environment, without requiring additional wind turbine tests using wind tunnels. The proposed method is verified by MATLAB/Simulink simulations and experiment tests of a WPGS with a permanent magnet synchronous generator (PMSG) and a three-phase back-to-back converter.

4.1 Introduction

There has been an increasing number of wind turbine installations in recent years and currently wind power has become one of the main renewable power sources. By the end of 2015, the total wind power generation capacity installed worldwide has reached 435 GW. As the increase of the share of wind power generation, wind power generation systems (WPGSs) are desirable to operate with high efficiency [91]. For this purpose, in moderate wind speed region, a WPGS is normally controlled to achieve MPPT, which enables the WPGS to extract the maximum power from the wind source [30].

MPPT algorithms have been widely used in the control system of a WPGS. There are many different methods for WPGS to achieve MPPT [30, 39, 59, 92, 93]. Among these methods, the perturbation and observation (P&O) based strategy is one of the most popular strategies as it does not require known wind turbine characteristics and wind speed [30]. However, it has the drawback that it may fail to track the optimal power points, or even lose its trackability in variable wind speed environment. Besides P&O, the WECS can also be controlled by the power signal feedback (PSF) strategy to achieve MPPT [30, 39, 49]. The MPPT efficiency of PSF depends on the accuracy of the pre-obtained optimal power-speed curve [39]. However, different turbines' optimal power-speed curves are different. Even for the same wind turbine, the optimal power-speed curve may change during the change of the environment or the operation of wind turbine, because of the aging and structure deformation at their lifelong operation period and the external factors, such as dirt and ice on the turbine blades [39, 94]. Thus, the optimal power-speed curve should ideally be independent of local conditions of the installation site and adjusted during its lifetime to ensure the MPPT efficiency.

Several methods have been proposed for improving the accuracy of the optimal power-speed curve or the energy conversion coefficient C_p, such as wind tunnel test method [48, 95–98], P&O method [48, 49, 99] and artificial intelligence methods [59, 92, 93]. Although the wind tunnel test method can obtain accurate optimal power-speed curve [48, 95–98], it cannot take into account the aging of the structure and the external disturbances during the operation. P&O method can estimate the

optimal power-speed curve via continuously searching for the peak output power of a wind turbine without requiring any prior knowledge of the wind turbine's characteristics [48, 49, 99]. The P&O is suitable for small-scale WT as it may fail to reach the maximum power points under rapid wind variations, especially for medium and large inertia wind turbines. Small-scale wind turbines have less response time to react the perturbation in rotor speed than medium and large inertia wind turbines. Besides, the perturbation given by P&O methods may bring disturbances into the system. As the difficulties to obtain the optimal power-speed curve lie in the uncertainties of wind turbines' power coefficient C_p, the optimal power-speed curve can be estimated from the physical modeling of the wind turbine's C_p curve [100–102]. Artificial intelligence based methods, such as neural network, are proposed to estimate the optimal power-speed curve or power coefficient C_p curve, based on the learning of input/output measurements of the wind turbine [59, 92, 93]. Those methods mentioned above require either additional experimental tests or may interrupt the operation of the wind turbines.

A method which is capable of obtaining the optimal power-speed curve without aerodynamic tests and prior knowledge of the wind turbine is proposed in this chapter. This method can be applied in control of an universal wind turbine as it can be used with different types of wind turbine generators. A PMSG-based WPGS is discussed in this chapter as an example to test the proposed method. In the condition that the wind turbine's optimal power-speed curve is unknown or the given optimal power-speed curve is not accurate as the changing in environment, the proposed method can be applied on the wind turbines' controller to detect the on-site optimal power-speed curve and used to capture maximum power from the wind in MPPT.

The accurate optimal power-speed curve is obtained by operating the wind turbine at specified rotational speed and recording the wind turbine's output power under variable wind speed and recording. This procedure will repeat for different pre-set rotational speed to obtain the whole relationship of power and speed. The rotational speed, wind turbine power and wind speed are all measured and recorded. By analyzing all the recorded operating data, the optimal power-speed curve are obtained. Then the detected optimal power-speed curve can be used in the PSF control

of the wind turbine to achieve MPPT or calibrating inaccurate optimal power-speed curve in PSF control to improve MPPT performance. Simulation studies are carried out to verify the proposed method at first, followed by experimental tests based on a WPGS test rig consisting of a PMSG and a DC motor which is coupled with the PMSG to imitate the wind turbine profile.

In the sections that follow, the WPGS model and PMSG vector control are presented in Section 4.2. Then, Section 4.3 presents the proposed optimal power-speed curve detection method. The simulation studies are conducted in Section 4.4 to examine the proposed method in different cases. Experimental implementation to verify the proposed method is presented in Section 4.5. Finally, conclusions are given in Section 4.6.

4.2 PMSG Based WPGS

A WPGS consists of a wind turbine, a generator, a drive train, a generator side converter and a grid side converter [93, 103]. The generator side converter is used to control wind turbine's rotational speed in order to extend the active power or keep in the rated value. The grid side converter maintains a constant DC-link capacitor voltage and transfers active power [104]. In a WPGS, MPPT is achieved by controlling the generator side converter to adjust the wind turbine rotational speed corresponding to the wind speed so as to maximize the power captured from the wind [32].

The power-speed curves of a WPGS at different wind speed are in Figure 4.1. It shows that, for each wind speed, there is a specific point in the output power P versus rotational speed ω characteristic where the output power is maximized [29]. The MPPT control of the wind turbine results in a variable speed operation, such that maximum power is extracted continuously from the wind. Therefore, MPPT can be achieved by controlling the wind turbine to follow its optimal power-speed curve as shown in Figure 4.1 [38].

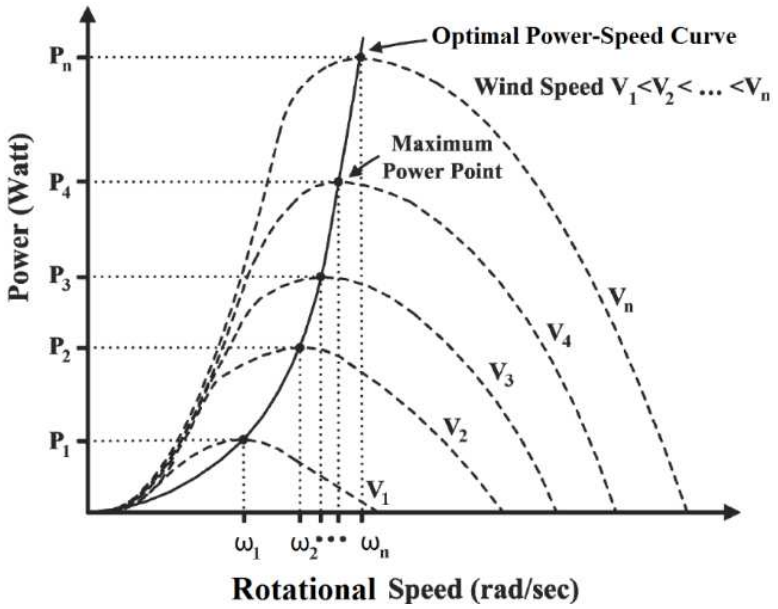

Figure 4.1: Power-speed curves of a WPGS

4.2.1 Permanent magnet synchronous generator model

The mathematical model of a PMSG can be described in d-q reference system as [103, 105]:

$$\frac{d}{dt}i_d = \frac{1}{L_d}v_d - \frac{R}{L_d}i_d + \frac{L_q}{L_d}p\omega_r i_q \tag{4.2.1}$$

$$\frac{d}{dt}i_q = \frac{1}{L_q}v_q - \frac{R}{L_q}i_q - \frac{L_q}{L_d}p\omega_r i_d - \frac{\psi_f p\omega_r}{L_q} \tag{4.2.2}$$

The electromagnetic torque equation is given by:

$$T_e = 1.5P[\psi_f i_q + (L_d - L_q)i_d i_q] \tag{4.2.3}$$

where L_q and L_d are q and d axis inductance, R is the resistance of the stator windings, v_q, v_d and i_q, i_d are the q and d axis voltages and currents, ω_r is the rotational speed of the rotor, and ψ_f is the magnitude flux of the permanent magnet. The electrical rotating speed of the generator ω_e is:

$$\omega_e = p\omega_r \tag{4.2.4}$$

where p is the number of pole pairs. The mechanical equation is given by:

$$\frac{d}{dt}\omega_r = \frac{1}{J}(T_e - B\omega_r - T_m) \tag{4.2.5}$$

$$\frac{d}{dt}\theta = \omega_r \tag{4.2.6}$$

where J is the combined inertia of rotor and load, B is the friction coefficient, θ is the rotor angular position, and T_m is the mechanical torque.

4.2.2 PMSG vector control

The generator side converter in a WPGS is used to regulate the output power of the generator. Vector control (VC) is normally used. As the generator is excited by permanent magnets, there is no exchange of reactive power between the generator and the machine side power converter [105]. The q-axis loop in vector control is used for wind turbine speed or torque control [106]. Considering the surface-mounted PMSG, the inductance of d and q axis are equal, that is, $L_d = L_q$, then it can be obtained [107]:

$$v_d = (k_{idP} + \frac{k_{idI}}{s})(i_d^* - i_d) - \omega_e L i_q \tag{4.2.7}$$

$$v_q = (k_{iqP} + \frac{k_{iqI}}{s})(i_q^* - i_q) - \omega_e L i_q + \omega_e \psi_f \tag{4.2.8}$$

where k_{idP} and k_{idI} are the parameters in PI controller for controlling i_d, k_{iqP} and k_{iqI} are the parameters in PI controller for controlling i_q. The current controllers PI_i_q and PI_i_d are used to regulate q-axis and d-axis stator current to follow the command, whereas a speed controller PI_ω is speed in order to follow the reference value ω_{ref} and produces corresponding q-axis current i_q^* [107]. The equation of the speed controller PI_ω can be summarized as:

$$i_q^* = (k_{\omega P} + \frac{k_{\omega I}}{s})(\omega - \omega_{ref}) \tag{4.2.9}$$

where $k_{\omega P}$ and $k_{\omega I}$ are the parameters in the PI controller for controlling rotational speed ω. Therefore, the WPGS is able to achieve MPPT through vector control with a provided rotational speed reference ω_{ref}. And the MPPT efficiency would be better if the ω_{ref} is according to a more accurate optimal power-speed curve.

4.3 Proposed Optimal Power-Speed Curve Detection Algorithm

The proposed method requires pre-set rotational speed reference. Assume the wind speed is variable, and the pre-set parameters value are appropriate for the wind turbine generation system. The optimal power-speed curve detection method can be obtained through the following five steps:

(i) Give the rotational speed reference ω_{ref} a specified constant value to control the wind turbine operating at a constant rotational speed.

(ii) Measure the wind speed and the output power. When the wind speed is at the pre-set values, record the operating data (wind speed, rotational speed and power).

(iii) When enough operating data is recorded for the current rotational speed reference, change to a new rotational speed reference value and repeat the first two steps.

(iv) When all the pre-set rotational speed reference values have been used and all the operating data has been recorded, stop recording the operating data. Compare the values of all recorded power under each wind speed and detect the maximum power points.

(v) Calculate the parameter k_{opt} in (iii) for each maximum power points. Obtain the mean value of all calculated k_{opt} as the overall optimal power-speed curve parameter. These five steps can be classified as two main operation processes: recording of operating data and detection of optimal power-speed curve and k_{opt}, which

will be described in details as follows.

4.3.1 Recording of operating data

Figure 4.2 shows the wind turbine power-speed curves under three different wind speed. ω_1^* is the rotational speed reference ω_{ref} at the beginning. By controlling the wind turbine's rotational speed, when the rotational speed ω is measured close to its reference value ω_{ref}, it will satisfy the Equation (4.3.1).

$$|\omega_{ref} - \omega| < \varepsilon_\omega \tag{4.3.1}$$

where ε_ω is a small constant to judge whether the rotational speed is controlled at the reference value. As shown in Figure 4.2, $P(1,1)$ is the measured power in the situation that the wind speed is v_1, and the rotational speed is ω_1. When wind speed changes from v_1 to v_2, $P(1,2)$ will be measured and recorded under the same rotational speed reference ω_1^*. Thus, there are n operating data recorded from $P(1,1)$ to $P(1,n)$ by varying wind speed between v_1 and v_n under the same rotational speed reference. Then the rotational speed reference changes from ω_1^* to ω_2^*, where $\omega_2^* = \omega_1^* + \Delta\omega$. $\Delta\omega$ is a constant step size between two reference rotational speeds. The operating data from $P(2,1)$ to $P(2,n)$ under ω_2^* will be recorded in the same way as in ω_1^*. By control the wind turbine rotational speed varying from ω_1^* to ω_m^*, there are $m \times n$ recorded operating points. Compare the recorded power value under each wind speed, the recorded maximum power points can be obtained, shown as red points in Figure 4.2.

Figure 4.3 shows the recording of operating data flowchart. Equation (4.3.2) is used to decide whether the operating data should be recorded.

$$|v - v_i| < \varepsilon_v \tag{4.3.2}$$

where ε_v is a constant to judge whether the wind speed is close to a pre-set value. Rotational speed changes from ω_1^* to ω_n^*. When all eligible operating points of the last rotational speed reference ω_n^* are recorded, the recording of operating data process ends. Then the controller will move on to the detection of the optimal power

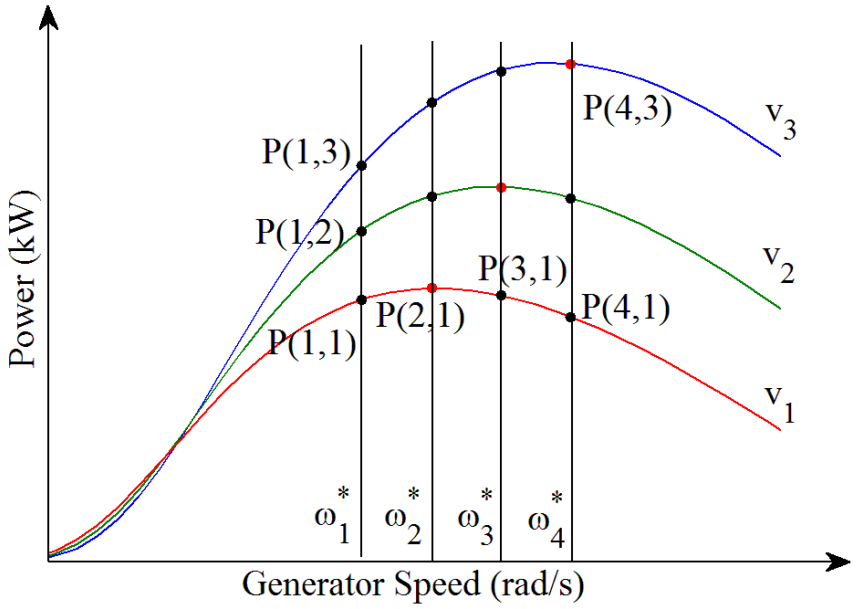

Figure 4.2: The recording of operating data on the power-speed curves of the WPGS

curve and k_{opt}. In the recording of operating data flowchart (Figure 4.3), there are two parts marked in blue and green. These two parts in the flowchart are negative power rejection and skipping unnecessary data.

Negative power rejection

The wind turbine rotational speed is controlled in specified constant values during the recording of operating data process. In the situation that wind speed decreases to a low value, it may make the WPGS have negative power in order to control the rotational speed to meet the specified constant reference. This can decrease the WPGS efficiency and should be avoided. A negative power rejection algorithm is proposed to avert the above situation. Decrease the rotational speed reference ω_{ref} to acclimate the decreasing in wind speed when the wind speed is not sufficiently high for the wind turbine to generate positive power at the pre-set rotational speed reference. Until the wind turbine increase to a value that the WPGS is able to generate positive power, the rotational speed reference ω_{ref} will switch back to the pre-set value and continue recording of the operating data. The blue area in Figure

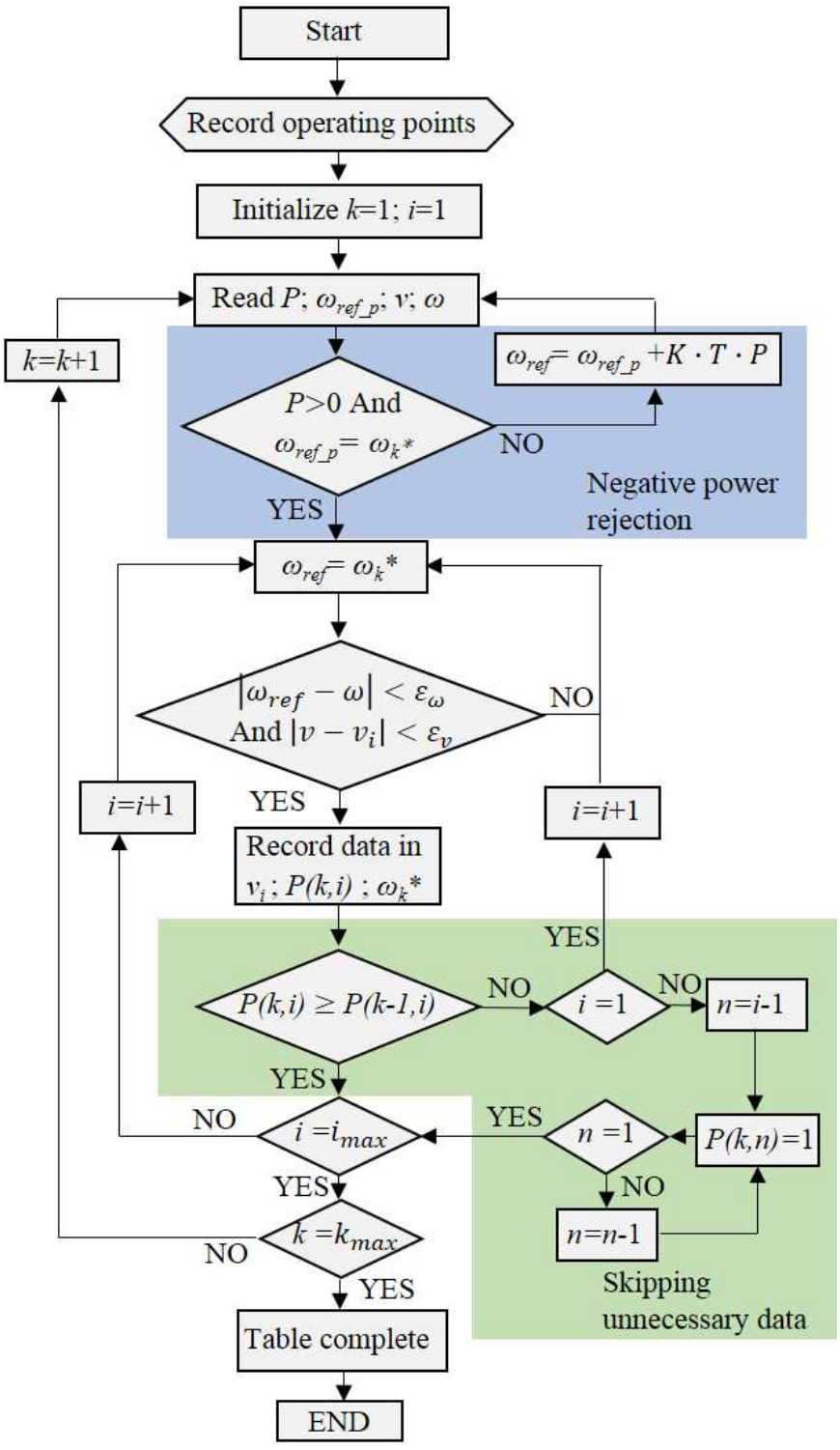

Figure 4.3: Flowchart of the recording of operating data

4.3 shows this algorithm in the method flowchart. When power is negative or the rotational speed reference of the previous step ω_{ref_p} is not the pre-set value ω_k^*, then the rotation speed reference is given by:

$$\omega_{ref} = \omega_{ref\_p} + K \cdot T \cdot P \tag{4.3.3}$$

where K is a parameter and T is the period of the control system. The aim is to control the rotational speed value in case power P is negative.

Skipping unnecessary data:

In the recording of operating data flowchart (Figure 4.3), there is a green area presenting the logic of skipping unnecessary data. During controlling the wind turbine rotational speed at specified constant values, if the measured power $P(k,i)$ is less than $P(k-1,i)$, then there is no need to record further operating data under wind speed v_i. For example, in Figure 4.2, when it is found that $P(3,1) < P(2,1)$, it signifies that it has passed the maximum power point under wind speed v_1. Then there is no need to record $P(4,1)$ and further data under wind speed v_1. Thus in Figure 4.3 green area, it recodes 1 to represent skipping these unnecessary data. This skipping unnecessary data process can reduce the time of recording of operating data.

4.3.2 Detection of optimal power-speed curve

Figure 4.4 shows the flowchart of the detection of optimal power-speed curve and k_{opt}. After the recording of operating data process, the maximum power points under each wind speed can be estimated. Then the optimal power-speed curve and k_{opt} for each wind speed can be calculated. For example, in wind speed v_i, the obtained maximum power point is P_{i_max}. When P_{i_max} is achieved, k_i is the calculated k_{opt} under wind speed v_i by equation:

$$k_i = \frac{P_{(k,i)}}{\omega_k^3} \tag{4.3.4}$$

where ω_k and $P_{(k,i)}$ represent the rotational speed and power of the MPP in wind speed v_i, respectively. After calculate k_i for each recorded wind speed, the optimal power-speed curve parameter k_{opt} can be estimated by calculating the average value of all obtained k_i. Then the wind turbine will operate PSF control with the detected optimal power-speed curve parameter k_{opt} to achieve MPPT.

Based on the pre-set values of wind speed v_i and reference rotational speed ω_i^*, it is probable that the maximum power points may not be detected directly. Thus, a remedy detection algorithm is designed to solve this problem. Implementation of this algorithm is shown in Figure 4.5. In Figure 4.5(a), the operating points are recorded at the rotational speed ω_k and ω_{k+1}. However, the actual MPP is between ω_k and ω_{k+1}, shown as the red point. Figure 4.5(b) shows the zoomed top part of the curve in Figure 4.5(a). Under wind speed v_i, the point A is the recorded MPP and point B and C are the two neighbouring recorded operating points. As point C is higher than B, then the real MPP must be between point A and C. The real MPP can be estimated if we assume the curve is symmetrical about the axis passed through the real MPP in a small region. Then the approximation MPP can be estimated as follows. Draw a line connecting point A and B. It will create an angle $\angle b$ with x-axis. Then Make a line pass through point C with angle $\angle c$ equal to $\angle b$. The extension of these two lines meet at point D. From geometric principle, point D would be very close to the central axis of this symmetric curve. As it was assumed the curve is symmetrical about the axis pass through the real MPP in a small region, point D will be recorded as the MPP under wind speed v_i instead of point A. Thus, the following formulas are deduced.

If the MPP is below the point A in Figure 4.5(b), it illustrated the MPP is between ω_{k-1} and ω_k. In this case, it can be regard as to reverse the Figure 4.5(b). The proposed method is still be able to detect the MPP. It can be summarized as:

If $P(k-1,i) > P(k+1,i)$, in Figure 4.5(b) it means the MPP is between the point A and B. Then the MPP would be calculated by:

$$\begin{cases} \omega_{i\_opt} = \frac{1}{2}\Big[\omega_k + \omega_{k-1} + \frac{P_{(k,i)}-P_{(k-1,i)}}{P_{(k,i)}-P_{(k+1,i)}}(\omega_{k+1} - \omega_k)\Big] \\ P_{i\_max} = P_{(k,i)} + \frac{P_{(k,i)}-P_{(k+1,i)}}{\omega_k-\omega_{k+1}}(\omega_{i\_opt} - \omega_k) \end{cases} \tag{4.3.5}$$

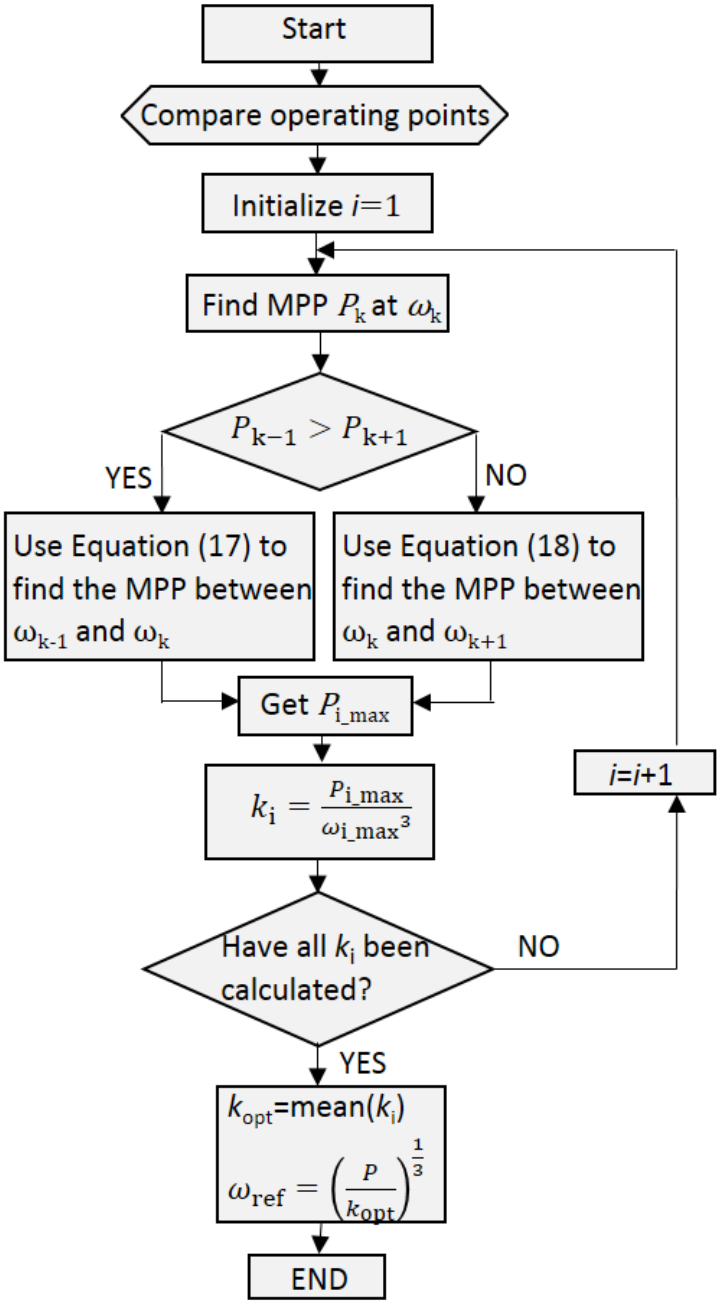

Figure 4.4: Flowchart of the detection of optimal power-speed curve and k_{opt}

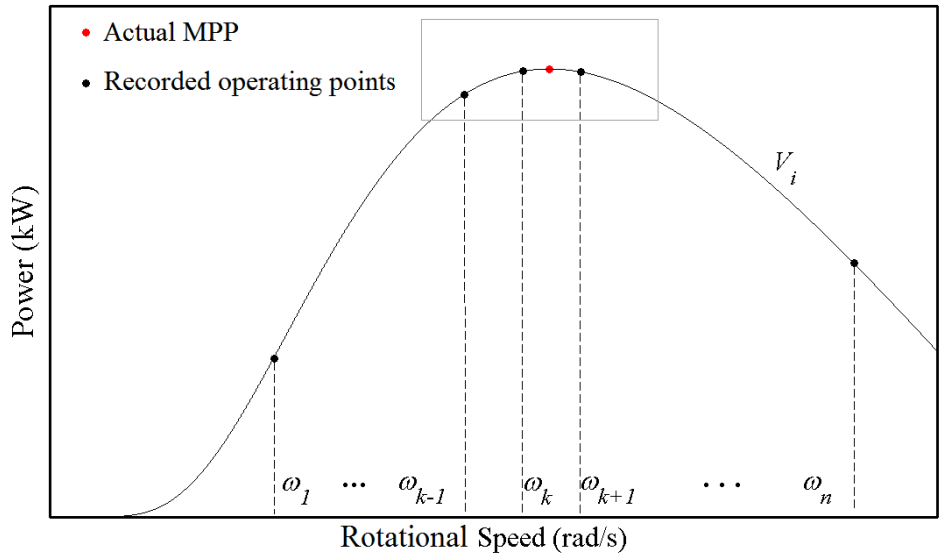

(a)

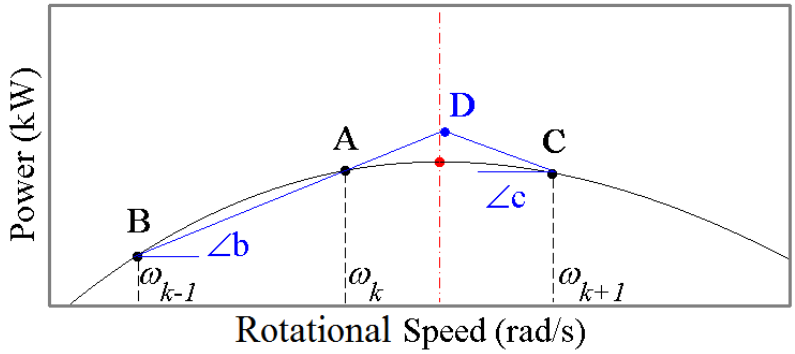

(b)

Figure 4.5: Remedy algorithm to estimate the MPP when the recorded operating points are not the MPP. (a) The overall recorded operating points in a particular wind speed. (b) Remedy algorithm illustrated on the zoomed top part of the curve.

If $P(k-1,i) < P(k+1,i)$, in Figure 4.5(b) it means the MPP is between the point A and C. Then the MPP would be calculated by:

$$\begin{cases} \omega_{i\_opt} = \frac{1}{2}\Big[\omega_k + \omega_{k+1} + \frac{P_{(k,i)}-P_{(k+1,i)}}{P_{(k,i)}-P_{(k-1,i)}}(\omega_k - \omega_{k-1})\Big] \\ P_{i\_max} = P_{(k,i)} + \frac{P_{(k,i)}-P_{(k-1,i)}}{\omega_k-\omega_{k-1}}(\omega_{i\_opt} - \omega_k) \end{cases} \tag{4.3.6}$$

Algorithm (4.3.5) and (4.3.6) can obtain a more accurate MPP when the recorded operation points are not locate accurately on the real MPP , and thus theoretically, there is no restrictions to pre-set the operation points if small enough step sizes are used. Equation (4.3.4) becomes:

$$k_i = \frac{P_{i,max}}{\omega_{i,opt}^3} \tag{4.3.7}$$

And the following PSF control will be based on the rotational speed reference ω_{ref} calculated by Equation (4.3.8) to achieve MPPT.

$$\omega_{ref} = \Big(\frac{P_e}{k_{opt}}\Big)^{\frac{1}{3}} \tag{4.3.8}$$

where

$$k_{opt} = \frac{1}{n}\sum_{i=1}^{n} k_i \tag{4.3.9}$$

4.4 Simulation Test

To verify the proposed detection method, a WPGS including PMSG and wind turbine is simulated in MATLAB/SIMULINK. The WPGS parameters are given in Table 4.1. Two simulation cases are carried out. Case 1 detects the optimal power-speed curve without any preliminary information of the optimal power-speed curve and operates the WT in MPPT mode. Case 2 is calibration the optimal power-speed curve and MPPT control of wind turbine based on an inaccurate optimal power-speed curve. In the simulation studies, the value of the wind turbine power coefficient C_p are given (Figure 4.7(b), Figure 4.9(b) and Figure 4.10) to verify the accuracy of the detected optimal power-speed curve.

Case 1: Detection of unknown optimal power-speed curve

Items	Specification
Blade radius R_b	35 m
Equivalent inertia J_r	3×10^6 kg $\cdot$ m^2
Rated power	1.5 MW
Rated wind speed	12 m/s
PMSG stator resistance R	0.19 Ω
PMSG stator inductance L_d, L_q	0.0005 H
Pole pairs p	5
PMSG field flux	0.0127 Wb

Table 4.1: Wind turbine and PMSG parameters in simulation and experiment

The simulation test detects the optimal power-speed curve at the beginning (from 0 s to 85 s) and then uses the detected optimal power-speed curve to control the turbine in MPPT mode (after 85 s). The simulation results of wind speed v, generator rotational speed ω_g, rotor power P_r, and the power coefficient of wind turbine C_p are given in Figure 4.6 and 4.7. The wind speed, shown in Figure 4.6(a), is generated by TurbSim [82], with an average speed of 8 m/s. Figure 4.6(b) shows that the rotational speed of the wind turbine is controlled in specified constant reference as mentioned in Section 4.3. Speed control the WT is achieved by vector control with PI loop. At time t = 30 s and 60 s in Figure 4.6 and 4.7, wind speed decreases and causes power drop, the rotation speed is controlled to decrease to keep positive output power, which demonstrates the effectiveness of the negative power rejection function mentioned in Section 4.3.1.

At t = 85 s in Figure 4.6, sufficient number of operating points are obtained to calculate k_{opt}. The calculated k_{opt} value is 1.702105 which is very close to the accurate k_{opt} value 1.729105 (with 2% estimation error). After the k_{opt} is detected, the WT is operated in MPPT mode. Figure 4.7(b) shows that after t = 85 s, the power coefficient C_p of the wind turbine can achieve its maximum value, which shows that the wind turbine is tracking accurate maximum power points.

Case 2: Calibration of inaccurate optimal power-speed curve

Figure 4.8 and 4.9 shows the simulation results that the proposed scheme is used

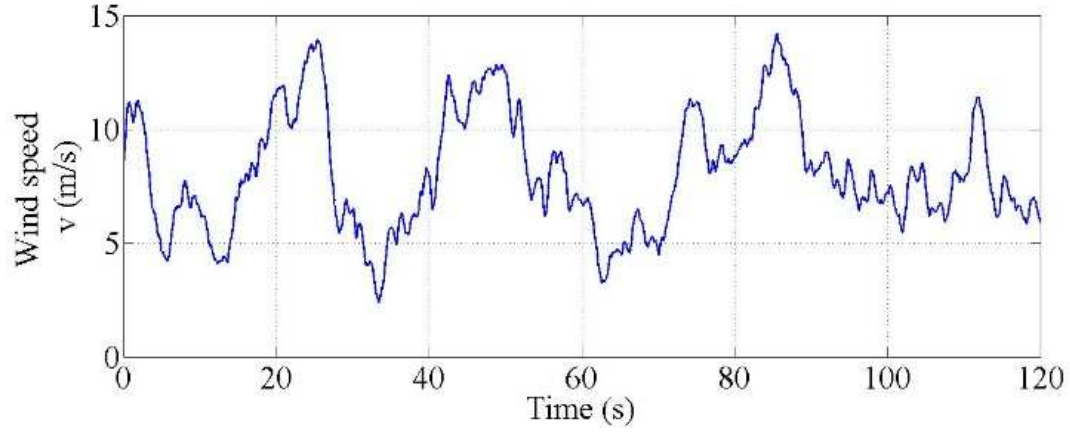

(a)

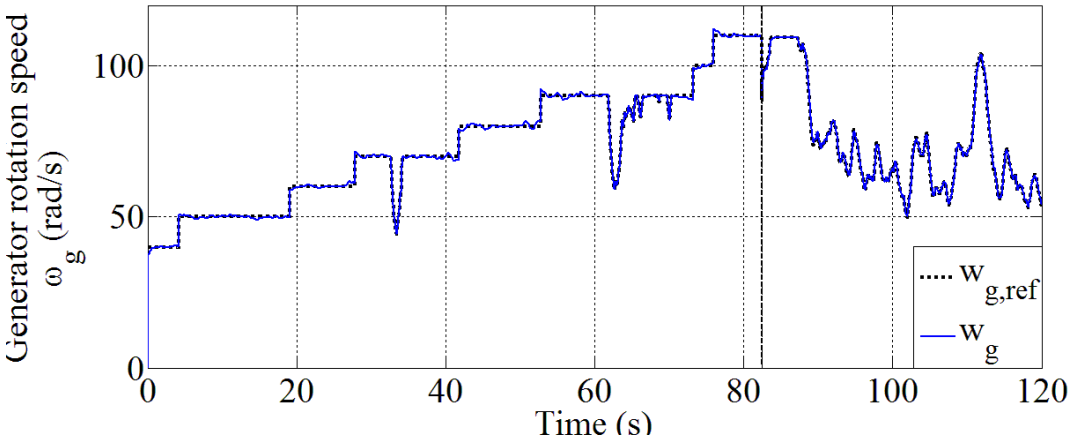

(b)

Figure 4.6: Wind speed and wind turbine rotational speed in the simulation of initialisation process. (a) Wind speed. (b) Generator rotational speed and reference rotational speed.

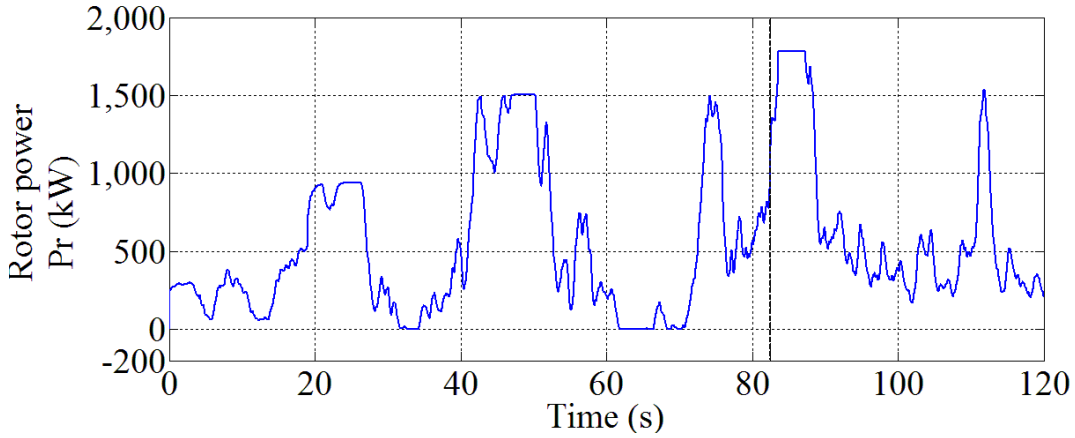

(a)

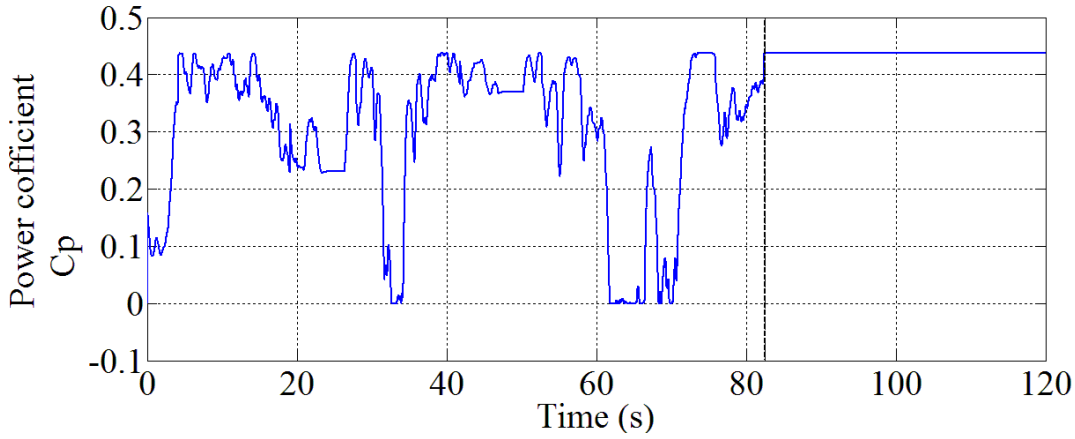

(b)

Figure 4.7: Wind turbine rotor power and power coefficient results in the simulation of initialisation process. (a) Wind turbine rotor power. (b) Wind turbine power coefficient.

Error in the optimal power-speed curve	Generation energy loss
10% Error	0.28%
20% Error	1.10%
30% Error	2.70%
40% Error	5.24%

Table 4.2: MPPT energy generation comparison

to calibrate an inaccurate optimal power-speed curve. Changes of environmental parameters, such as the air density, and other external factors such as dirt and ice augmented on the turbine blades, generally happening during the daily operation of the WT, will change the WT optimal power-speed curve. To simulate this kind of inaccuracy, the turbine is controlled with k_{opt} in 20% error in the first 30 s, as shown in Figure 4.8 and 4.9. The calibration process takes 112 s and ends at 152 s. Subsequently, the system is controlled in the MPPT mode with the calibrated k_{opt} value.

Figure 4.10 compares the power coefficient before and after the calibration process, which shows that before calibration there is a gap between the power coefficient and its maximum value. After the calibration process, shown in Figure 4.10(b), C_p can almost track its maximum value.

To illustrate the effect of the optimal power-speed curve error generated in energy generation, more simulation studies were done and the results are given in Table 4.2. The results show that 10% error of k_{opt} will cause 0.28% loss of generation energy. When the error increases, the loss will increase as well. When k_{opt} has a 40% error, the generation energy will lose 5.24%.

4.5 Experiment Results

The hardware-in-the-loop experiment platform is the same as in Chapter 3. The schematics of the controller and the experimental test rig is illustrated in Figure 3.9 and Figure 3.10.The experiment is implemented in the dSPACE 1104 environment. A DC motor is controlled as a wind turbine to produce a mechanical torque corre-

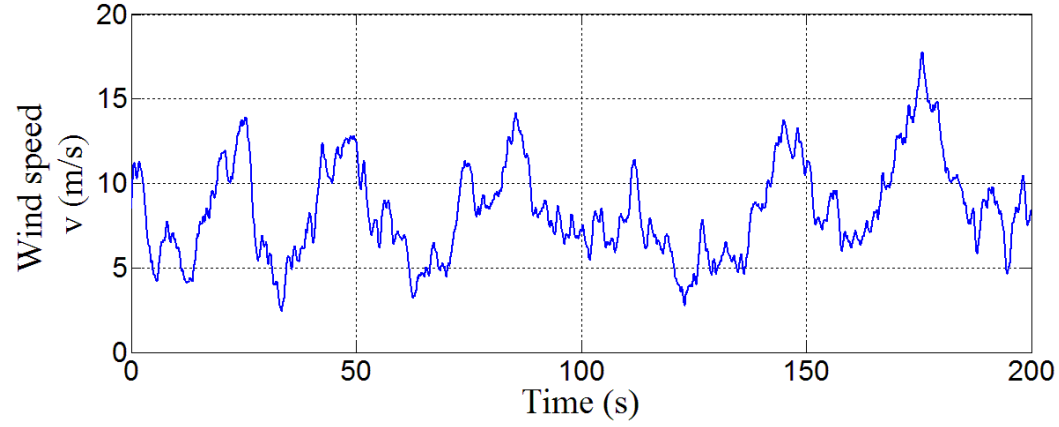

(a)

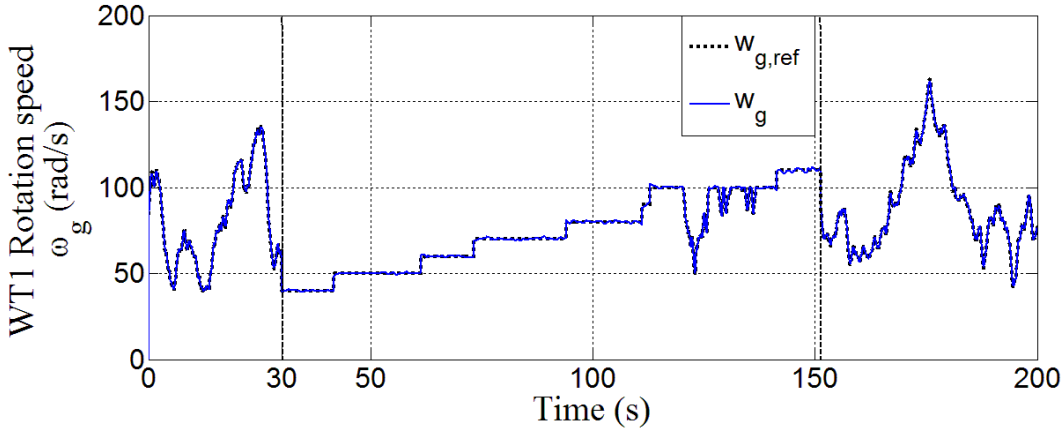

(b)

Figure 4.8: Wind speed and wind turbine rotational speed in the simulation of calibration process. (a) Wind speed. (b) Generator rotational speed and reference rotational speed.

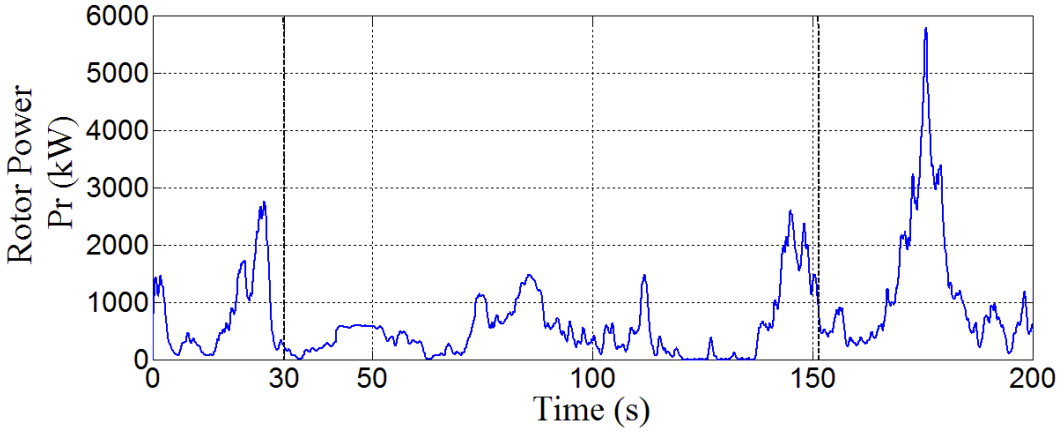

(a)

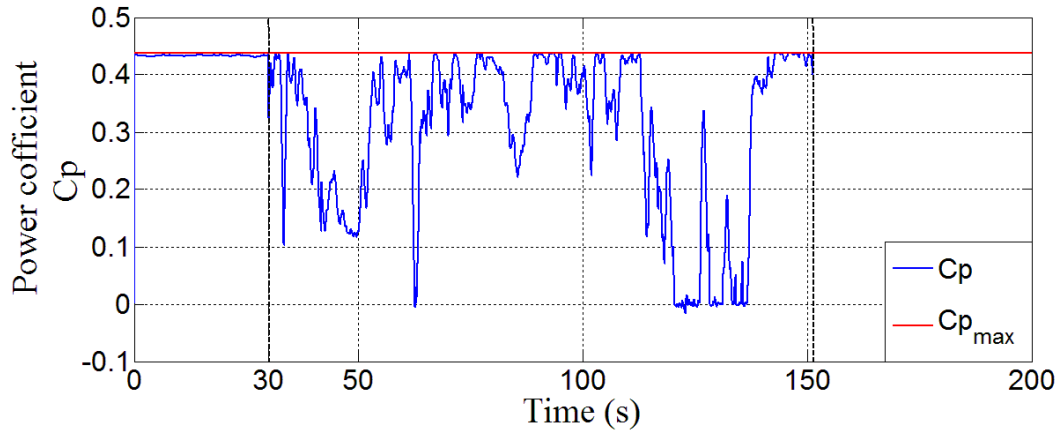

(b)

Figure 4.9: Wind turbine rotor power and power coefficient results in the simulation of calibration process. (a) Wind turbine rotor power. (b) Wind turbine power coefficient and the wind turbine maximum power coefficient value.

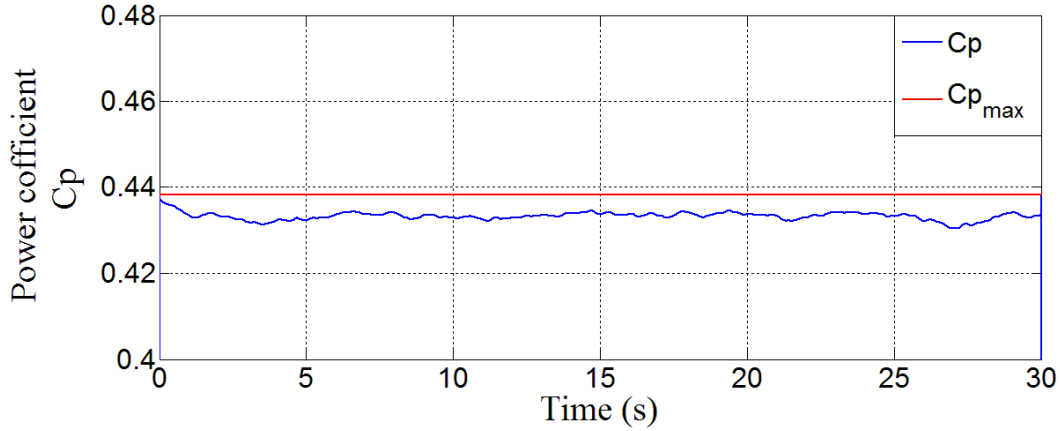

(a)

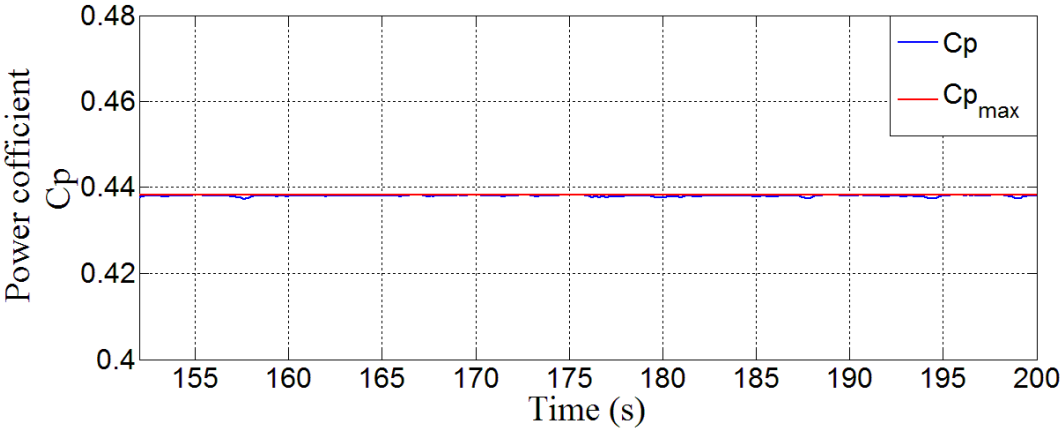

(b)

Figure 4.10: Comparison of power conversation coefficient C_p in the simulation of calibration process. (a) Before the calibration process. (b) After the calibration process.

sponding to the turbine model under variable wind conditions. A PMSG is driven by the DC motor to provide output electrical power. An IGBT based power electronics board is used as the PMSG side converter to control the WPGS with the PWM signals from the dSPACE control board.

The experiment is carried out under a 120 s variable wind speed. Figure 4.11 and Figure 4.12 present the experimental results of the recording of operating data and detection of the optimal power-speed curve (0 s to 60 s) and validation in MPPT mode (60 s to 120 s), respectively. Figure 4.11(a) and Figure 4.11(b) show the wind speed and rotational speed of the WT-PMSG system. The power captured by the wind turbine is shown in Figure 4.12. From t = 35 s to 50 s, there is a decrease in rotational speed to adopt the decrease in the wind speed. It verifies the negative power rejection mentioned in Section 4.3.1.

After enough operating points are recorded, the optimal power-speed curve and the k_{opt} is calculated at t = 60 s. Then it is used in PSF to control the wind turbine achieve MPPT. The calculated k_{opt} in the experiment is 1.787105, which is close to the accurate value 1.729105. The accuracy is around 97%. Figure 4.15 shows the comparison between the detected and the real optimal power-speed curve in the experiment. It can be seen that the optimal power-speed curve detected by the proposed method is close to the accurate curve. Figure 4.13(a), Figure 4.13(b) and Figure 4.14 show the experiment results in the MPPT validation mode, with wind speed, wind turbine rotational speed and power coefficient C_p, respectively. The experimental verification results show that the proposed method can obtain the wind turbine optimal power-speed curve under the variable wind speed condition, which can improve the performance of WPGS MPPT.

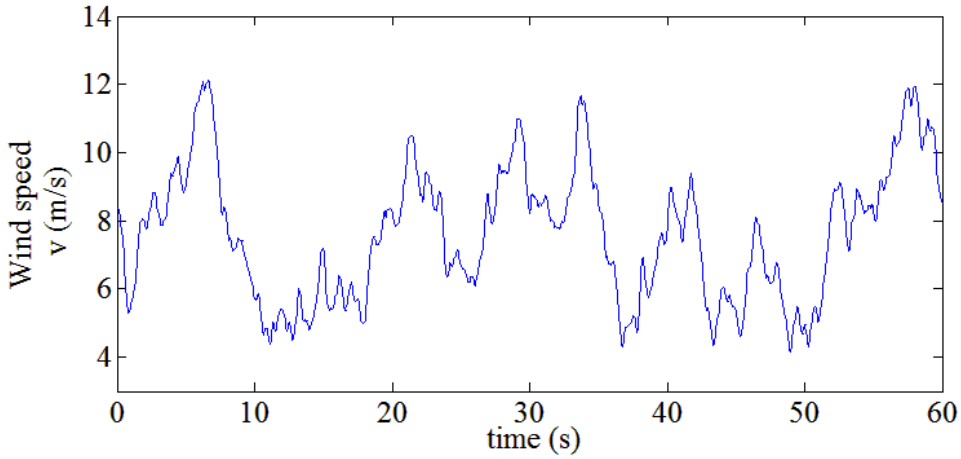

(a)

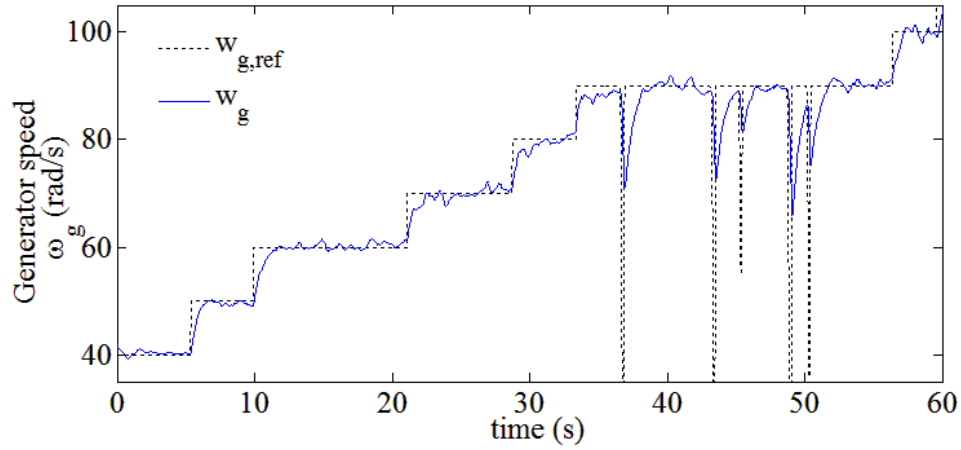

(b)

Figure 4.11: Wind speed and generator speed when the WPGS is in recording of operating data process in hard-ware-in-the-loop test. (a) Wind speed. (b) Generator rotational speed.

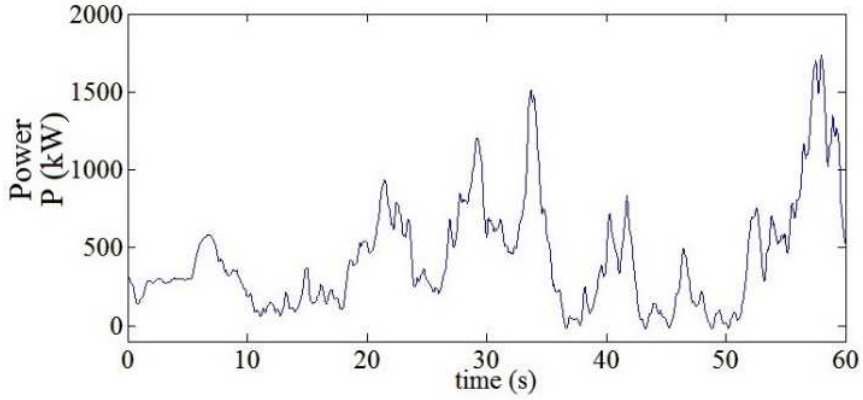

Figure 4.12: Experiment results of the output power when the WPGS is in recording of operating data process in hard-ware-in-the-loop test.

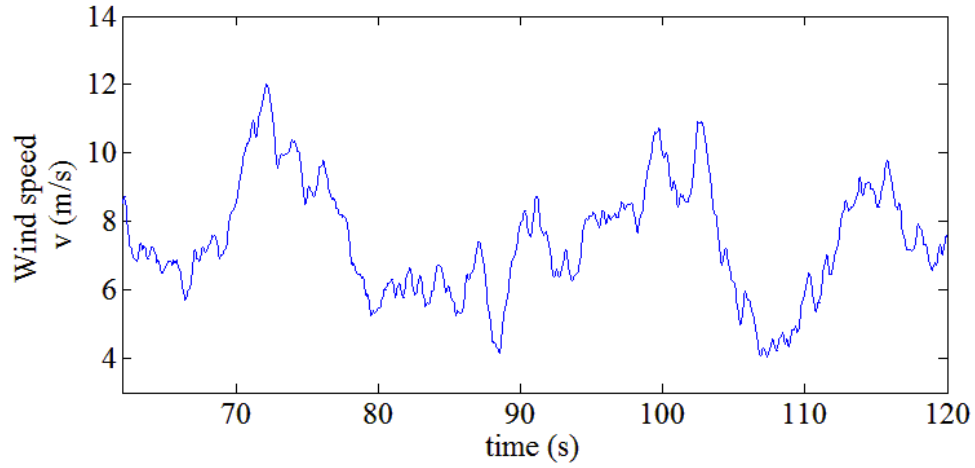

(a)

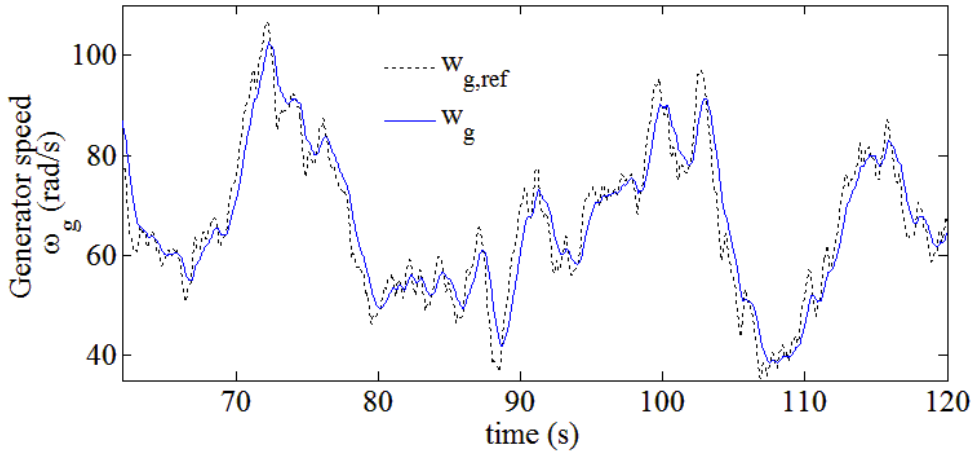

(b)

Figure 4.13: Wind speed and generator speed when the WPGS detected the optimal power-speed curve and in MPPT process in hard-ware-in-the-loop test. (a) Wind speed. (b) Generator rotational speed and reference rotational speed.

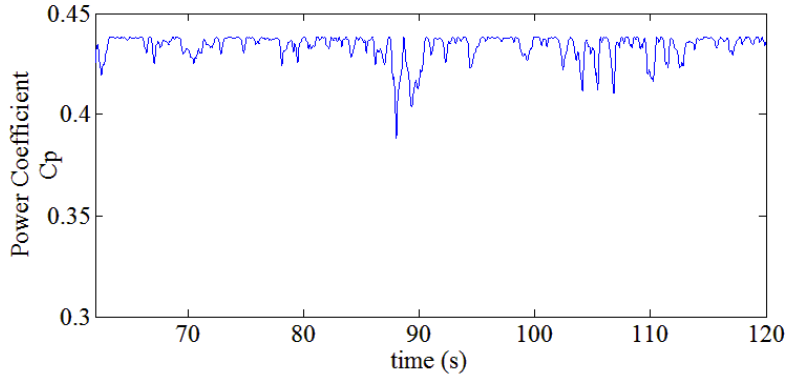

Figure 4.14: Experiment results of the power coefficient when the WPGS detected the optimal power-speed curve and in MPPT process in hard-ware-in-the-loop test.

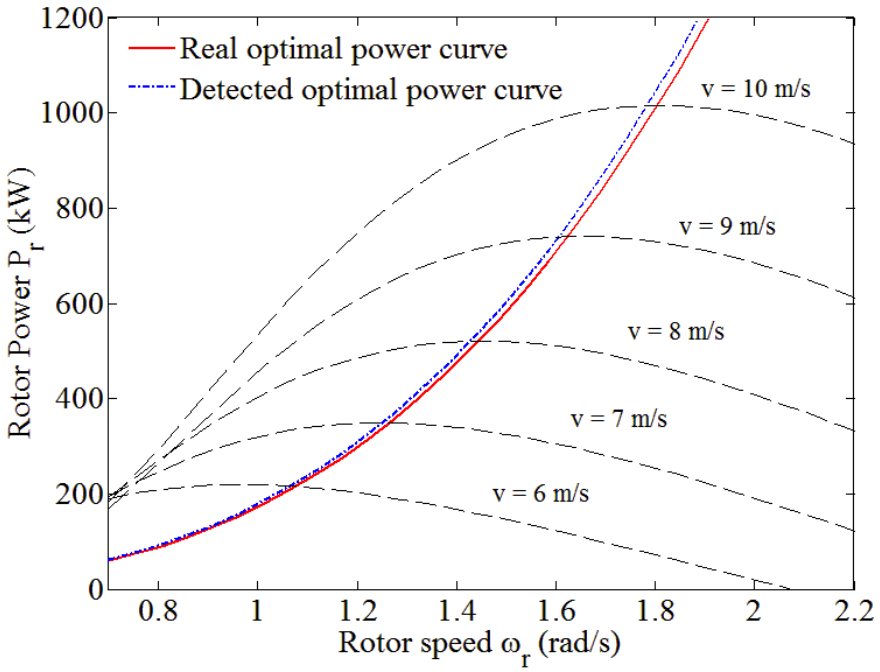

Figure 4.15: Comparison of the detected optimal power-speed curve and the real optimal power-speed curve

4.6 Conclusions

A new method to detect the optimal power-speed curve of a wind turbine under natural variable wind speed conditions has been proposed. The method obtains the maximum power points by controlling the WPGS in specified constant rotational speed and recoding the power and wind speed at the same time. Methods to estimate accurate MPP values and accelerate the detection time were proposed. After the recording of the operating data and calculating the optimal power-speed curve, the WPGS is controlled based on the obtained optimal power-speed curve to achieve MPPT. The optimal power-speed curve detected by the proposed method can also improve the MPPT performance and increase the WPGS energy generation when an inaccurate optimal power-speed curve was used in PSF. This proposed method does not require the system preknowledge and can obtian accurate optimal power-speed curve under natural variable wind speed conditions. The accuracy of the detected optimal power-speed curve and k_{opt} is about 97%. MATLAB/Simululink simulation and practical results confirm the validity and performance of the proposed method. Future work will focus on the design of a wind speed observer to remove the requirement of measuring wind speed, and the field test of the proposed algorithm on a real wind turbine.

Chapter 5

DC/DC Boost Converter Based PMSG Wind Turbine

Power electronics converters are the key and important part of a wind power generation system for controlling its output current or voltage and consequently, its rotational speed [108]. For a PMSG based wind power generation system, due to the fact that the synchronous generator provides the rotor flux by itself through permanent magnets or rotor field winding and, thus, diode rectifiers can be used as generator-side converters [109]. The configuration of a rectifier and DC-DC boost converter in a WPGS is given in Figure 5.1. The diode rectifier converts variable generator voltage to a DC voltage, which is boosted to a higher DC voltage by the boost converter. It is important that the generator voltage at low wind speeds be boosted to a sufficiently high level for the inverters, which ensures the delivery of the maximum captured power to the grid in the full wind speed range. Compared with the back-to-back VSCs, the diode rectifier and boost converter are simpler and more cost-effective [18].

As the stator current waveform could be distorted due to the use of the diode rectifier, which may increase the losses in the generator and causes torque ripple as well, the research of DC-DC boost converter operation and design is necessary. Also the designed and implemented DC-DC boost converter would be used in prototype experiments.

In this chapter, the operation of a DC-DC boost converter is presented at first, followed by the modeling of a DC-DC boost converter. Then the controller design and the simulation test of a WPGS with the DC-DC boost converter in MATLAB/SIMULINK is given. moreover, the hardware implementation of a diode and DC-DC boost converter is summarized in this chapter. Related hardware-in-the-loop test results are given to verify the ability of the implemented converter hardware.

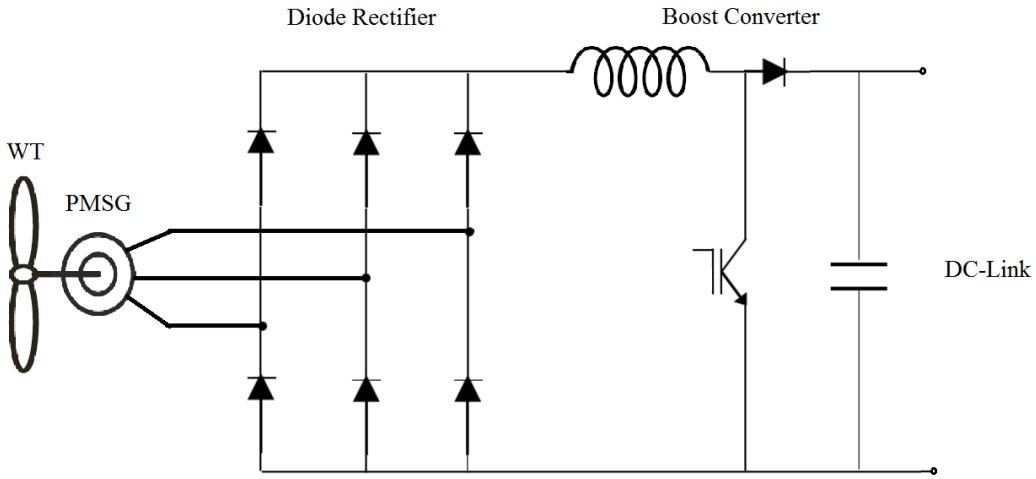

Figure 5.1: The configuration of a rectifier and DC-DC boost converter in a WPGS

5.1 Operation of a DC-DC Boost Converter

A DC-DC boost converter can produce an output dc voltage at a level greater than input dc voltage by employing pulse-width modulation (PWM) control techniques [110]. The standard topology of a DC-DC boost converter consists of a boost inductor, an output capacitor, a power switch and a diode. The configuration is shown in Figure 5.2(a).

In continuous current conduction mode (CCM), the current flowing continuously in the inductor during the entire switching cycle. There are two states during a switching cycle of the operation of a DC-DC boost converter: ON state and OFF state. At ON state, the power switch is on and the diode is off. The equivalent circuit is shown in Figure 5.2(b). At OFF state, the power switch is off and the diode is on. The equivalent circuit is shown in Figure 5.2(c).

The state-state equation that describes the dynamics of the DC-DC boost converter is given by Equation (5.1.1).

$$\begin{bmatrix} \frac{dI_{dcg}}{dt} \\ \frac{V_o}{dt} \end{bmatrix} = \begin{bmatrix} 0 & -\frac{1-S_{dc}}{L} \\ \frac{1-S_{dc}}{C} & 0 \end{bmatrix} \begin{bmatrix} I_{dcg} \\ V_o \end{bmatrix} + \begin{bmatrix} \frac{1}{L} & 0 \\ 0 & -\frac{1}{C} \end{bmatrix} \begin{bmatrix} V_{dcg} \\ I_o \end{bmatrix} \tag{5.1.1}$$

where I_{dcg} is the converter input current, V_o is the converter output voltage, V_{dcg} is

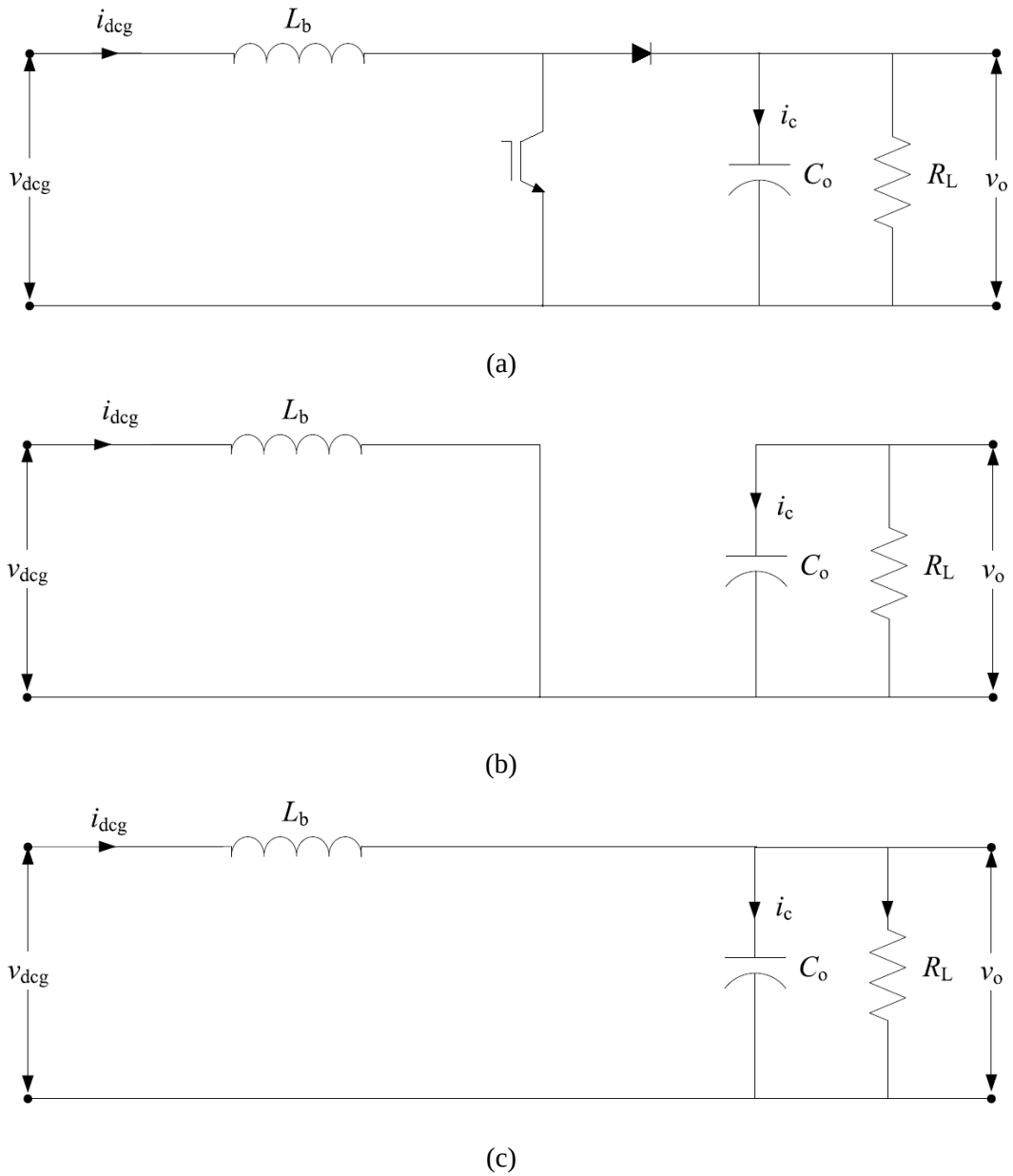

Figure 5.2: A DC-DC boost converter (a) Schematic diagram. (b) ON state. (c) OFF state

the converter input voltage, I_o is the converter output current, and S_{dc} is the switching function of the power converter, defined as follows:

$$S_{dc} = \begin{cases} 0, \text{ for OFF state} \\ 1, \text{ for ON state} \end{cases} \tag{5.1.2}$$

The ratio of time during the power switch is turned on to the period of one complete switching cycle is defined as duty cycle D. The discontinuous model in Equation (5.1.1) can be approximated by a continuous state-space averaged model in Equation (5.1.3).

$$\begin{bmatrix} \frac{dI_{dcg}}{dt} \\ \frac{V_o}{dt} \end{bmatrix} = \begin{bmatrix} 0 & -\frac{1-D}{L} \\ \frac{1-D}{C} & 0 \end{bmatrix} \begin{bmatrix} I_{dcg} \\ V_o \end{bmatrix} + \begin{bmatrix} \frac{1}{L} & 0 \\ 0 & -\frac{1}{C} \end{bmatrix} \begin{bmatrix} V_{dcg} \\ I_o \end{bmatrix} \tag{5.1.3}$$

Since there is no net change of the inductor current from cycle to cycle in steady-state conditions. Thus, in steady-state conditions, the input-to-output voltage conversion relationship of the boost converter is:

$$V_o = \frac{V_{dcg}}{1-D} \tag{5.1.4}$$

In the same way, the relationship between the average inductor current I_L and the DC-DC converter output current I_o is as follows:

$$i_o = \frac{V_{dcg}}{1-D} \tag{5.1.5}$$

5.2 Modeling of a DC-DC Boost Converter

The steady-state equations of a DC-DC boost converter is given in Equation (5.1.3). To get the transfer function of the DC-DC boost converter, perturbation signals, e.g. the perturbed duty cycle $\tilde{D}(t)$, the perturbed DC input current of the converter, $\tilde{I_{dcg}}(t)$, and the pertubed DC output voltage of the converter, $\tilde{V_o}(t)$. Thus, with the perturbation signals, Equation (5.1.3) can be rewritten as [111]:

$$\begin{bmatrix} \frac{d(I_{dcg}+\tilde{I_{dcg}}(t))}{dt} \\ \frac{d(V_o+\tilde{V_o}(t))}{dt} \end{bmatrix} = \begin{bmatrix} 0 & -\frac{1-(D+\tilde{D(t)})}{L} \\ \frac{1-(D+\tilde{D(t)})}{C} & 0 \end{bmatrix} \begin{bmatrix} I_{dcg}+\tilde{I_{dcg}}(t) \\ V_o+\tilde{V_o}(t) \end{bmatrix} + \begin{bmatrix} \frac{1}{L} & 0 \\ 0 & -\frac{1}{C} \end{bmatrix} \begin{bmatrix} V_{dcg} \\ I_o \end{bmatrix} \tag{5.2.1}$$

As $\tilde{d(t)}\tilde{V_o(t)}$ is the product of two small perturbation signals, it can be ignored in the linearisation. Substitute Equation (5.1.4) into (5.2.1). Also considering that in the loading conditions, $I_o = V_o/R_L$, Then simplify Equation (5.2.1). It can be rewritten as Equation (5.2.2) and (5.2.3).

$$\frac{\hat{I_{dcg}}}{dt} = \frac{1}{L}\big(V_o\tilde{D}(t) - (1-D)\tilde{V_o}(t)\big) \tag{5.2.2}$$

$$\frac{d\hat{V_o}}{dt} = \frac{1}{C}\big((1-D)\tilde{I_{dcg}}(t) - I_{dcg}\tilde{D}(t) - \frac{ztildeV_o(t)}{R_L} \tag{5.2.3}$$

The Laplace transform equation of (5.2.2) and (5.2.3) are as follows:

$$d\hat{I}_{dcg}(s) = \frac{1}{Ls}(V_o\tilde{D}(t) - (1-D)\tilde{V_o}(s)) \tag{5.2.4}$$

$$\hat{V_o}(s) = \frac{1}{Cs}((1-D)\tilde{I_{dcg}}(s) - I_{dcg}\tilde{D}(s) - \frac{\tilde{V_o}(s)}{R_L}) \tag{5.2.5}$$

From Equation (5.2.4) and (5.2.5) the control-to-output transfer function $G_{vd}(s)$ can be obtained:

$$G_{vd} = \frac{V_o(s)}{D(s)} = \frac{(1-D)V_o - LI_{dcg}s}{LCs^2 + \frac{L}{R_L}s + (1-D)^2} \tag{5.2.6}$$

Equations (5.1.4) and (5.1.5) are employed to substitute V_o and I_{dcg} in (5.2.6). Therefore, $G_{vd}(s)$ is obtained in (5.2.7).

$$G_{vd} = \frac{V_o(s)}{D(s)} = \frac{V_{dcg}(R_L - (1-D)^{-2}Ls)}{R_LL_os^2 + Ls + (1-D)^2R_L} \tag{5.2.7}$$

The derivation of $G_{id}(s)$ is similar to the one made above for obtaining $G_{vd}(s)$. Thus, the control-to-input current transfer function $G_{id}(s)$ is obtained in (5.2.8).

$$G_{id} = \frac{I_{dcg}(s)}{D(s)} = \frac{(1-D)^{-1}V_{dcg}(RCs+2)}{R_LLCs^2 + Ls + (1-D)^2R_L} \tag{5.2.8}$$

Finally, transfer functions (5.2.7) and (5.2.8) are used to obtain the current-to-output transfer function G_{dc-dc}

$$G_{dc-dc} = \frac{V_o(s)}{I_{dcg}(s)} = \frac{(1-D)R_L - (1-D)^{-1}Ls}{R_LCs+2} \tag{5.2.9}$$

For stability analysis, Equation (5.2.9) is validated under the variations of duty cycle D and load R_L.

5.3 Controller Design of a Boost Converter in a W-PGS

The control algorithm of the dc-dc boost converter in wind power system contains two PI controllers. The boost converter can be used to control the dc current I_{dcg} by adjusting the value of duty cycle D and getting V_{dcg} as a feedback. From the voltage equation in continuous current mode in Equation (5.1.3), we can get that:

$$L\frac{I_{dcg}}{dt} = V_{dcg} - (1-D)V_o \tag{5.3.1}$$

Then Equation (5.3.2) can be obtained from Equation (5.3.1).

$$I_{dcg} = \frac{1}{L}\int (V_{dcg} - (1-D)V_o)dt \tag{5.3.2}$$

Besides, in wind power generation system, current I_{dcg} is related to the generator speed ω_m. The PMSG model given in Chapter 4 illustrated the relationship between current and rotational speed. Consequently, the controller with compensation of feedforward term can be formed as shown in Figure 5.3.

5.4 Prototype Boost Converter

Prior calculations of the minimum and maximum absolute values of state variables are important in order to accurately design components of a DC-DC boost

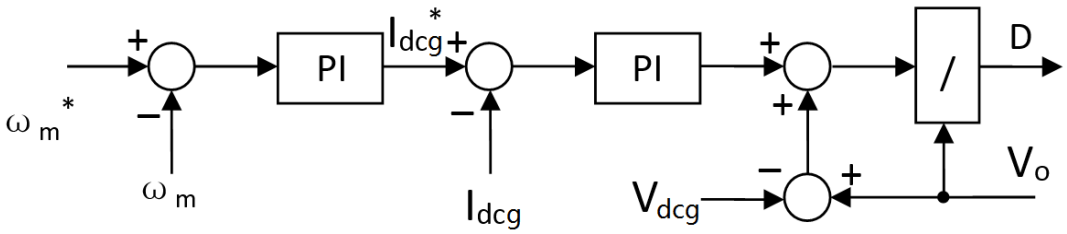

Figure 5.3: Control diagram of a DC-DC boost converter in a wind power generation system

converter. Table 5.1 lists the state variables, which are obtained from experimental characteristics of the PMSG in prototype experiments. Hence, the maximum output DC current of a diode rectifier can be calculated at 500 rpm and neglecting the losses inside the diode rectifier as follows:

$$I_{dcg-max} = \frac{P_o}{V_{dcg-max}} = \frac{640}{52} = 12.31A \tag{5.4.1}$$

Finally, Table 5.2 gives the design results of the DC-DC boost converter used in this work by employing 5.4.2 to 5.4.5 [112].

$$D_{min} = 1 - \frac{V_{dcg-min}}{V_{o-min}} \tag{5.4.2}$$

$$D_{max} = 1 - \frac{V_{dcg-max}}{V_{o-max}} \tag{5.4.3}$$

$$L_{min} \geq \frac{V_{dcg-max} D_{max} T_{sw}}{I_{dcg-max}} \tag{5.4.4}$$

$$C_{min} \leq \frac{(1 - D_{max}) I_{dcg-max} T_{sw}}{V_{r-min}} \tag{5.4.5}$$

As shown in Table 5.1 that minimum output voltage ripple is chosen as 0.1V, which can be decreased by increasing L, C, or switching frequency, f_{sw}. However, there are some disadvantages by increasing these parameters, e.g.: (i) if L is chosen large, the time required for I_{dcg} to reach its peak value is increased, (ii) if L or C are chosen large, the capacity and the cost of a DC-DC converter are increased and

Description	Symbol	Unit	Value
Minimum input DC voltage	V_{dcg_min}	V	5
Maximum input DC voltage	V_{dcg_max}	V	52
Minimum output DC voltage	V_{o_min}	V	5
Maximum output DC voltage	V_{o_max}	V	220
Minimum output voltage ripple	V_{r_min}	V	0.1

Table 5.1: The minimum and maximum absolute values of the state variables used for designing the DC-DC boost converter

Description	Symbol	Unit	Value
Minimum duty cycle	d_{min}	%	0
Maximum duty cycle	d_{max}	%	70
Minimum boost inductor	L_{b_min}	mH	0.32
Maximum output capacitor	C_{o_max}	μF	2900

Table 5.2: The design results of the DC-DC boost converter

(iii) if f_{sw} is chosen large, the switching loss in a power switch, e.g. an IGBT, is increased.

5.5 Simulation Test

A PMSG based wind power generation system with diode rectifier and DC-DC boost converter based on the given model was simulated in MATLAB/SIMULINK. By varying the power switch duty cycle of the boost converter, the rotational speed of the wind turbine can be controlled. The purpose of simulation test is to verify the performance of control rotational speed in a WPGS with diode rectifier and DC-DC boost converter.

Figure 5.4 shows the simulation model in MATLAB/SIMULINK. When control the WPGS rotational speed in constant under a step change wind speed, the control system can change the duty to keep the rotational speed tracking its reference value. The simulation results are shown in Figure 5.5. From the results, it can be found

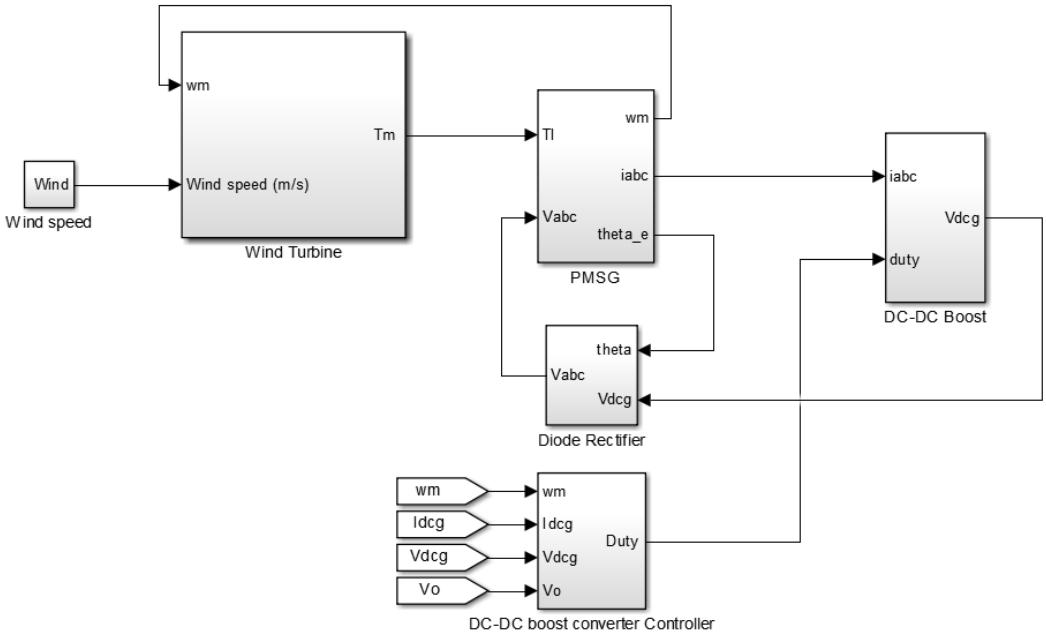

Figure 5.4: Simulation model in Simulink/Matlab

that, when wind speed changes, the controller will change the duty cycle to ensure the rotational speed keeps tracking its reference value. Thus, the designed controller is able to control the wind turbine rotational speed in a WPGS with diode rectifier and DC-DC boost converter.

5.6 Generator-Side Converter Hardware Implementation

The schematic diagram of a diode bridge-VSC with a DC-DC boost converter in a wind power generation system is as shown in Figure 5.1. The generator-side converter contains a diode rectifier and a DC-DC boost converter.

For the hardware implementation of the generator side converter, there are three parts need to be mentioned. As the PWM control signal is output from dSPACE control panel, a coupler board need to be installed to transfer the PWM signal into the IGBT driver. Also, a particular IGBT driver should be connected to drive the

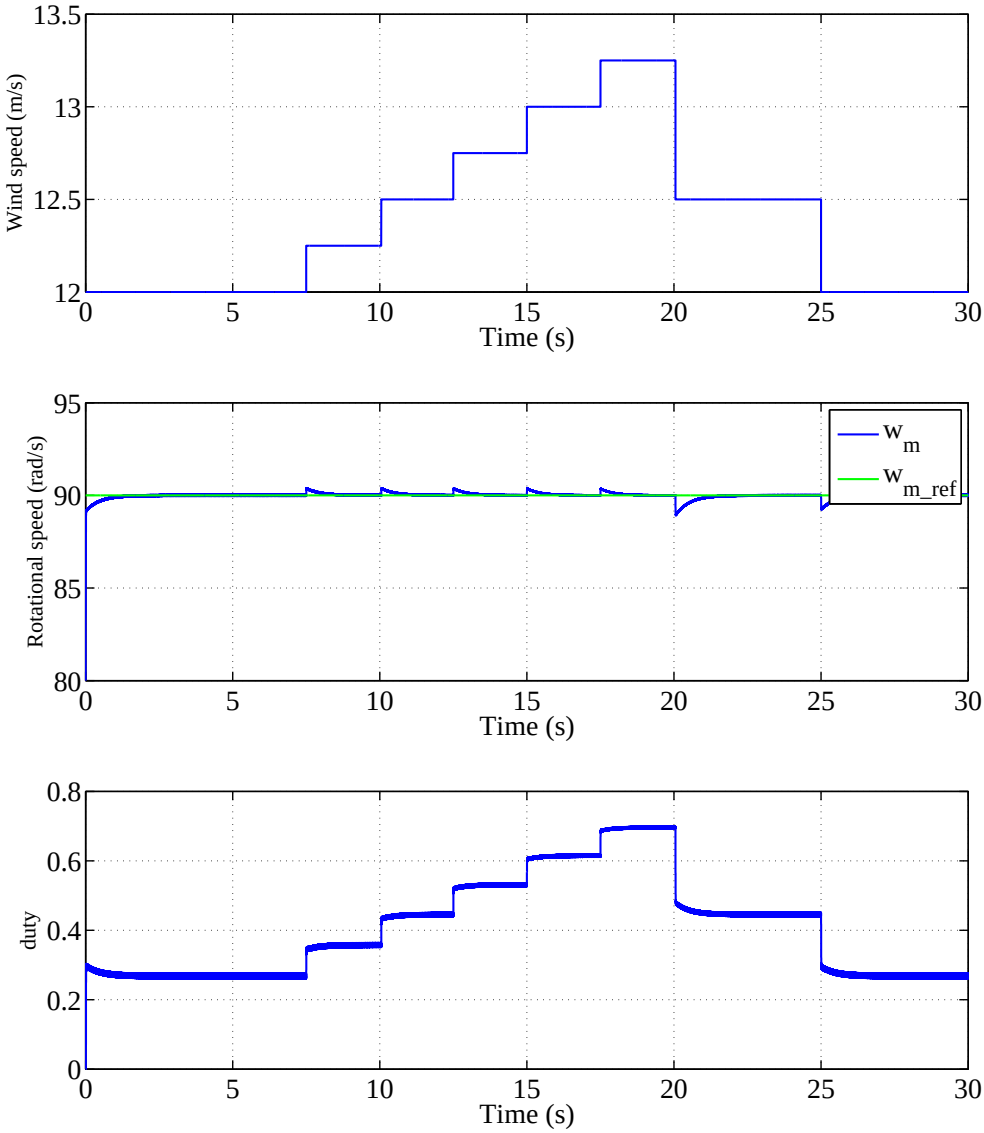

Figure 5.5: Simulation results of control rotational speed of WPGS with DC-DC boost converter under step change wind speed

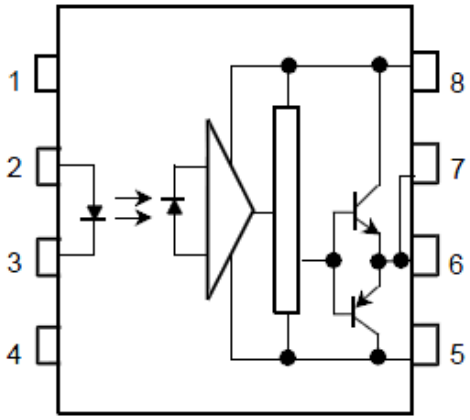

Figure 5.6: Schematic of the photocoupler

IGBT power switch in the boost converter. Finally, all the components and boards are installed together on a heat sink as a build diode rectifier and boost converter.

5.6.1 Coupler board connection

As the PWM signal output from dSPACE control pannel is 0 to 5 V voltage signal, it should go through a photocoupler for circuit protection and signal voltage step up. The TOSHIBA TLP250 consists of a light emitting diode and a integrated photodetector. It is suitable for gate driving circuit of IGBT or power MOSFET. Its schematic is as Figure 5.6 shows.

On the coupler board, +15 V voltage power supply connects the pin 8 V_{cc} and pin 5 GND. Pin 2 connects the PWM signal output from dSPACE control panel. Pin 3 is connected with the digital ground of dSPACE control panel. The voltage between pin 6/7 and 5 is the output of the board. A 0.1 μF bypass capacitor must be connected between pin 8 and 5 to stabilize the operation of the high gain linear amplifier. Failure to provide the bypassing may impair the switching property. Thus, the design of coupler board is as Figure 5.7 shows.

Based on the coupler board circuit design, the soldered coupler interface board is shown in Figure 5.8. The PWM and Digital Ground pins connect with dSPACE control panel. The socket is connected with IGBT driver adaptor board.

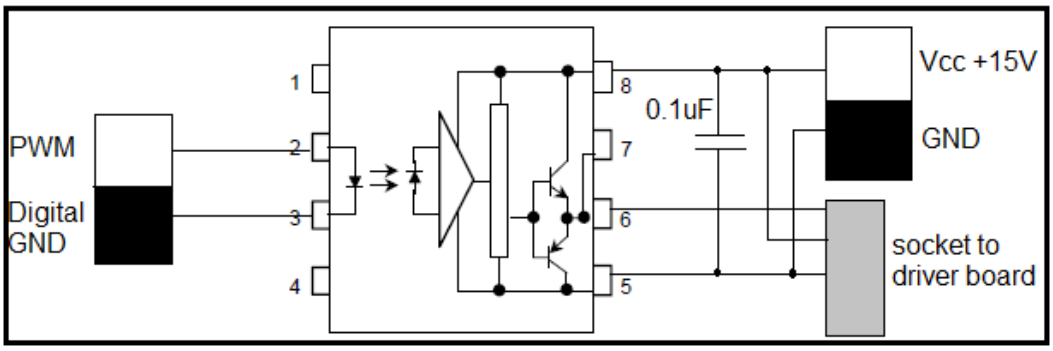

Figure 5.7: Coupler board circuit design

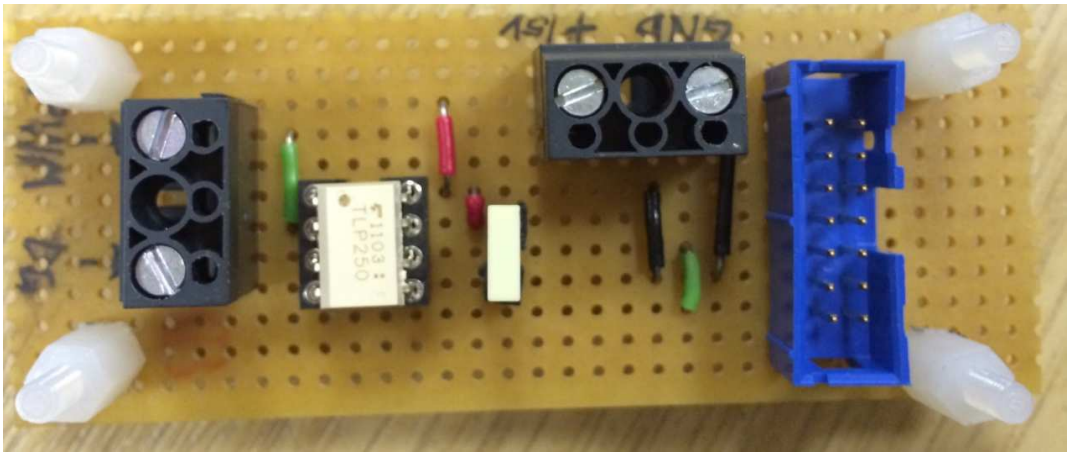

Figure 5.8: Coupler interface board

5.6.2 IGBT modules and driver connection

The SKYPER 32 core constitutes an interface between IGBT modules and the controller. This core is a half bridge driver. Basic functions for driving, potential separation and protection are integrated in the driver. Thus it can be used to build up a driver solution for IGBT modules. There is an adaptor board for the driver. The one used is Board 1 SKYPER 32. The board can be customized allowing adaptation and optimization to the used IGBT module. The input signal of the driver is switching active to +15 V and 0 V. A capacitor is connected to the input to obtain high noise immunity. Besides, an external resistor to the controller logic high level is required. On the output side, the external components R_{ce} and C_{ce} are applied for adjusting the steady-state threshold the blanking time. According to the component datasheet, the values we used are: $Rce = 18k\Omega$ and $C_{ce} = 330\,pF$. There are some external boost capacitors connected on the board as the rated gate charge of the driver may be increase by additional boost capacitors to drive IGBT with large gate capacitance. The whole connection schematic is shown as Figure 5.9.

R_{on} and R_{off} in Figure 5.9 are gate resistors. The output transistors of the driver are MOSFETs. The sources of the MOSFETs are separately connected to external terminals in order to provide setting of the turn-on and turn-off speed of each IGBT by the external resistors R_{on} and R_{off}. The gate resistor influences the switching time, switching losses, etc. By increasing R_{on} and R_{off} the turn-on and turn-off speed will decrease. According to the datasheets, R_{on} and R_{off} used in our hardware are both 220 Ω. Some of the components are not equipped on the adaptor board. Thus the following steps should be done for complete the board:

$R262$	R_{ce}	$18k\Omega$
$C260$	C_{ce}	$332pF$
$R250$	R_{VCE}	0Ω
$R251, R252, R253$	R_{Gon}	220Ω
$R254, R255, R256$	R_{Goff}	220Ω

After equipped the components, the IGBT driver and its adaptor board are shown in Figure 5.10.

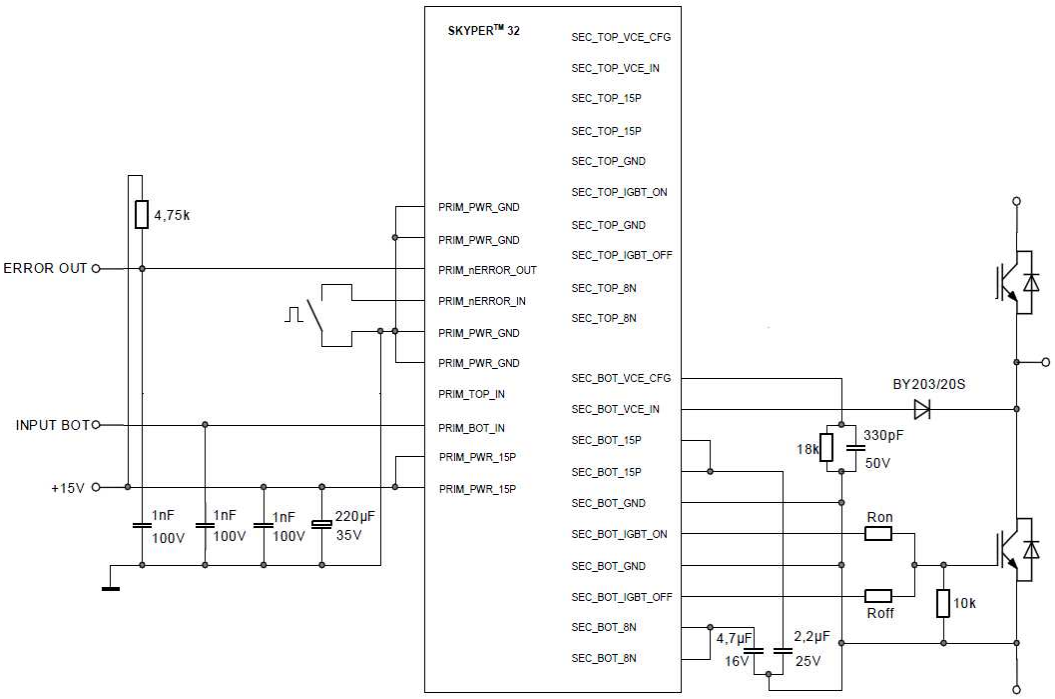

Figure 5.9: Connection schematic of the driver core and IGBT module

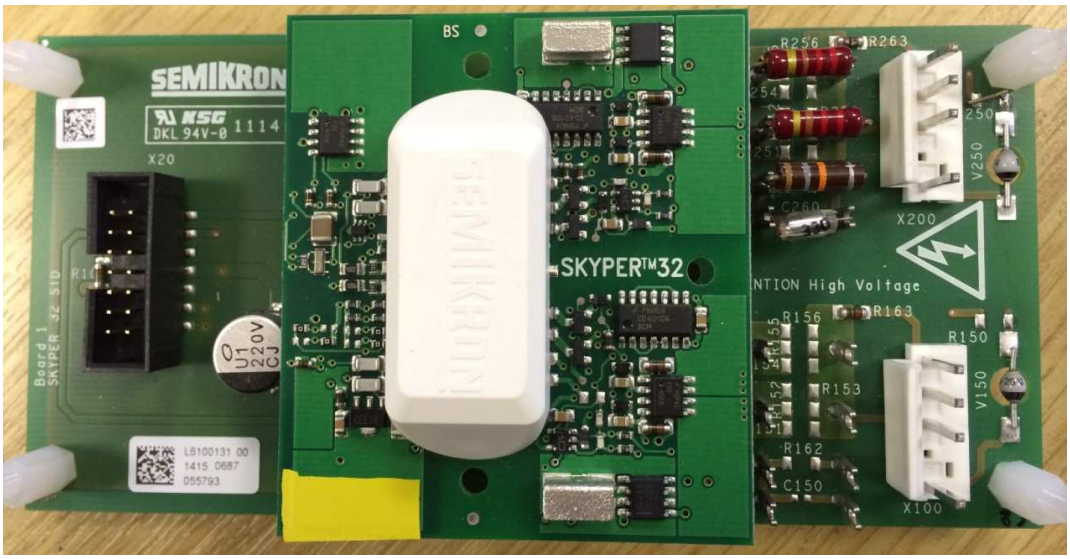

Figure 5.10: IGBT driver and adaptor board

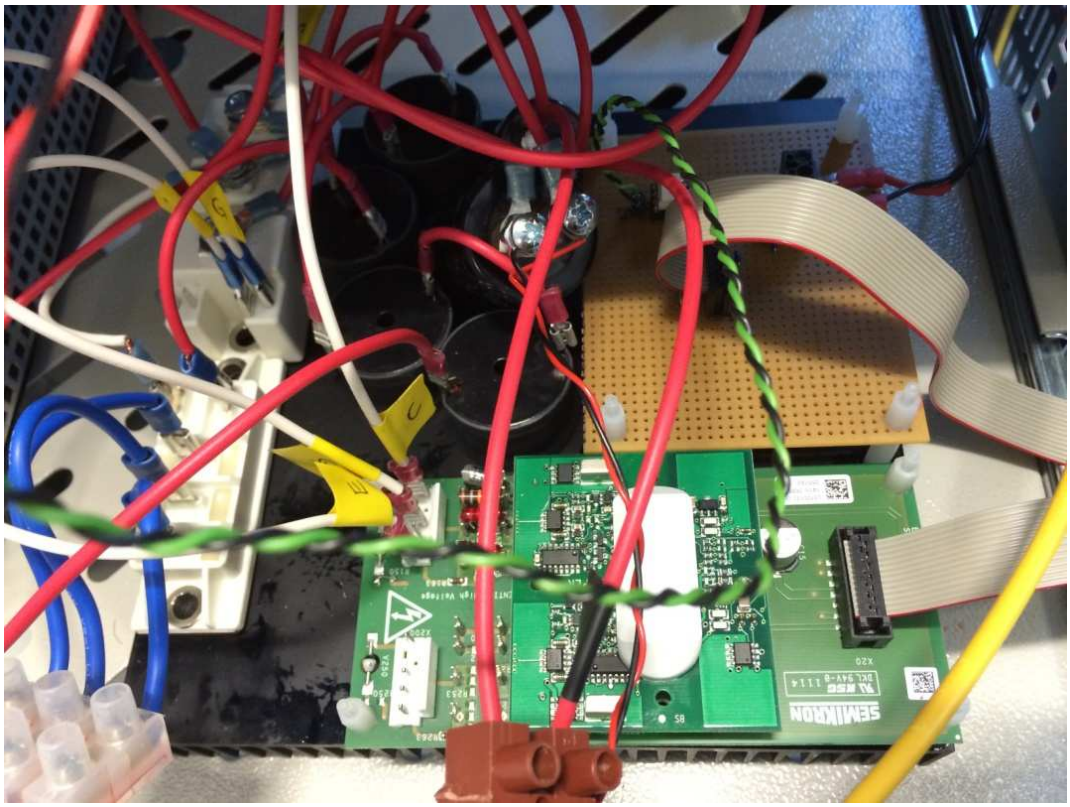

Figure 5.11: Wind turbine converter hardware installation

The output of the adaptor board are Emitter output, Gate output, and Collector output which can directly connect with IGBT module.

5.7 Hardware-In-The-Loop Test

Combine the above parts together as Figure 1.6 shows. The final hardware for the generator-side converter is as Figure 5.11.

The control signal is provided by dSPACE control panel.

To test the installed generator-side converter hardware, hardware-in-the-loop tests have been implemented with an experimental PMSG. The test bench is shown in Figure 5.12. The constructed test bench consists of a PMSG which is coupled to a three-phase induction motor. The measurements are sampled by a dSPACE DS1104 controller. The constructed teest bench is equipped with voltage transducers (type

Rated output power	W	500
Rated rotation speed	A	20
Phase resistance	Ω	0.66
Rotor inertia	Kg$\cdot m^2$	0.006
Generator configuration		3 phase star connected AC output

Table 5.3: Experimental PMSG specification

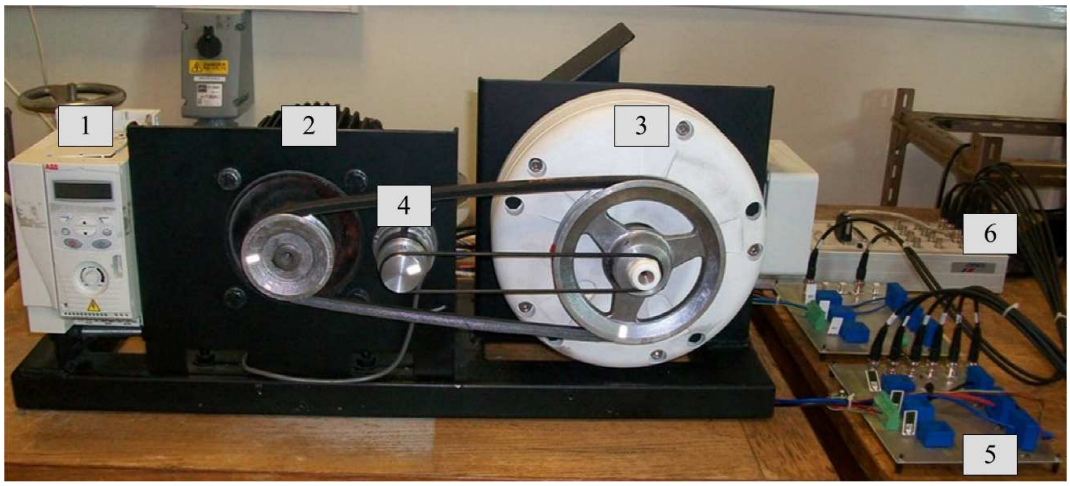

Figure 5.12: The experiment bench for generator-side converter test: (1) a variable-frequency AC driver, (2) a three-phase induction motor, (3) a PMSG, (4) an encoder, (5) voltage and current sensor boards, (6) a dSPACE control panel

LV25-p), current transducers (type LA55-p) and an encoder to measure the rotor speed and position. It is worth noting that all the components used in the constructed test bench are commercially available. The paprameters of the PMSG (which includes a back-EMF observer) are listed in Table 5.3.

The results obtained form the hardware-in-the-loop test are presented in Figure 5.13 and 5.14. Figure 5.13 is the results in the case that the wind turbine is controlled to tracking a constant rotational speed reference in variable wind speed. It shows that when wind speed changes, the duty cycle of the converter changes keep the rotational speed stay around 20 rad/s. Figure 5.14 shows the results in the case that controlling the wind turbine rotates in variable rotational speed under a constant

wind speed environment. And it can be seen that, duty cycle changes to make the rotational speed varies following the reference value.

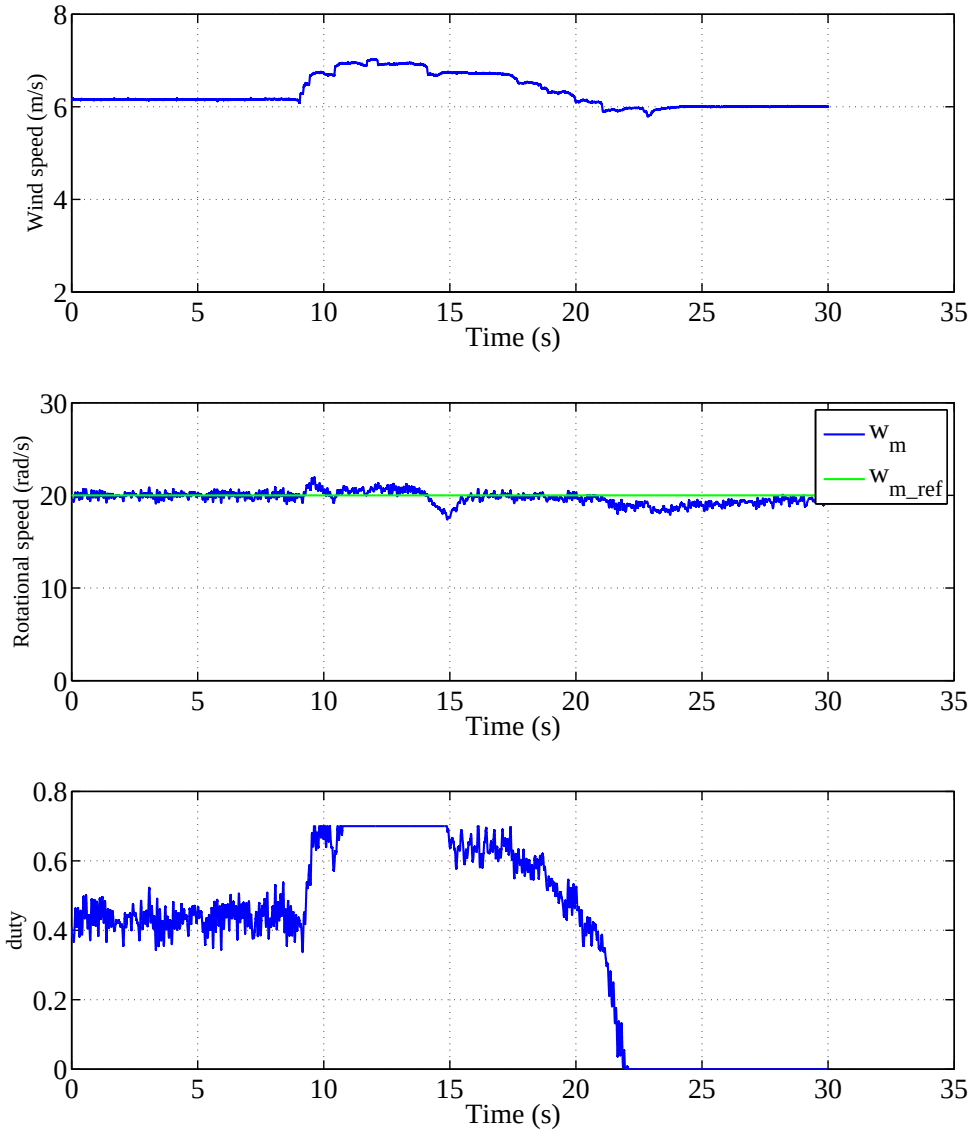

Figure 5.13: Hardware-in-the-loop test of varying wind speed with constant rotational speed reference

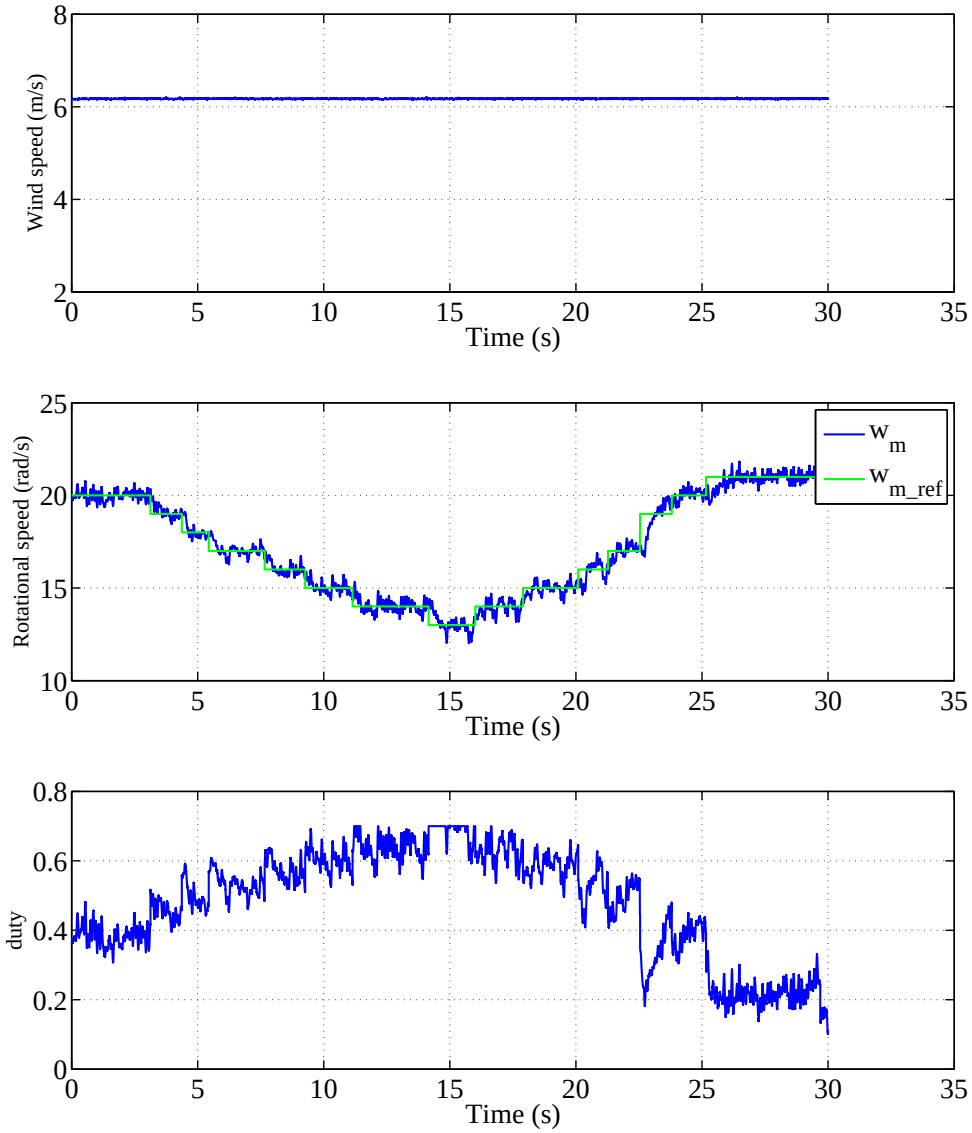

Figure 5.14: Hardware-in-the-loop test of constant wind speed with changing reference speed

5.8 Conclusions

This chapter presents the diode rectifier with DC-DC boost converter as the generater-side converter in a WPGS. The operation principle and model of a DC-DC boost converter have been given. Then the design of the DC-DC boost converter and controller are investigated followed by the simulation test. The implementation of the designed generator-side converter has been tested in hardware-in-the-loop experiments. Both simulation and experiment results verified the designed DC-DC boost converter is reliable, efficient and suitable to be used in the PMSG based WPGS. Thus prototype experiments can use the designed DC-DC boost converter for wind turbine control.

Chapter 6

Small-Scale Prototype Implementation and Field Test

There are two small scale wind turbines installed on the department roof and cable connected to the office for experiment and condition monitoring. It has been used to build a micro-smart grid platform to demonstrate renewable energy generation, control and condition monitoring systems. With this prototype, the further green energy conversion ideas are enable to be developed, tested and validated. This chapter describes the prototype settings, experiment design, field test and experiments results based on the controller designed from previous chapters and installed on the roof turbines. The designed DC-DC boost converter is used in the prototype experiment WPGS. The comparison experiments results in this chapter illustrate show with the designed DC-DC boost converter, the WPGS can generate more power than the wind turbine's original controller.

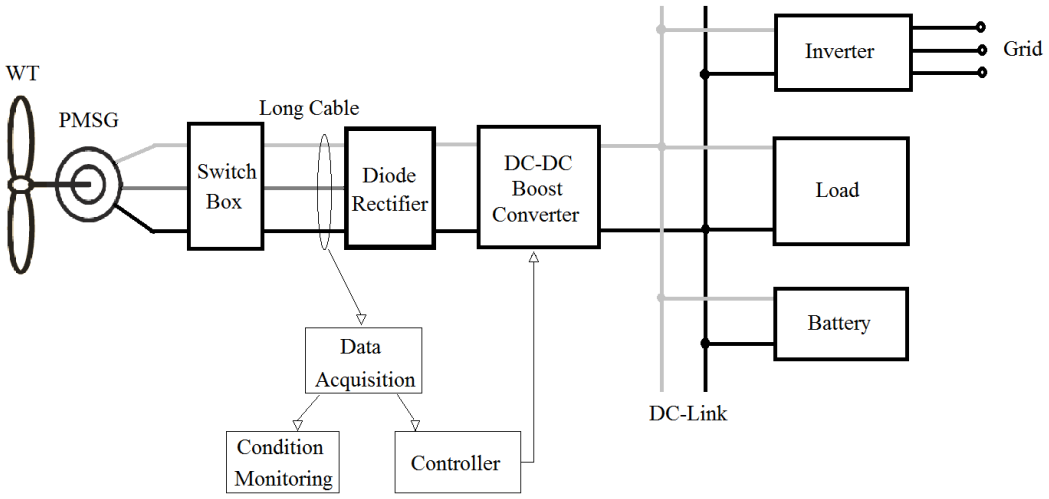

Figure 6.1: Configuration of the prototype WPGS

6.1 Prototype Design and Implementation

The configuration of the prototype WPGS is shown in Figure 6.1. The whole platform includes: WT, PMSG, switch box, diode rectifier, DC-DC boost converter, load, battery and inverter connect to the grid.

The power generated by the PMSG transfer to the diode rectifier and then pass through the DC-DC boost converter, eventually transfer to the grid or load or in charge battery. There are some sensors installed with the WPGS, i.e. voltage transducer (VT) and current transducer (CT) for voltage and current measurement, anemometer to measure wind speed and WebCam to monitor the turbines on the roof. The measurement results transfer to the data acquisition system for the condition monitoring and controller. The controller output PWM signal through dSPACE platform to the DC-DC boost converter power electronics. The details are given below.

6.1.1 Hardware implementation

There are two full-scale vertical-axis wind turbine on the department roof as shown in Figure 6.2. The two turbines are in the same size and have the same

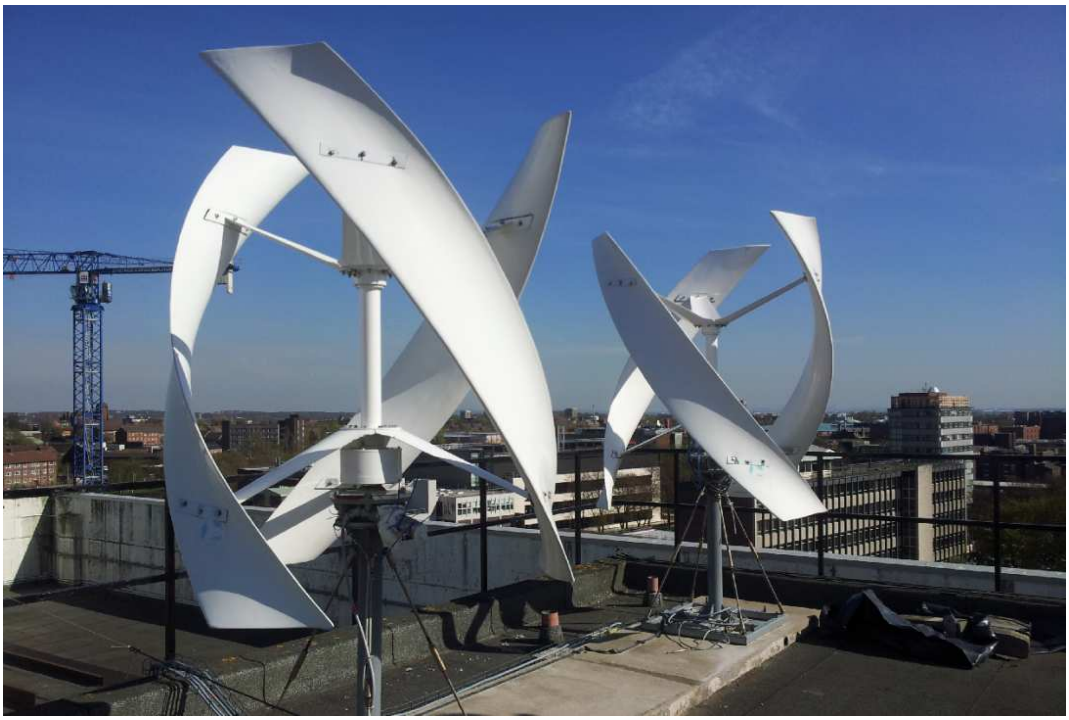

Figure 6.2: The two full-scale vertical-axis wind turbines installed on the building roof of the EEE department

parameters as Table 6.1 and 6.2 shown below. In this case, they can be used for comparison experiments.

Each wind turbine is coupled with a direct drive Three-Phase Permanent Magnet Synchronous Generator (PMSG). The performance parameters of the wind turbines with their generators are in Table 6.2.

In Figure 6.3, there are switches on the roof installed between the turbines' generators and the Lab A405 to turn the connection. The turbines' generators are connected with the wind turbine control systems which were installed in the Lab as shown in Figure 6.4.

Relevant parameters of the control system are measured and send to the PC for data analysis. An anemometer was installed on the roof to get wind speed. The returned value send to the PC as well. Besides, a web camera was installed for monitoring the wind turbines.

As shown in Figure 6.1, the wind turbines' control and monitoring systems need

Axis	Vertical
Height	1.80 m
Width	1.38 m
Weight	92 kg
Swept Area	2.36 m^2
Blade Materials	Carbon Fiber and Fiberglass

Table 6.1: Eddy wind turbine physical information

Rated Power	600 W
Cut-in Wind Speed	3.5 m/s
Cut-out Wind Speed	32 m/s
Rated RPM	200 RPM
Survival Wind Speed	55 m/s
Rated Wind Speed	12m/s
Annual Energy at 5 m/s	780 kWh
Noise from IEC 61400-11 at 12 m/s	36 dB

Table 6.2: Eddy wind turbine performance information

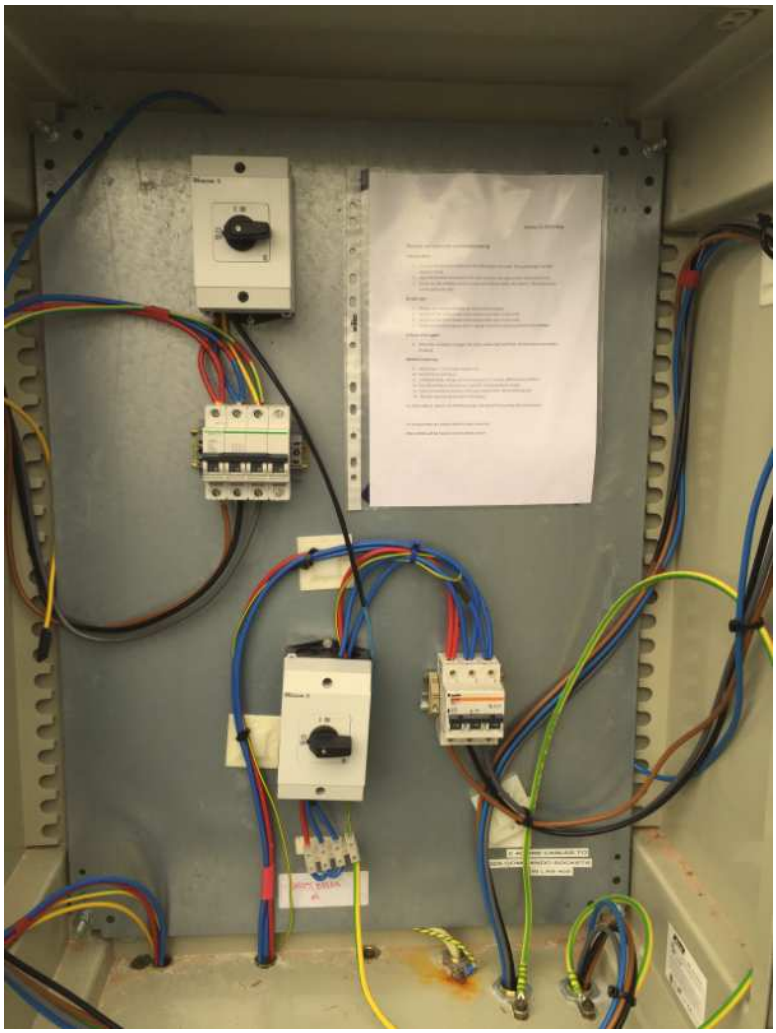

Figure 6.3: Switch box on the roof for cables connection

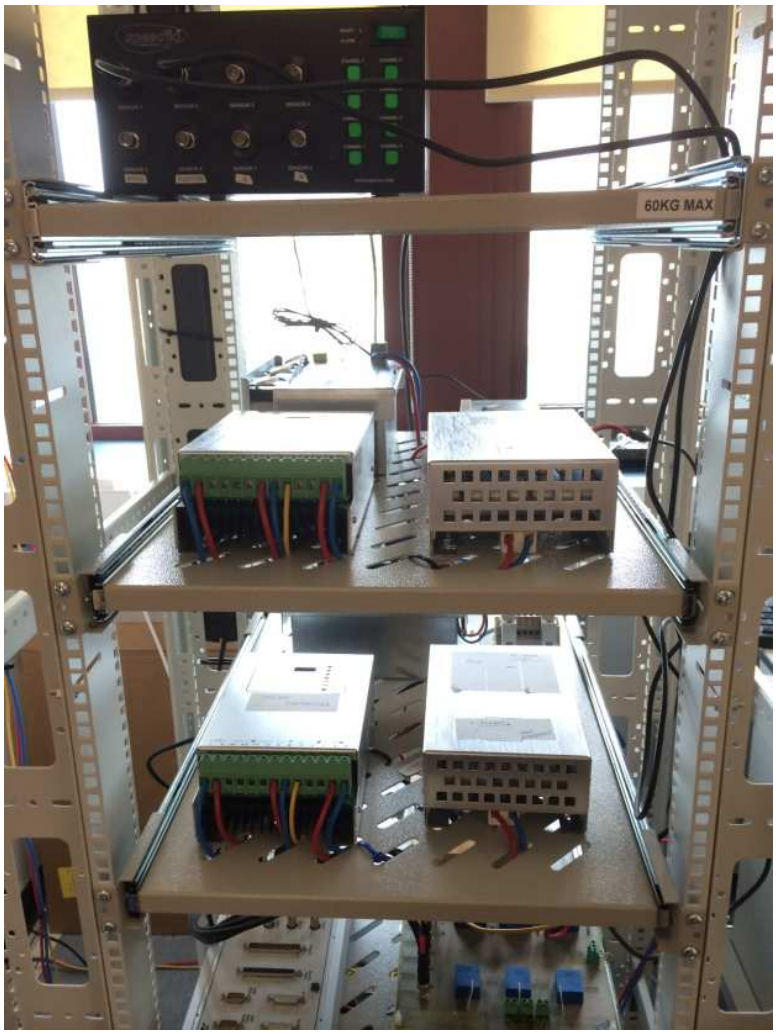

Figure 6.4: Power electronics of the WPGS in a cabinet

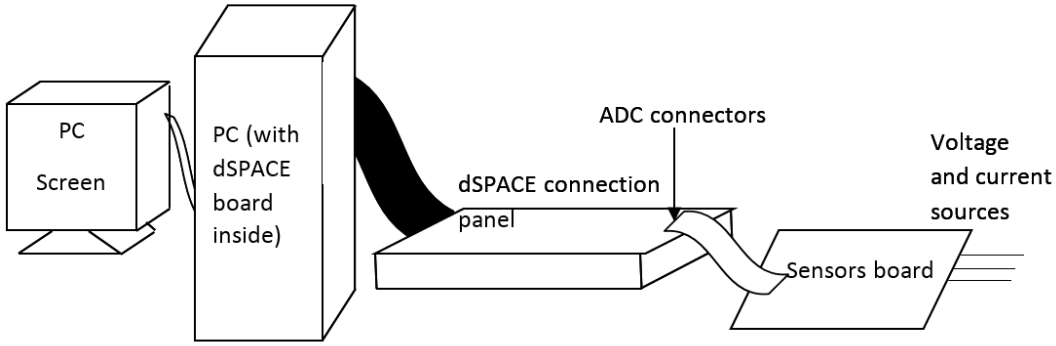

Figure 6.5: Schematic diagram of control and monitoring system

to measure voltage, current and wind speed to feedback the signal to the pc in the Lab. The whole monitoring system contains: current transducers (CT); voltage transducers (VT); wind speed sensor (anemometer); WebCam. The VT/CT board connects with the dSPACE platform and transfer signal to the PC as shown in Figure 6.5.

In Figure 6.5, the sensors board is connected with the voltage and current sources for measuring and sending the output analogue signals to the dSPACE connection panel. The dSPACE board is able to transfer the analogue signals to digital signals and directly display on the connected PC screen. An example of the PC screen monitoring display is shown in Figure 6.6.

Figure 6.7 shows the connection of the VT/CT (voltage transducer type LV25-p, current transducer type LA55-p) circuit board.

The direct measured voltages are the generator output voltage Vab, Vbc, and Vca. Besides voltage and current measurement, the wind speed is also measure by an anemometer on the department roof (Figure 6.8). It is also connected with the dSPACE to display the value on the PC screen (Figure 6.6).

Figure 6.8 also shows that there is a webcam installed on the roof to monitor the condition of the turbines. And the webcam image was sent to the internet. So that by typing in the password, the webcam image can be monitored on any PC in the university.

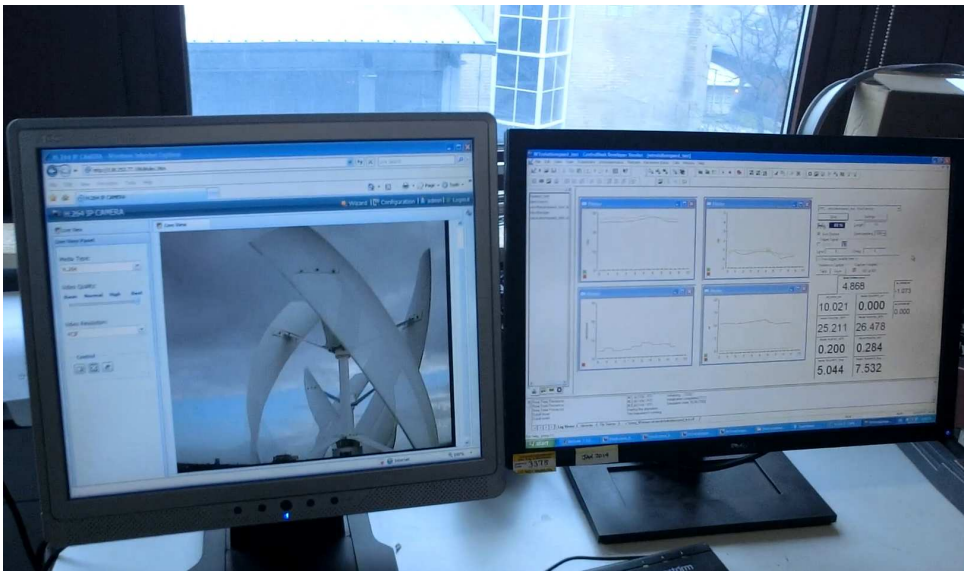

Figure 6.6: The monitoring screen through the WebCam and dSPACE

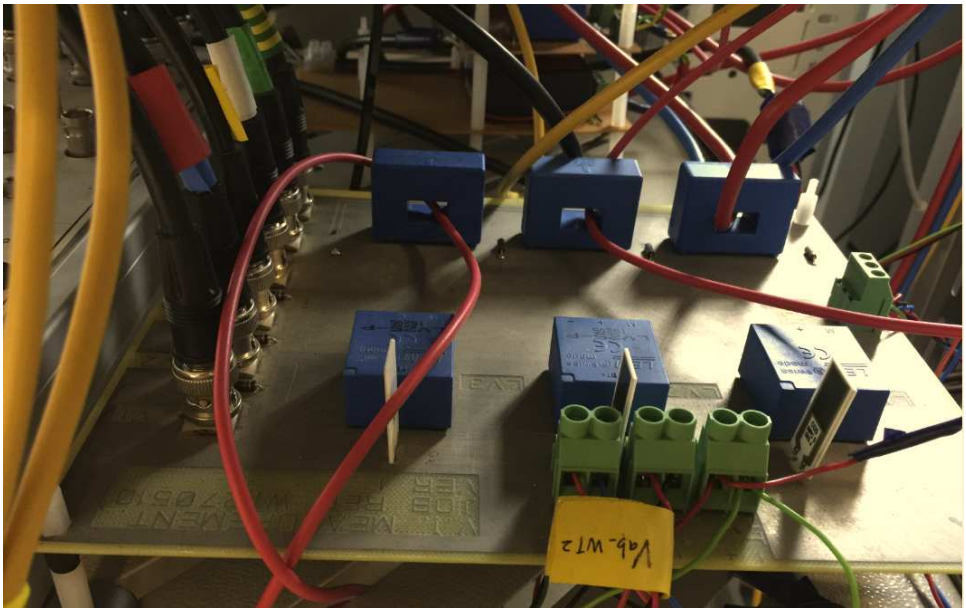

Figure 6.7: VT/CT circuit board for voltage and current measurement

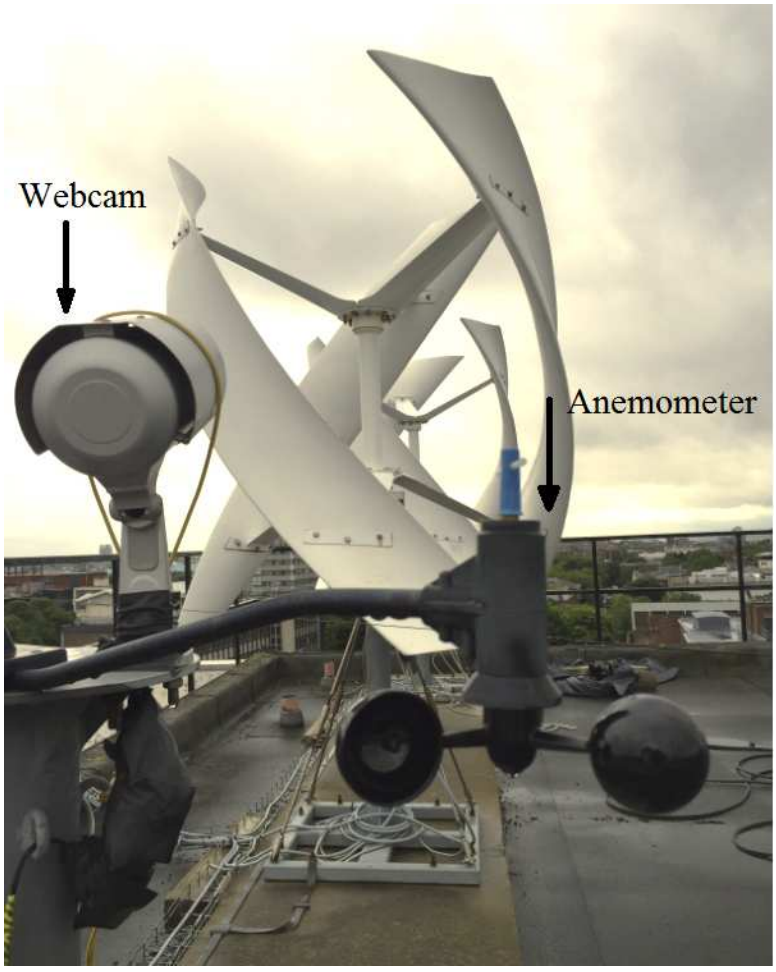

Figure 6.8: Anemometer and webcam on the roof for wind speed measurement and wind turbine monitoring

6.1.2 Condition monitoring system

Phase voltage calculation

To save the connection pins, not all values need to be measured. Some of them can be estimated. For example, as:

$$V_{ab} + V_{bc} + V_{ca} = 0 \tag{6.1.1}$$

Then Vca can be calculated by the value of V_{ab} and V_{bc}. The phase voltage V_a, V_b and V_c have a relation:

$$V_a + V_b + V_c = 0 \tag{6.1.2}$$

From Equation (6.1.1) and (6.1.2), the phase voltages V_a, V_b and V_c can be calculated by:

$$\begin{cases} V_a = \frac{2V_{ab}+V_{bc}}{3} \\ V_b = \frac{V_{bc}-V_{ab}}{3} \\ V_c = \frac{-(V_{ab}+2V_{bc})}{3} \end{cases} \tag{6.1.3}$$

In this way, by measuring V_{ab} and V_{bc}, the value of V_{ac}, V_a, V_b and V_c can all be calculated.

Figure 6.9 is the screen shot of the monitoring module in Matlab Simulink.

Wind turbine rotational speed estimation

Both AC and DC generators produce a frequency that is proportional and linear to the rotational speed of the generator shaft. By measuring this frequency it is possible to measure the rotation speed of the generator without the use of a conventional tachometer. This is achieved through the use of a resistor/capacitor high pass filter. The pure AC signal is then fed into a frequency to voltage converter which outputs a DC voltage proportional to the input frequency. The voltage is then boosted by an amplifier and high frequency noise is removed by a low pass filter.

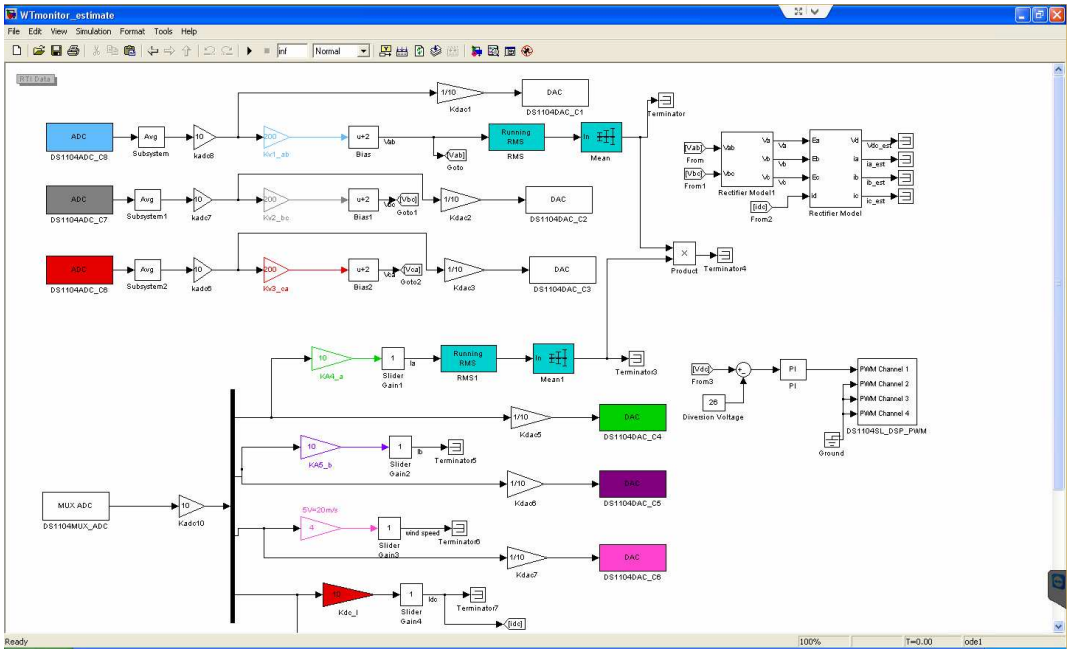

Figure 6.9: The monitoring module for long term running and recording

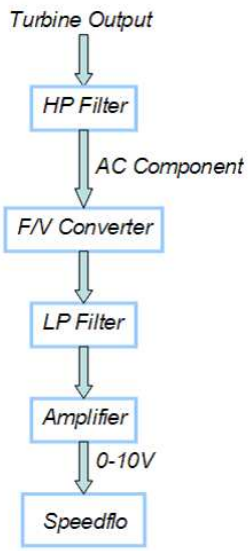

Figure 6.10: Rotational speed measurement signal flow diagram

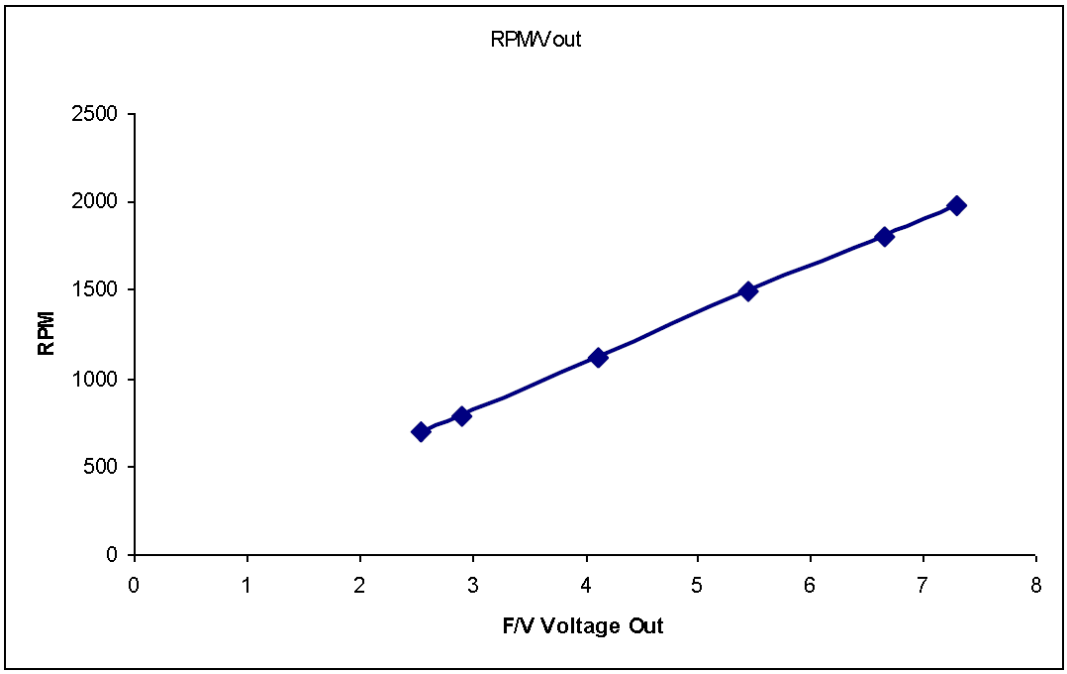

Figure 6.11: Relationship between RPM and rotation speed measurement voltage output

The output from the rotational speed measurements were validated by comparing the voltage output to the RPM read by an optical tachometer at increasing wind speed.

The results demonstrate that there is a clear linear and proportional relationship between the rotational speed measurement voltage output and the actual rotational speed.

Data acquisition and condition monitoring system

The hardware implementation architecture is shown in Figure 6.12. The wind turbines and generators are installed on the roof of the building. The turbines with generators are connected to the dSPACE data collection system in the lab for data measurement and collection, which forms a simple data acquisition system. The data is collected and then distributed by a data distribution server. In another lab, several PCs are set as the server in the same local area network. Users can access the the application for data monitoring using their PCs, mobile phones and tablet

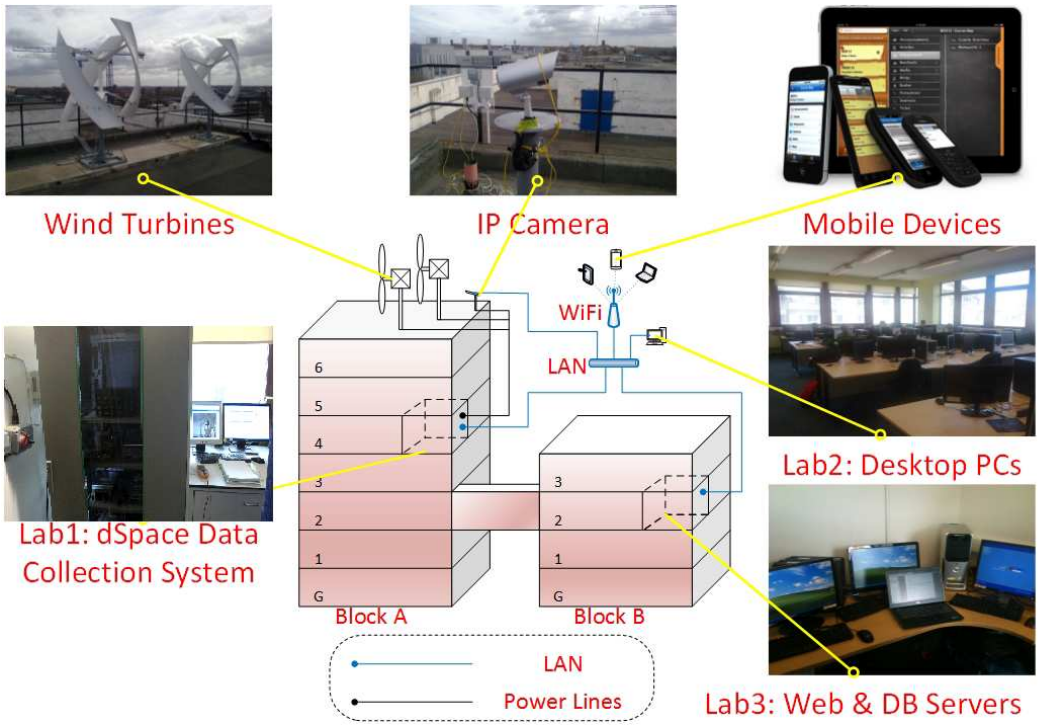

Figure 6.12: Hardware implementation platform with data acquisition system

devices by wired or wireless connection with the LAN. The web camera also connected to the network that works together with web server to provide the real-time image display of wind turbines.

The data acquisition system with real-time data publisher is shown in Figure 6.13. The data acquisition and condition monitoring system include data measurement, dSPACE control panel board, and MATLAB/SIMULINK environment.

6.1.3 Controller and power electronics

The controller and power electronics in prototype WPGS is the same as in Chapter 5. The schematic diagram of control the prototype WPGS is shown in Figure 5.3. The measurement of voltage and current transfers to the data acquisition system. Then the value of ω_m, I_{dc}, V_{in} and V_o can be got and transfer in the control system. The controller outputs duty cycle D to the IGBT switch in the DC-DC boost converter.

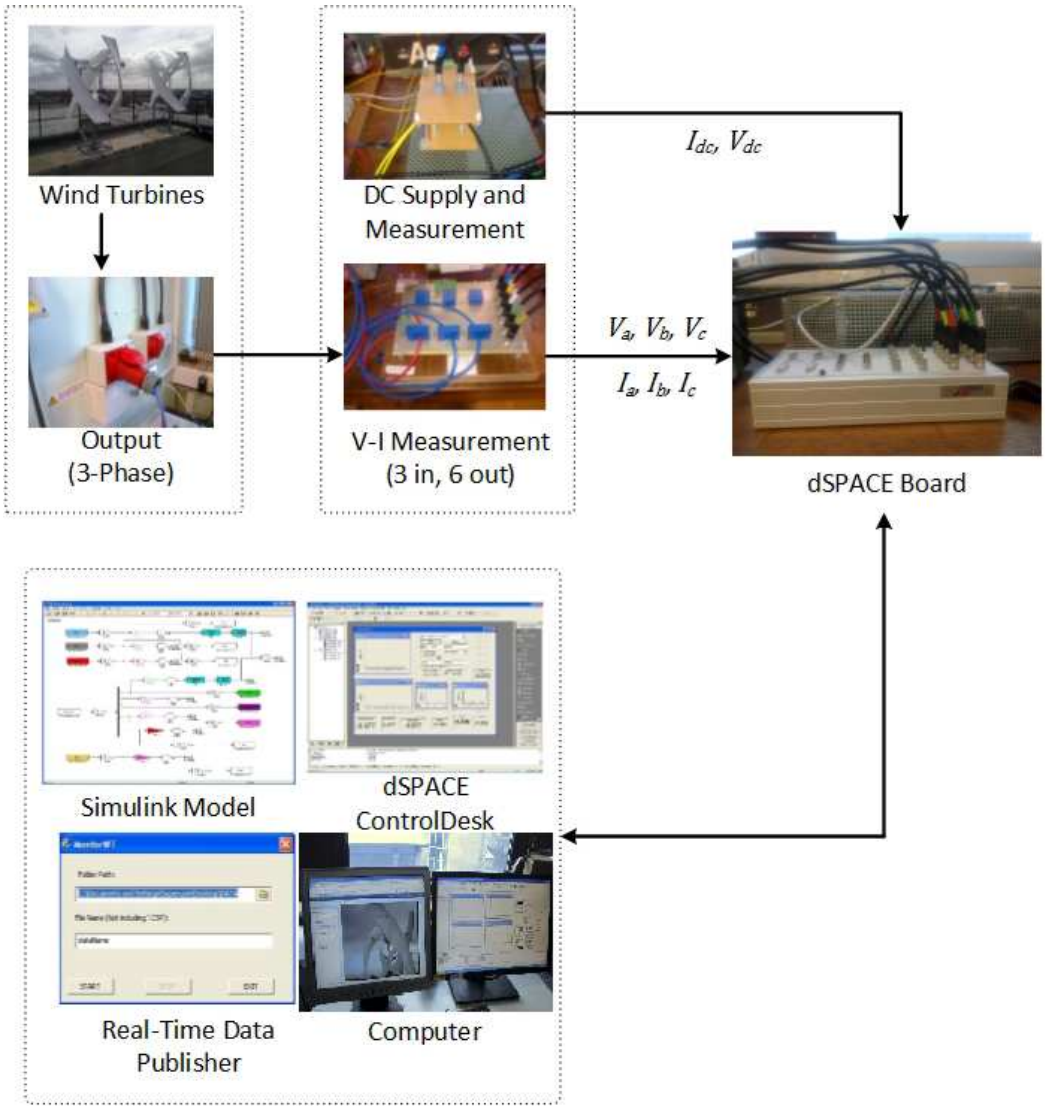

Figure 6.13: Data acquisition system with dSPACE

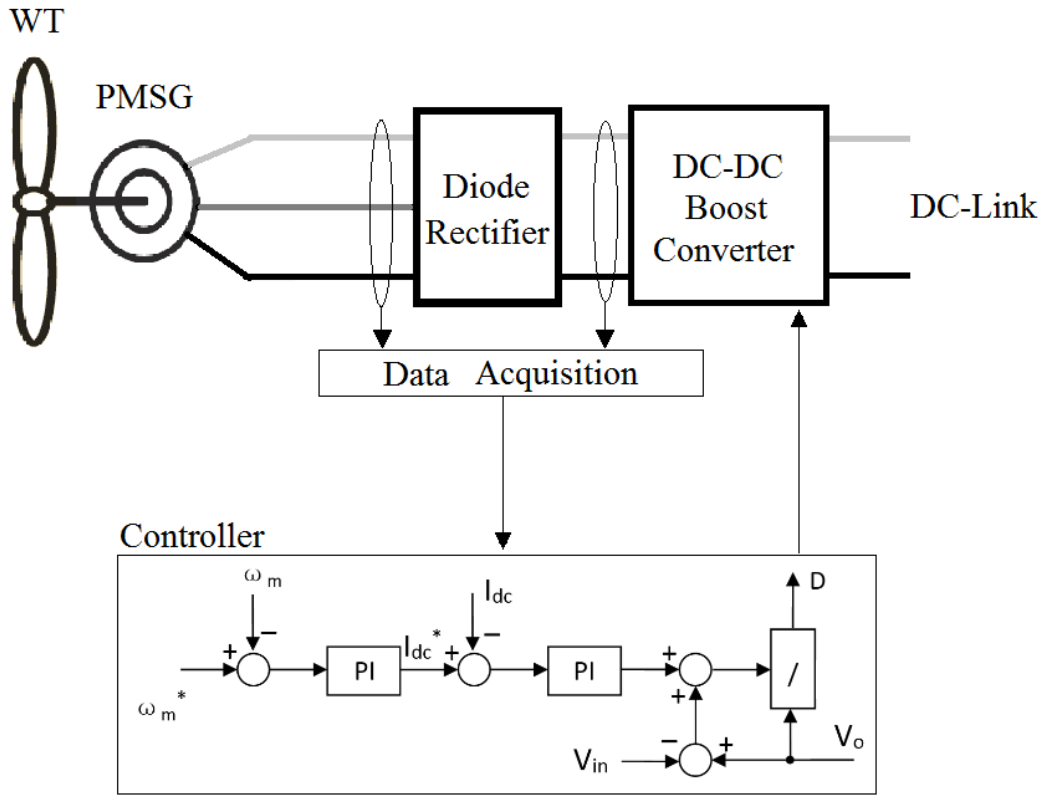

Figure 6.14: The schematic diagram of control the prototype WPGS

6.2 Experiments Design and Set-Up

6.2.1 The comparison experiment of charging battery

Because there are two wind turbines with their generators and one anemometer to measure wind speed on the roof. For the comparison experiment, the two turbine generators are connected with different energy conversion systems in the lab. One is with designed conversion system and controller; the other is with the turbine's original controller. They both are charging batteries. The experiments aim to compare the two turbines generation systems performance. The schematic diagram of experiment hardware setting is shown in Figure 6.15.

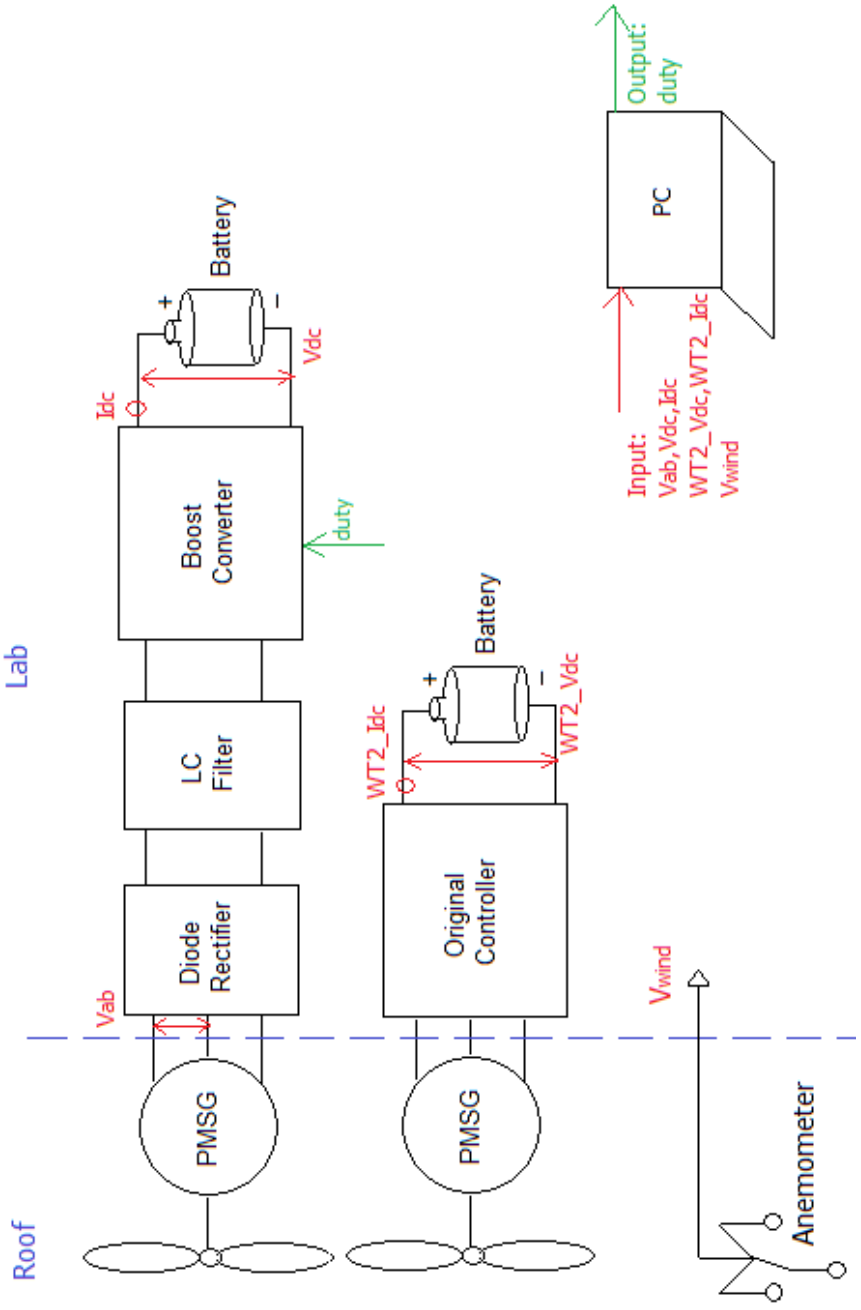

Figure 6.15: The schematic diagram of prototype hardware for controller comparison

The variables in red are measured and send to the PC. The controller calculates the value of duty based on the inputs and sends to the converter to control the turbine. The control objective is maximum power point tracking. The experiment is designed to compare the power charging the batteries from the two turbines.

Figure 6.16 is the schematic block diagram of comparing the two generation systems of generating power transferred to charge the batteries. The wind turbine 1 (WT1) is connected with the designed DC/DC converter hardware which was mentioned in Chapter 6. The wind turbine 2 (WT2) is connected with the original controller. Both the two turbines are connected to charging the same type of battery.

6.2.2 The comparison experiment of power transfer to the grid by inverters

Figure 6.17 shows the diagram of the two turbines' experiment connection. Different from Figure 6.16 in Section 2.1, in Figure 6.17 the two turbines are both connected with grid side inverter and the generated power are transferred to the grid.

6.3 Experiments Results

6.3.1 Two wind turbines rotational speed comparison

The experiment of comparing the two wind turbines rotational speed is to verify that when the two turbine are both connected with their original controllers in the same environment, their operation and generation would be almost the same.

Figure 6.18 shows the comparison of the two turbines in 2 hours. From the results, it shows that the total rotating time of WT1 is a little bit more than WT2. By comparing the results in time=3000 to 4000 (Figure 6.19), the time of turbines charging batteries are similar. Comparing $K = Pe/\omega_r^3$ and $K_v = Pe/v^3$ of the turbines, their values are very similar. It means when the system are charging the batteries, the power coefficient of the two turbines are almost the same. From the turbine's datasheet, the estimated optimal value of K is 0.072 and the estimated op-

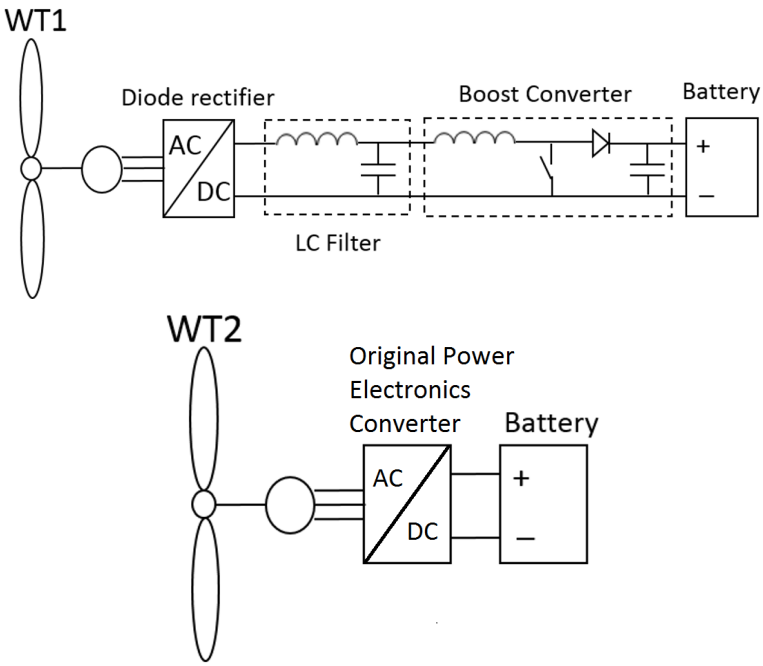

Figure 6.16: Experiment of generated power transferred to charge the batteries

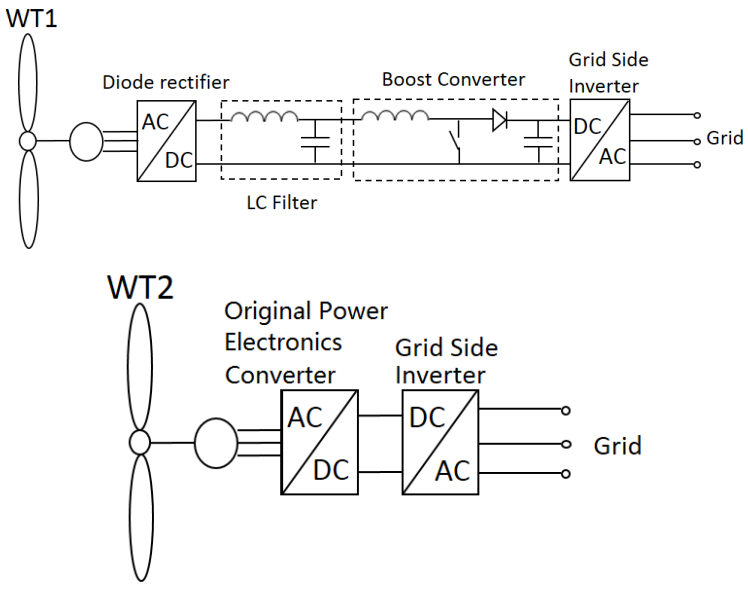

Figure 6.17: Experiment of generated power transferred to the grid

timal value of K_v is 0.38. The experiment results are much lower than the estimated optimal values.

From the two wind turbines rotational speed comparison results, it can be seen that when the two turbines are both connected with their original controllers in the same environment, their operation are quite similar. Thus, further experiments can be done for one wind turbine with different control and conversion system and compare to the other wind turbine with the original control and conversion system.

6.3.2 PSF control experiment results

The amount of mechanical power captured from wind by a wind turbine could be formulated as:

$$P_m = \frac{1}{2}\rho A C_p v^3 \tag{6.3.1}$$

where, ρ is the air density, A is the wind turbine swept area, C_p is the wind turbine power coefficient, v is the wind speed. Therefore, if the air density, swept area, and wind speed are constant the output power of the turbine will be a function of power coefficient of the turbine. As the power coefficient maximum value and the C_{p-TSR} curve of the roof turbine is unknown, we assume C_p is a constant as well. Thus from equation(6.3.1) we can get:

$$P_e = K v^3 \tag{6.3.2}$$

Assume there is no loss during the transportation, the input power should be equal to the output power:

$$P_e = V_i I_i = V_o I_o \tag{6.3.3}$$

Combine equation(6.3.2) and (6.3.3), it can be deduced that:

$$I_i = K\frac{v^3}{V_i} \tag{6.3.4}$$

From the equations above, the boost converter control algorithm used in the experiment is shown in Figure 6.20.

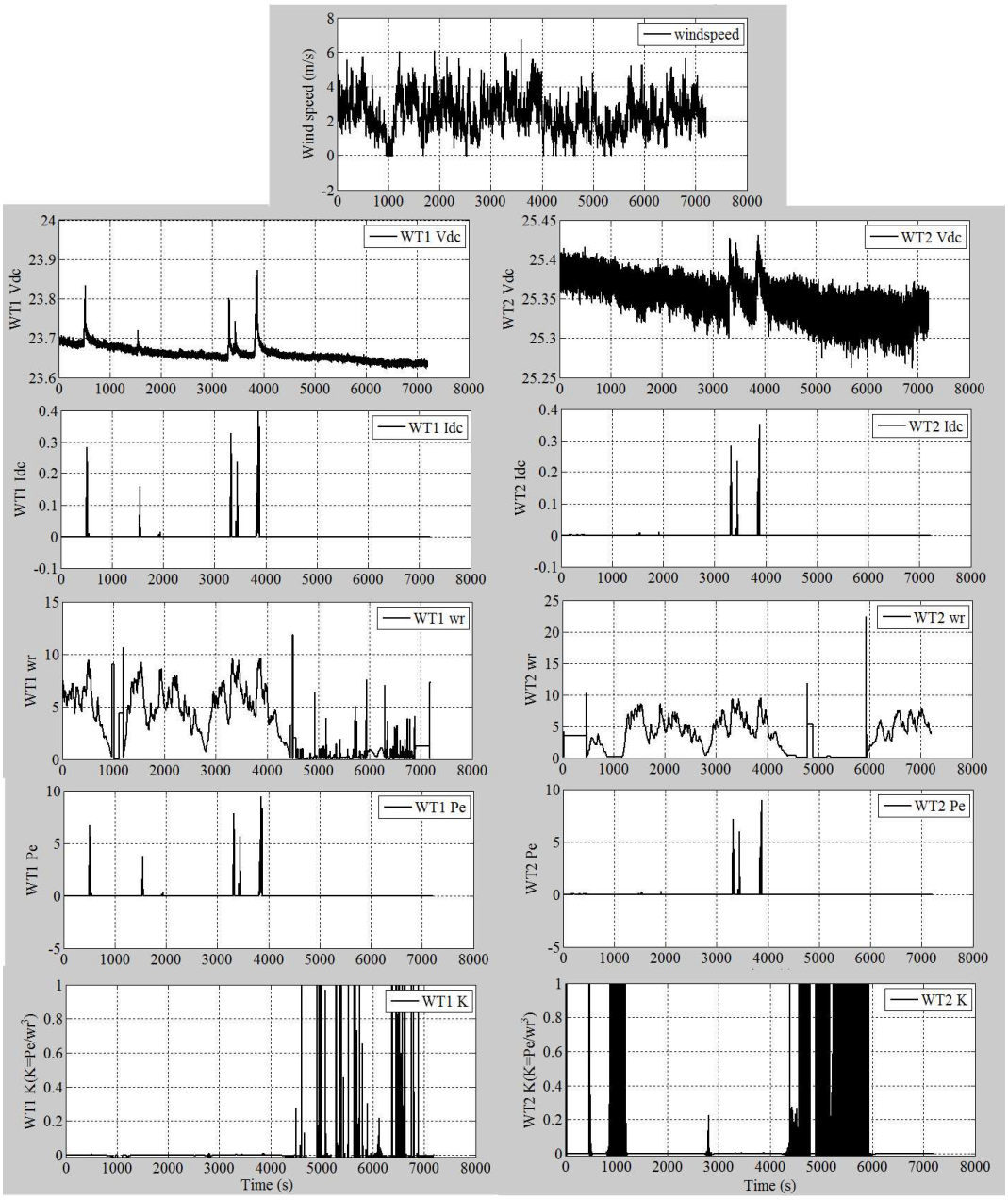

Figure 6.18: Two turbines operating data record in 2 hours

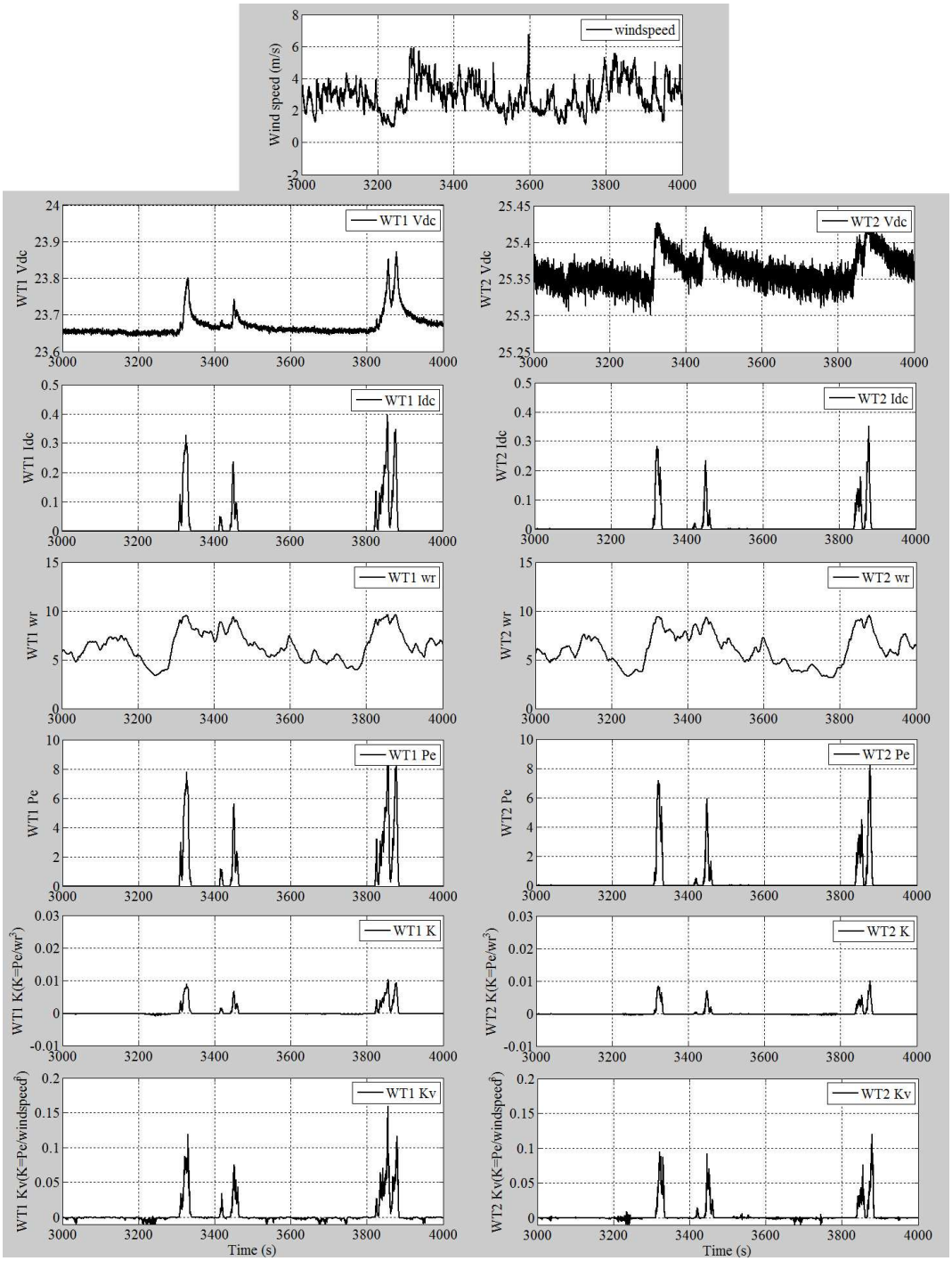

Figure 6.19: Zoom in of Figure 6.18 for time in 3000 to 4000s

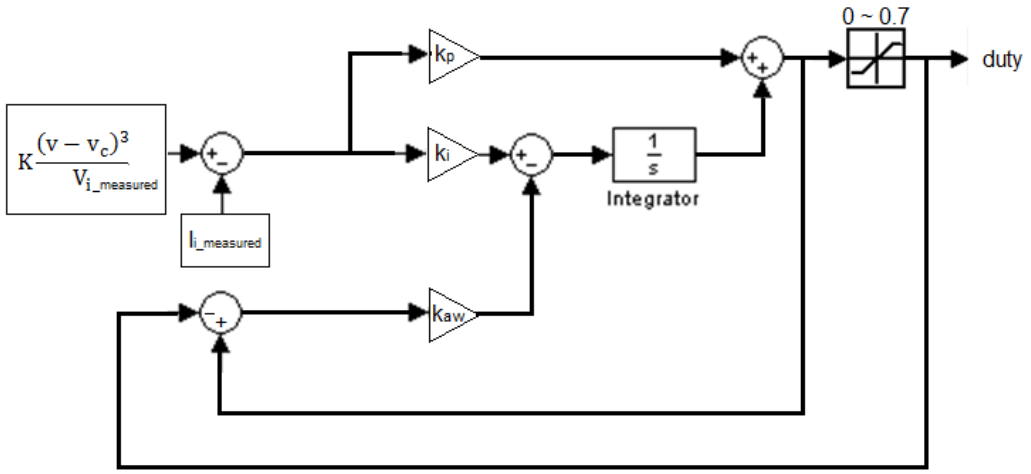

Figure 6.20: PI controller for boost converter in the experiment

Wind Turbine 1 is the one connected with boost converter hardware. Wind Turbine 2 is connected with its original controller. The experiment results of the Wind Turbine 1 is shown in Figure 6.21. Figure 6.22 shows the experiment results of Wind Turbine 2 in the same time.

In Figure 6.21 and 6.22, at t=1.5s, there is a gust wind. The wind speed has a step change. At that moment, WT1 is controlled to increase the current, thus the rotation speed is decreased. WT2 is dropped to dumper as the battery voltage is higher than 28 V. As there is no rotation speed sensor on the two turbines, WT1 $I_{in\_measured}$ can represent the tendency of rotor speed.

At t=9s, the gust wind left. The wind speed is slowly decreasing. WT1 is controlled to decrease the current. Thus the generator torque is decreased. The rotor speed stays at a particular value. While WT2 switches to dumper at t=14 s and no generated power when it switches back to controller.

From the experiment results, we can conclude that the designed diode rectifier and boost converter hardware is suitable for our experiment use. The controller algorithm could be replaced in the future.

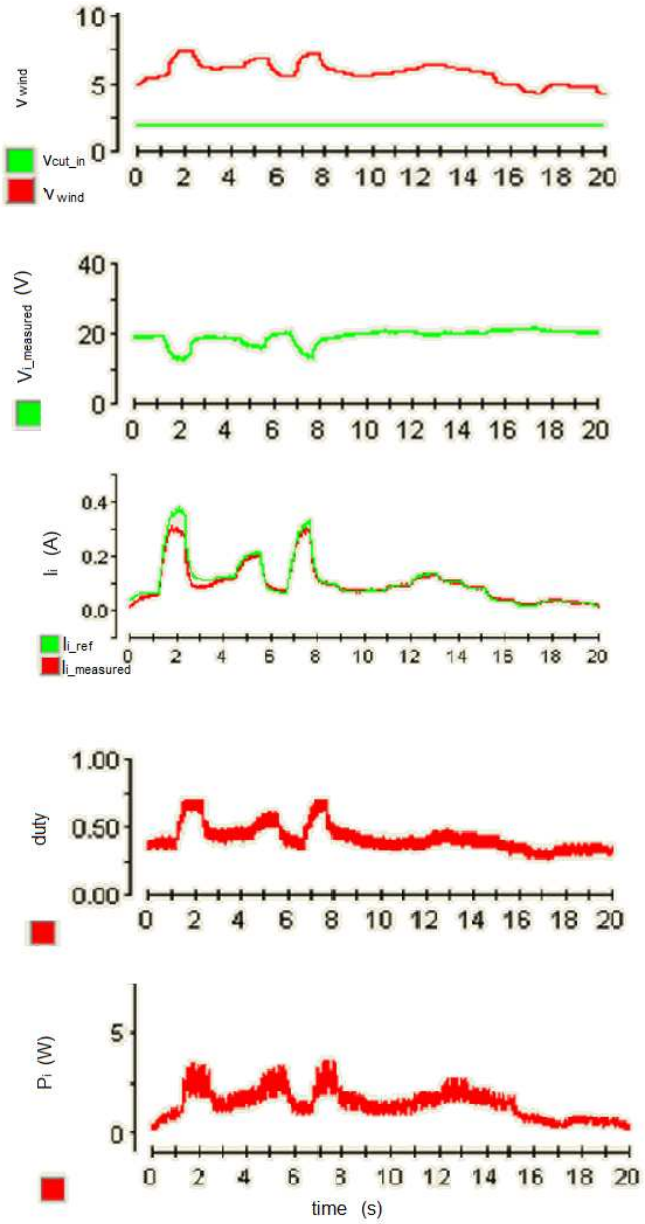

Figure 6.21: Experiment results of wind turbine 1 controlled by PSF method

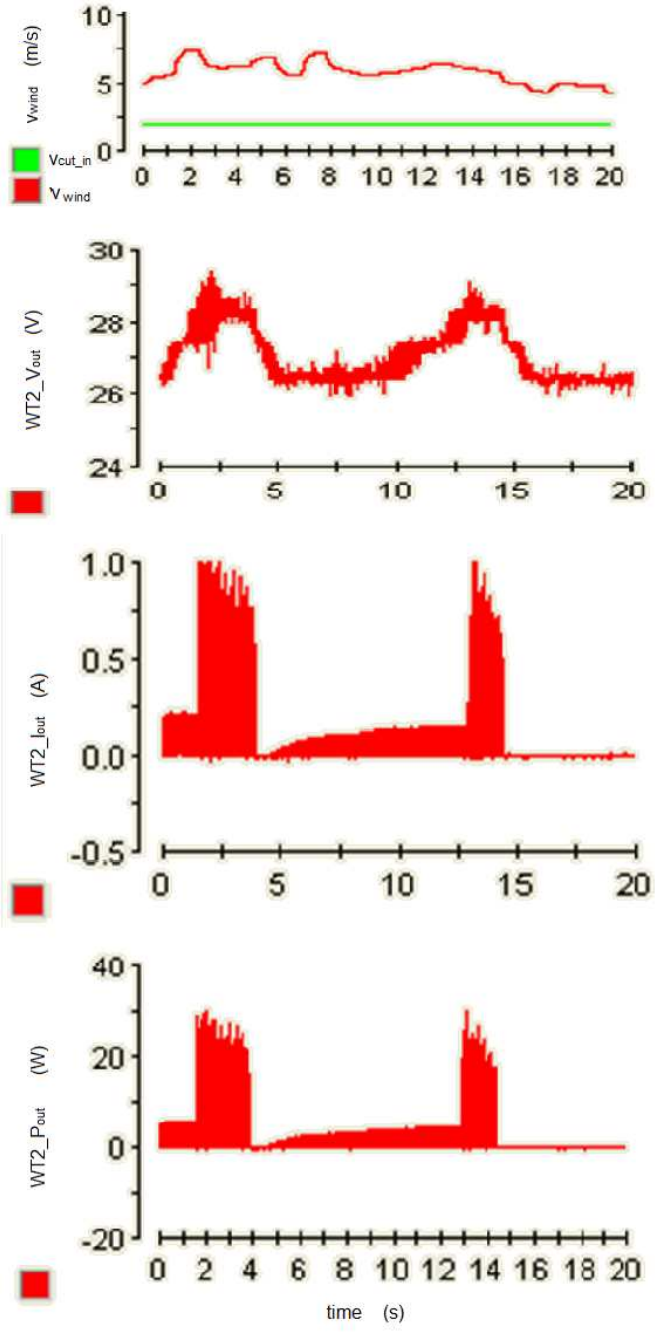

Figure 6.22: Experiment results of wind turbine 2 controlled by the wind turbine original controller

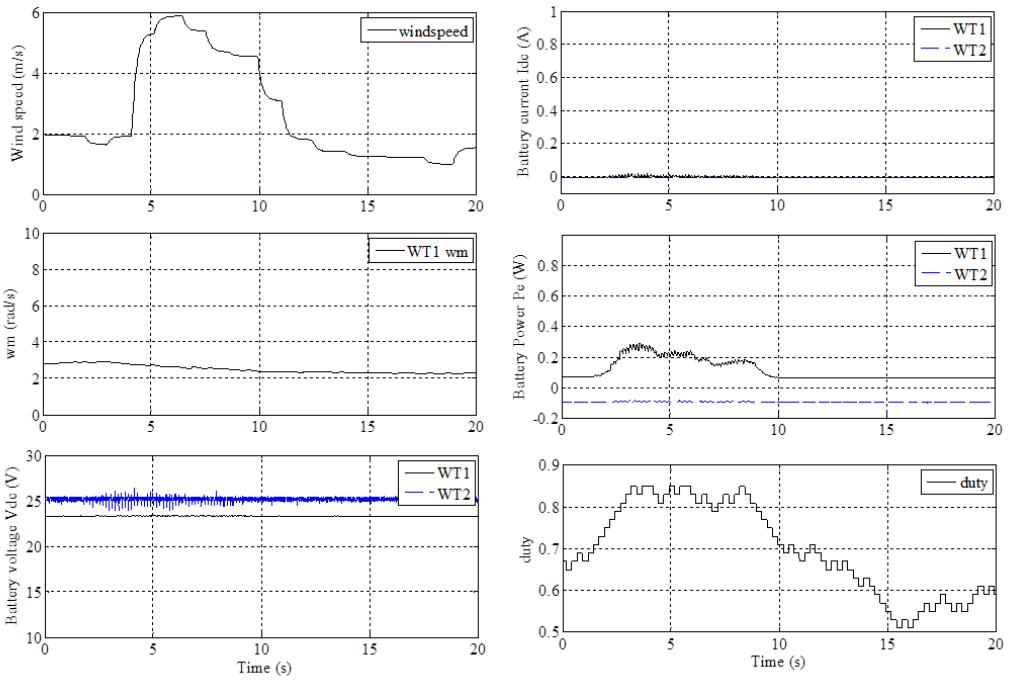

Figure 6.23: Comparison results of two wind turbines operation in a gust wind. WT1 is controlled by HCS method

6.3.3 Conventional HCS control experiment results

Experiments of control wind turbine 1 (WT1) with conventional HCS method and wind turbine 2 (WT2) with its original controller were done. Figure 6.23 and Figure 6.24 are some experiment results. The results show that, when the two turbines are under the same wind environment, the generation of WT1 is affected by controlling the duty cycle of the boost converter to generate more power than WT2. Although the results show that the conventional HCS method is able to control the duty cycle and effect the generating power of WT1. In rapid changing wind speed, conventional HCS method may lose its traceability.

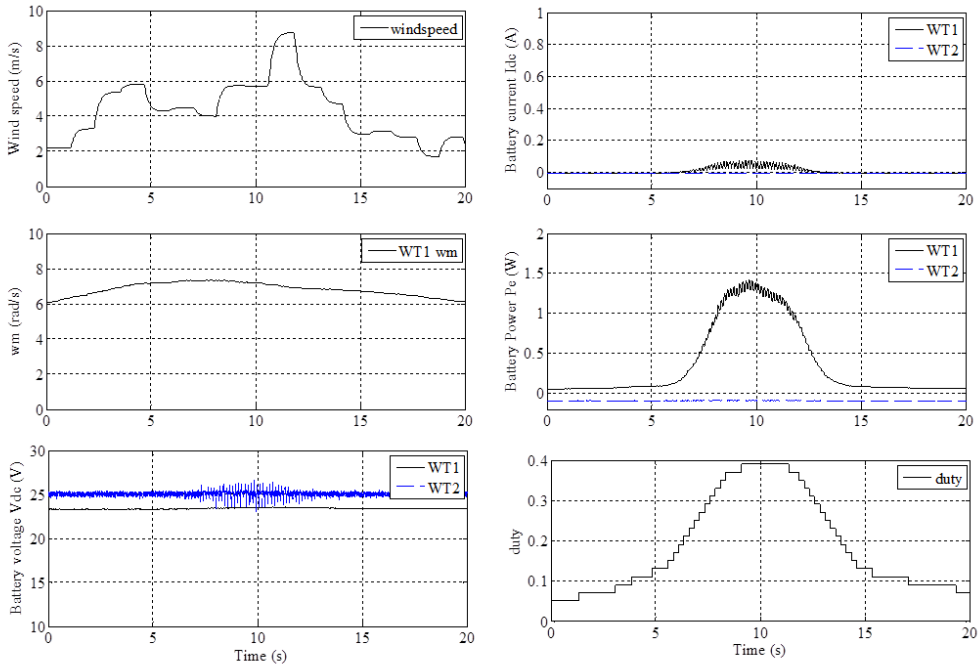

Figure 6.24: Another comparison results of two wind turbines operation in a gust wind. WT1 is controlled by HCS method

Time period	Average wind speed	WT1 generated energy (Wh)	WT2 generated energy (Wh)	E_{nWT1}/E_{nWT2}
18:42 to 20:42	1.82 (m/s)	2.6	0.5	520%
20:42 to 22:42	2.50 (m/s)	7.3	3.3	221.2%
22:42 to 00:42	2.66 (m/s)	9.5	5.9	161%
00:42 to 02:42	2.35 (m/s)	6.8	3.65	186.3%
02:42 to 04:42	2.02 (m/s)	2.9	0.15	/
04:42 to 06:42	1.93 (m/s)	3	0.1	/
06:42 to 08:42	2.44 (m/s)	6.5	3	216.7%
08:42 to 10:42	3.28 (m/s)	15.5	4	387.5%
	Total	54.1	30.5	177.4%

Table 6.3: Generated energy comparison of power transfer to charge the batteries

6.3.4 Long term operating results

The comparison experiment of power transferred to charge batteries

Data was recorded from 18:42 in 10/09/2015 to 10:42 in 11/09/2015. Final results shows that WT1 generated electricity 54.1 Wh and WT2 generated electricity 30.5 Wh. Thus in total WT1 generated 177.4 % electrical energy of WT2. Table 6.3 shows the comparison of the two turbines generated energy in every 2hrs in different average wind speed. From Table 6.3, the experiment results show that the designed controller presents better than the turbines' original controller especially in lower wind speed. More experiment would be done in the future. Table 6.4 shows comparison results in every hour on 22 September. From the results, it can be seen that sometimes WT2 generated more power than WT1 for a short time. This means the controller can be improved in the future to be more efficient.

The comparison experiment of power transferred to the grid

Data was recorded every 10 minutes from 04/09/2015 afternoon to 07/09/2015 morning. The results shows that in about 67hrs the final generated energy of WT1 is 292.3Wh and WT2 is 129Wh. Thus WT1 generated 226.6% electrical energy of

Time period	Average wind speed	WT1 generated energy (Wh)	WT2 generated energy (Wh)	E_{nWT1}/E_{nWT2}
10:02 to 11:02	2.24 (m/s)	0.49	0.45	108.9%
11:02 to 12:02	2.83 (m/s)	1.76	1.2	146.7%
12:02 to 13:02	3.60 (m/s)	5	5.35	93.5%
13:02 to 14:02	4.93 (m/s)	11.3	14.9	75.8%
14:02 to 15:02	4.95 (m/s)	4	4.2	95.2
	Total	22.55	25.65	88%

Table 6.4: Generated energy comparison of power transfer to charge the batteries in 22/09

WT2. Table 6.5 shows the comparison of the two turbines generated energy in every 6hrs with different wind speed.

From Table 6.5, it shows that WT1 always generates more electricity than WT2, especially in low wind speed.

Time period	Average wind speed	WT1 generated energy (Wh)	WT2 generated energy (Wh)	E_{nWT1}/E_{nWT2}
15:50 to 21:50	4.86 (m/s)	78	50.5	154.5%
21:50 to 9:50	3.77 (m/s)	52	28.5	182.5%
9:50 to 15:50	1.40 (m/s)	7	1	700%
15:50 to 21:50	2.39 (m/s)	10.5	5.5	190.9%
21:50 to 9:50	2.50 (m/s)	24.9	8.6	289.5%
9:50 to 15:50	2.27 (m/s)	10.1	1.9	531.6%
15:50 to 21:50	2.72 (m/s)	21.5	4	537.5%
21:50 to 9:50	3.24 (m/s)	32	10	320%
9:50 to 15:50	3.54 (m/s)	40	15	266.7%
15:50 to 21:50	2.48 (m/s)	24	4	600%
21:50 to 9:50	0.64 (m/s)	2	1	200%
	Total	302	130	232.3%

Table 6.5: Generated energy comparison of power transfer to the grid experiments

6.4 Conclusions

This chapter has illustrated the prototype experiment platform and monitoring system. The experiment results shows the installed hardware works well with the roof turbine. From the long term comparison results, it can be concluded that the wind turbine with designed hardware and control system can capture more power from wind than the wind turbine with its original controller.

Chapter 7

Conclusions and Future Work

This chapter has summarised the results obtained in this thesis and contributions. At the end of this chapter, suggestions for future investigations are also listed.

7.1 Conclusions

This thesis aims to develop maximum power control for PMSG-based WPGS. In industry, wind power generation systems require controllers to smoothly switch between different control objectives in different regions and capture maximum power from the wind when the wind speed is low. This thesis discussed the development of wind turbine controllers on different aspects: the switching between different operating regions and control objectives; the HCS method to achieve MPPT, the detection of optimal power-speed curve and experimental verification.

At the beginning of this thesis, the overview and typical configuration and components of wind power generation systems have been presented. Different MPPT methods have been reviewed. This thesis has focused on the operation and control of PMSG based WPGSs.

In Chapter 2, a method for controlling a variable speed wind turbine over its complete operating wind speed regions has been presented. The control method attempts to minimise structure and mechanical loading while maximising energy conversion from the wind. This involved designing a switching logic to enable s-

mooth switching between different control objectives of torque controllers and pitch controllers. All these controllers used PDF control algorithm for smoothing performance and simplifying parameter tuning process. The simulation of a wind turbine with a hardware-in-the-loop industrial controller, that uses the presented switching logic, demonstrates good results; the switching is smooth between different control objectives over a large wind speed range. In the three operation regions, Region 1 aims to capture maximum power from the wind. This region determines the WPGS generated power in low wind speed. HCS method and PSF method are two methods generally used in industry. Chapter 2 and 3 are mainly discussing the development in these two methods.

In Chapter 3, a hybrid HCS algorithm for wind speed sensorless maximum power point tracking of wind turbine generation systems under varying wind speeds has been presented. The proposed algorithm introduces a new detection method of wind speed variation and combines it with the conventional HCS algorithm. It can obtain a real-time optimal power curve coefficient based on the optimal power under constant wind condition. The simulation compares the proposed hybrid HCS algorithm and the conventional HCS algorithm method on a PMSG based wind turbine. Under rapidly changing wind speeds, the proposed hybrid HCS algorithm performs much better in tracking the maximum power coefficient without the requirement of directly sensing wind speed and knowing wind turbine characteristics.

In Chapter 4, a new method to detect the optimal power-speed curve of a wind turbine under natural variable wind speed conditions has been proposed. The method obtains the maximum power points by controlling the WPGS in specified constant rotational speed and recording the power and wind speed at the same time. Methods to estimate accurate MPP values and accelerate the detection time were proposed. After the recording of the operating data and calculating the optimal power-speed curve, the WPGS is controlled based on the obtained optimal power-speed curve to achieve MPPT. The optimal power-speed curve detected by the proposed method can also improve the MPPT performance and increase the WPGS energy generation when an inaccurate optimal power-speed curve was used in PSF. This proposed method does not require the system pre-knowledge and can obtain accurate optimal

power-speed curve under natural variable wind speed conditions. The accuracy of the detected optimal power-speed curve and k_{opt} is about 97%. MATLAB/Simulink simulation and practical results confirm the validity and performance of the proposed method. Future work will focus on the design of a wind speed observer to remove the requirement of measuring wind speed, and the field test of the proposed algorithm on a real wind turbine.

Power electronics plays an important role in WPGSs. In Chapter 5, it represents the diode rectifier with DC-DC boost converter as the generator-side converter in a WPGS. The operation and model of a DC-DC boost converter have been given. The implementation of the designed generator-side converter has been tested in hardware-in-the-loop experiments. Both simulation and experiment results verified the designed DC-DC boost converter is reliable, efficient and suitable to be used in the PMSG based WPGS.

The proposed wind turbine control methods and power electronics hardware need to be verified in hardware experiments. Chapter 6 has illustrated the prototype experiment platform and monitoring system. The experiment results show the installed hardware works well with the roof turbine. From the long-term comparison results, it can be concluded that the wind turbine with designed hardware and control system can capture more power from the wind than the wind turbine with its original controller.

In conclusion, the study in this thesis contributes on developing the control of PMSG based WPGSs. A switching logic has been proposed to smooth switch between different control strategies and avoid sudden changes in WPGS. In the first operation region, the control objective is to achieve MPPT. Thus, a developed HCS method has been proposed which can detect wind speed variation from the operating data analysis thus to avoid the misleading of conventional HCS method during variable wind speed. Besides, a method has been proposed for wind turbines to on-site detect the optimal power-speed curve. With an accurate optimal power-speed curve, the WPGS can efficiently achieve MPPT by PSF control. To verify the proposed methods, a designed power electronics hardware has been tested with a PMSG based WPGS and finally implemented in a small scale prototype WPGS.

Nevertheless, there are some further research can continue in the future.

7.2 Future Work

- The proposed smooth switch method in Chapter 2 can combine with the different MPPT methods to adapt different WPGSs. Also, some parameters in the switching logic need to be set before operating. The parameter values can affect the switching results and the mechanical load. Besides, the twist angle in the wind turbine drive train can be presented and compared with other switching methods.

- In Chapter 3, the developed HCS method can solve the problem of miss-trackable of conventional HCS method in variable wind speed. The setting of the HCS step size and parameters in the wind speed variation detection need to be developed more adaptively. Besides, the method can be developed to capture accurate k_{opt} value and calibrate the value during the WPGS normal operating.

- In Chapter 4, the method to detect the optimal power curve needs wind speed as a reference. In the future, a wind speed observer will be added. By detecting the wind speed variation and estimating the wind speed value, the optimal power curve detection method can be developed sensorless. Also, the method needs to collect data in different wind speed and the system needs to wait for wind speed change. This makes the detection time undetermined. In the future, the method to detect the wind turbine optimal power curve in a fixed time can be designed and verified.

- The hardware implemented in Chapter 5 can be combined with a grid-side converter together. The grid-side converter can be implemented with PWM-VSC and controller for grid-side converter should be designed and combined with the previous system. Besides, back-to-back converter configuration can be implemented to compare with the diode rectifier and boost converter.

- The prototype implemented in Chapter 6 used to compare the wind turbine original power electronics and controller with the implemented power electronics and PSF control. The developed HCS method can be applied to the control system thus verifying it in the prototype experiments. In the future, different control methods and power electronics configurations can be compared by using the prototype wind turbines.

References

[1] Dennis YC Leung and Yuan Yang. Wind energy development and its environmental impact: a review. *Renewable and Sustainable Energy Reviews*, 16(1):1031–1039, 2012.

[2] Olimpo Anaya-Lara, Nick Jenkins, Janaka Ekanayake, Phill Cartwright, and Michael Hughes. *Wind energy generation: modelling and control*. John Wiley & Sons, 2011.

[3] L Fried. Global wind statistics 2015. 2016.

[4] Thomas Ackermann et al. *Wind power in power systems*, volume 140. Wiley Online Library, 2005.

[5] SH Chichester. Grid integration of wind energy conversion systems, 1999.

[6] Vladislav Akhmatov. *Induction generators for wind power*. Multi-Science Pub., 2005.

[7] Brendan Fox. *Wind power integration: connection and system operational aspects*, volume 50. Iet, 2007.

[8] L Holdsworth, XG Wu, JB Ekanayake, and N Jenkins. Comparison of fixed speed and doubly-fed induction wind turbines during power system disturbances. *IEE Proceedings-Generation, Transmission and Distribution*, 150(3):343–352, 2003.

[9] Zhe Chen, Josep M Guerrero, and Frede Blaabjerg. A review of the state of

the art of power electronics for wind turbines. *IEEE Transactions on power electronics*, 24(8):1859–1875, 2009.

[10] Set Muller, M Deicke, and Rik W De Doncker. Doubly fed induction generator systems for wind turbines. *IEEE Industry applications magazine*, 8(3):26–33, 2002.

[11] Lie Xu and Yi Wang. Dynamic modeling and control of dfig-based wind turbines under unbalanced network conditions. *IEEE Transactions on Power Systems*, 22(1):314–323, 2007.

[12] James F Manwell, Jon G McGowan, and Anthony L Rogers. *Wind energy explained: theory, design and application*. John Wiley & Sons, 2010.

[13] Tony Burton, David Sharpe, Nick Jenkins, and Ervin Bossanyi. *Wind energy handbook*. John Wiley & Sons, 2001.

[14] Vladislav Akhmatov, Arne Hejde Nielsen, J Kaas Pedersen, and Ole Nymann. Variable-speed wind turbines with multi-pole synchronous permanent magnet generators. part i: Modelling in dynamic simulation tools. *Wind Engineering*, 27(6):531–548, 2003.

[15] Kathryn E Johnson, Lucy Y Pao, Mark J Balas, and Lee J Fingersh. Control of variable-speed wind turbines: standard and adaptive techniques for maximizing energy capture. *IEEE control systems*, 26(3):70–81, 2006.

[16] Tore M. Undeland Ned Mohan and William P. Robbins. *Power electronics: converters, applications, and design*. John Wiley & Sons, 2003.

[17] Lars Henrik Hansen, Lars Helle, Frede Blaabjerg, E Ritchie, Stig Munk-Nielsen, Henrik W Bindner, Poul Ejnar Sørensen, and Birgitte Bak-Jensen. Conceptual survey of generators and power electronics for wind turbines. Technical report, 2002.

[18] Bin Wu, Yongqiang Lang, Navid Zargari, and Samir Kouro. *Power conversion and control of wind energy systems*. John Wiley & Sons, 2011.

[19] Ricardo J. Mantz Fernando D. Bianchi, Hernan De Battista. Wind turbine control systems. principles, modelling and gain scheduling design. fernando d. bianchi, hernán de battista and ricardo j. mantz, springer, london, 2006., 2006.

[20] WE Leithead, S De la Salle, and D Reardon. Role and objectives of control for wind turbines. In *IEE Proceedings C-Generation, Transmission and Distribution*, volume 138, pages 135–148. IET, 1991.

[21] Poul Ejnar Sørensen, Anca Daniela Hansen, Florin Iov, Frede Blaabjerg, and Martin H Donovan. Wind farm models and control strategies. Technical report, 2005.

[22] EA Bossanyi. The design of closed loop controllers for wind turbines. *Wind energy*, 3(3):149–163, 2000.

[23] WE Leithead and Bill Connor. Control of variable speed wind turbines: design task. *International Journal of Control*, 73(13):1189–1212, 2000.

[24] Thommy Ekelund. Yaw control for reduction of structural dynamic loads in wind turbines. *Journal of Wind Engineering and Industrial Aerodynamics*, 85(3):241–262, 2000.

[25] Jianzhong Zhang, Ming Cheng, Zhe Chen, and Xiaofan Fu. Pitch angle control for variable speed wind turbines. In *Electric Utility Deregulation and Restructuring and Power Technologies, 2008. DRPT 2008. Third International Conference on*, pages 2691–2696. IEEE, 2008.

[26] Karl Stol and Mark Balas. Periodic disturbance accommodating control for speed regulation of wind turbines. In *ASME 2002 Wind Energy Symposium*, pages 310–320. American Society of Mechanical Engineers, 2002.

[27] Lucy Y Pao and Kathryn E Johnson. Control of wind turbines. *IEEE Control Systems*, 31(2):44–62, 2011.

[28] Jason H Laks, Lucy Y Pao, and Alan D Wright. Control of wind turbines: Past, present, and future. In *2009 American Control Conference*, pages 2096–2103. IEEE, 2009.

[29] Dipesh Kumar and Kalyan Chatterjee. ”a review of conventional and advanced mppt algorithms for wind energy systems”. *Renewable and Sustainable Energy Reviews*, 55:957–970, 2016.

[30] MA Abdullah, AHM Yatim, CW Tan, and R Saidur. ”a review of maximum power point tracking algorithms for wind energy systems”. *Renewable and sustainable energy reviews*, 16(5):3220–3227, 2012.

[31] Shravana Musunuri and HL Ginn. Comprehensive review of wind energy maximum power extraction algorithms. In *2011 IEEE power and energy society general meeting*, pages 1–8. IEEE, 2011.

[32] Syed Muhammad Raza Kazmi, Hiroki Goto, Hai-Jiao Guo, and Osamu Ichinokura. ”review and critical analysis of the research papers published till date on maximum power point tracking in wind energy conversion system”. In *2010 IEEE Energy Conversion Congress and Exposition*, pages 4075–4082. IEEE, 2010.

[33] M Nasiri, J Milimonfared, and SH Fathi. Modeling, analysis and comparison of tsr and otc methods for mppt and power smoothing in permanent magnet synchronous generator-based wind turbines. *Energy Conversion and Management*, 86:892–900, 2014.

[34] Shigeo Morimoto, Hideaki Nakayama, Masayuki Sanada, and Yoji Takeda. Sensorless output maximization control for variable-speed wind generation system using ipmsg. In *Industry Applications Conference, 2003. 38th IAS Annual Meeting. Conference Record of the*, volume 3, pages 1464–1471. IEEE, 2003.

[35] Haritza Camblong, I Martinez de Alegria, M Rodriguez, and G Abad. Ex-

perimental evaluation of wind turbines maximum power point tracking controllers. *Energy Conversion and Management,* 47(18):2846–2858, 2006.

[36] Abdeldjalil Dahbi, Mabrouk Hachemi, Nasreddine Nait-Said, and Mohamed-Said Nait-Said. Realization and control of a wind turbine connected to the grid by using pmsg. *Energy Conversion and Management*, 84:346–353, 2014.

[37] Ki-Yong Oh, Joon-Young Park, Jun-Shin Lee, and JaeKyung Lee. Implementation of a torque and a collective pitch controller in a wind turbine simulator to characterize the dynamics at three control regions. *Renewable Energy*, 79:150–160, 2015.

[38] Eftichios Koutroulis and Kostas Kalaitzakis. ”design of a maximum power tracking system for wind-energy-conversion applications”. *IEEE transactions on industrial electronics*, 53(2):486–494, 2006.

[39] Mariusz Malinowski, Adam Milczarek, Radoslaw Kot, Zbigniew Goryca, and Jan T Szuster. ”optimized energy-conversion systems for small wind turbines: Renewable energy sources in modern distributed power generation systems”. *IEEE Power Electronics Magazine*, 2(3):16–30, 2015.

[40] Kelvin Tan and Syed Islam. Optimum control strategies in energy conversion of pmsg wind turbine system without mechanical sensors. *IEEE Transactions on Energy Conversion*, 19(2):392–399, 2004.

[41] Kazmi Syed Muhammad Raza, Hiroki Goto, Hai-Jiao Guo, and Osamu Ichinokura. A novel algorithm for fast and efficient maximum power point tracking of wind energy conversion systems. In *Electrical Machines, 2008. ICEM 2008. 18th International Conference on*, pages 1–6. IEEE, 2008.

[42] Luisa C Pagnini, Massimiliano Burlando, and Maria Pia Repetto. Experimental power curve of small-size wind turbines in turbulent urban environment. *Applied Energy*, 154:112–121, 2015.

[43] Yue Zhao, Chun Wei, Zhe Zhang, and Wei Qiao. A review on position/speed sensorless control for permanent-magnet synchronous machine-based wind

energy conversion systems. *IEEE Journal of Emerging and Selected Topics in Power Electronics*, 1(4):203–216, 2013.

[44] Rana Ahmed, A Namaane, and NK M'Sirdi. Improvement in perturb and observe method using state flow approach. *Energy Procedia*, 42:614–623, 2013.

[45] Rajib Datta and VT Ranganathan. A method of tracking the peak power points for a variable speed wind energy conversion system. *IEEE Transactions on Energy Conversion*, 18(1):163–168, 2003.

[46] Aryuanto Soetedjo, Abraham Lomi, and Widodo Puji Mulayanto. Modeling of wind energy system with mppt control. In *Electrical engineering and informatics (ICEEI), 2011 international conference on*, pages 1–6. IEEE, 2011.

[47] Syed Muhammad Raza Kazmi, Hiroki Goto, Hai-Jiao Guo, and Osamu Ichinokura. A novel algorithm for fast and efficient speed-sensorless maximum power point tracking in wind energy conversion systems. *IEEE Transactions on Industrial Electronics*, 58(1):29–36, 2011.

[48] Quincy Wang and Liuchen Chang. An intelligent maximum power extraction algorithm for inverter-based variable speed wind turbine systems. *IEEE Transactions on power electronics*, 19(5):1242–1249, 2004.

[49] Yuanye Xia, Khaled H Ahmed, and Barry W Williams. A new maximum power point tracking technique for permanent magnet synchronous generator based wind energy conversion system. *IEEE Transactions on Power Electronics*, 26(12):3609–3620, 2011.

[50] Maher Azzouz, A-I Elshafei, and Hasan Emara. Evaluation of fuzzy-based maximum power-tracking in wind energy conversion systems. *IET renewable power generation*, 5(6):422–430, 2011.

[51] Mukhtiar Singh and Ambrish Chandra. Application of adaptive network-based fuzzy inference system for sensorless control of pmsg-based wind tur-

bine with nonlinear-load-compensation capabilities. *IEEE transactions on power electronics*, 26(1):165–175, 2011.

[52] M Godoy Simoes, Bimal K Bose, and Ronald J Spiegel. Fuzzy logic based intelligent control of a variable speed cage machine wind generation system. *IEEE Transactions on Power Electronics*, 12(1):87–95, 1997.

[53] Amal Z Mohamed, Mona N Eskander, and Fadia A Ghali. Fuzzy logic control based maximum power tracking of a wind energy system. *Renewable energy*, 23(2):235–245, 2001.

[54] Z Chen, S Arnalte Gomez, and M McCormick. A fuzzy logic controlled power electronic system for variable speed wind energy conversion systems. In *Power Electronics and Variable Speed Drives, 2000. Eighth International Conference on (IEE Conf. Publ. No. 475)*, pages 114–119. IET, 2000.

[55] Vincenzo Galdi, Antonio Piccolo, and Pierluigi Siano. Designing an adaptive fuzzy controller for maximum wind energy extraction. *IEEE Transactions on Energy Conversion*, 23(2):559–569, 2008.

[56] V Calderaro, V Galdi, A Piccolo, and P Siano. A fuzzy controller for maximum energy extraction from variable speed wind power generation systems. *Electric Power Systems Research*, 78(6):1109–1118, 2008.

[57] Bunlung Neammanee, Korawit Krajangpan, Somporn Sirisumrannukul, and S Chatrattana. Maximum peak power tracking-based control algorithms with stall regulation for optimal wind energy capture. In *Power Conversion Conference-Nagoya, 2007. PCC'07*, pages 1424–1430. IEEE, 2007.

[58] Wei Qiao, Wei Zhou, José M Aller, and Ronald G Harley. Wind speed estimation based sensorless output maximization control for a wind turbine driving a dfig. *IEEE Transactions on Power Electronics*, 23(3):1156–1169, 2008.

[59] Hui Li, KL Shi, and PG McLaren. "neural-network-based sensorless maximum wind energy capture with compensated power coefficient". *IEEE transactions on industry applications*, 41(6):1548–1556, 2005.

[60] Mona N Eskander. Neural network controller for a permanent magnet generator applied in a wind energy conversion system. *Renewable Energy*, 26(3):463–477, 2002.

[61] Kyoungsoo Ro and Han-ho Choi. Application of neural network controller for maximum power extraction of a grid-connected wind turbine system. *Electrical Engineering*, 88(1):45–53, 2005.

[62] Marcello Pucci and Maurizio Cirrincione. Neural mppt control of wind generators with induction machines without speed sensors. *IEEE Transactions on Industrial Electronics*, 58(1):37–47, 2011.

[63] Rasit Ata. Artificial neural networks applications in wind energy systems: a review. *Renewable and Sustainable Energy Reviews*, 49:534–562, 2015.

[64] Trishan Esram, Patrick L Chapman, et al. Comparison of photovoltaic array maximum power point tracking techniques. *IEEE Transactions on Energy Conversion EC*, 22(2):439, 2007.

[65] Lijun He, Yongdong Li, and Ronald Harley. "novel adaptive power control of a direct-drive pm wind generation system in a micro grid". In *2012 IEEE Power Electronics and Machines in Wind Applications*, pages 1–8. IEEE, 2012.

[66] Alan Mullane, G Lightbody, R Yacamini, and S Grimes. Adaptive control of variable speed wind turbines. *Rev. Energ. Ren.: Power Engineering*, pages 101–110, 2001.

[67] Vivek Agarwal, Rakesh K Aggarwal, Pravin Patidar, and Chetan Patki. A novel scheme for rapid tracking of maximum power point in wind energy generation systems. *IEEE Transactions on Energy Conversion*, 25(1):228–236, 2010.

[68] M Kesraoui, N Korichi, and A Belkadi. Maximum power point tracker of wind energy conversion system. *Renewable energy*, 36(10):2655–2662, 2011.

[69] E. A. Bossanyi. ”wind turbine control for load reduction”. *Wind energy*, 6(3):229–244, 2003.

[70] Yao Xingjia, Wang Xiaodong, Xing Zuoxia, and Liu Jun. ”coordinate control strategy based on expert decision system of wind turbine”. In *2008 IEEE International Conference on Sustainable Energy Technologies*, pages 464–468. IEEE, 2008.

[71] Lucy Y Pao and Kathryn E Johnson. ”a tutorial on the dynamics and control of wind turbines and wind farms”. In *2009 American Control Conference*, pages 2076–2089. IEEE, 2009.

[72] Kathryn E Johnson et al. *”Adaptive torque control of variable speed wind turbines”*. Citeseer, 2004.

[73] Sven Creutz Thomsen. *”Nonlinear control of a wind turbine”*. PhD thesis, Technical University of Denmark, DTU, DK-2800 Kgs. Lyngby, Denmark, 2006.

[74] Siegfried Heier. *Grid integration of wind energy: onshore and offshore conversion systems*. John Wiley & Sons, 2014.

[75] Roberto Cardenas, Ruben Pena, Marcelo Perez, Jon Clare, Greg Asher, and Patrick Wheeler. ”control of a switched reluctance generator for variable-speed wind energy applications”. *IEEE transactions on Energy conversion*, 20(4):781–791, 2005.

[76] Hamidreza Jafarnejadsani, Jeff Pieper, and Julian Ehlers. ”adaptive control of a variable-speed variable-pitch wind turbine using rbf neural network”. In *Electrical Power and Energy Conference (EPEC), 2012 IEEE*, pages 216–222. IEEE, 2012.

[77] Arkadiusz Kulka. ”pitch and torque control of variable speed wind turbines”. 2004.

[78] Dal Y Ohm et al. ”pid and pdff compensators for motion control”. *Drivetech, Inc., Blacksburg, Virginia, Teknik Rapor*, 1994.

[79] Brice Beltran, Tarek Ahmed-Ali, and Mohamed El Hachemi Benbouzid. ”sliding mode power control of variable-speed wind energy conversion systems”. *IEEE Transactions on Energy Conversion*, 23(2):551–558, 2008.

[80] A Kumar and K Stol. ”simulating feedback linearization control of wind turbines using high-order models”. *Wind Energy*, 13(5):419–432, 2010.

[81] Victor Bellido-González, Benoit Daniel, John Counsell, and D Monaghan. Reactive gas control of non-stable plasma conditions. *Thin solid films*, 502(1):34–39, 2006.

[82] Bonnie J Jonkman. ”turbsim user’s guide: Version 1.50”, 2009.

[83] Jogendra Singh Thongam and Mohand Ouhrouche. *”MPPT control methods in wind energy conversion systems”*. INTECH Open Access Publisher, 2011.

[84] Liuying Li, Yaxing Ren, Lin Jiang, Joseph Brindley, and Victor Bellido-Gonzalez. ”hardware implementation of smooth region switching for wind turbine control using pdf controller”. In *Renewable Energy Research and Applications (ICRERA), 2013 International Conference on*, pages 115–120. IEEE, 2013.

[85] John Sandoval-Moreno, Gildas Besancon, and John J Martinez. ”observer-based maximum power tracking in wind turbines with only generator speed measurement”. In *2013 European Control Conference (ECC)*, pages 478–483, 2013.

[86] Petar Mateljak, Vlaho Petrovic, and Mato Baotic. ”dual kalman estimation of wind turbine states and parameters”. In *Proceedings of the International Conference on Process Control*, pages 85–91, 2011.

[87] GumTae Son, Hee-Jin Lee Lee, and Jung-Wook Park. ”estimation of wind turbine rotor power coefficient using rmp model”. In *Industry Applications Society Annual Meeting, 2009. IAS 2009. IEEE*, pages 1–8. IEEE, 2009.

[88] K Busawon, L Dodson, and M Jovanovic. ”estimation of the power coefficient in a wind conversion system”. In *Proceedings of the 44th IEEE Conference on Decision and Control*, pages 3450–3455. IEEE, 2005.

[89] Ying Zhu, Ming Cheng, Wei Hua, and Wei Wang. ”a novel maximum power point tracking control for permanent magnet direct drive wind energy conversion systems”. *Energies*, 5(5):1398–1412, 2012.

[90] Sofia Lalouni, Djamila Rekioua, Kassa Idjdarene, and Abdelmounaim Tounzi. ”maximum power point tracking based hybrid hill-climb search method applied to wind energy conversion system”. *Electric Power Components and Systems*, 43(8-10):1028–1038, 2015.

[91] Vahid Rezaei. ”advanced control of wind turbines: Brief survey, categorization, and challenges”. In *2015 American Control Conference (ACC)*, pages 3044–3051. IEEE, 2015.

[92] Shahaboddin Shamshirband, Dalibor Petković, Hadi Saboohi, Nor Badrul Anuar, Irum Inayat, Shatirah Akib, Žarko Ćojbašić, Vlastimir Nikolić, Miss Laiha Mat Kiah, and Abdullah Gani. ”wind turbine power coefficient estimation by soft computing methodologies: comparative study”. *Energy Conversion and Management*, 81:520–526, 2014.

[93] Frede Blaabjerg, Remus Teodorescu, Marco Liserre, and Adrian V Timbus. ”overview of control and grid synchronization for distributed power generation systems”. *IEEE Transactions on industrial electronics*, 53(5):1398–1409, 2006.

[94] Iain Staffell and Richard Green. ”how does wind farm performance decline with age?”. *Renewable energy*, 66:775–786, 2014.

[95] M Predescu, A Bejinariu, A Nedelcu, O Mitroi, C Nae, M Pricop, and A Craciunescu. ”wind tunnel assessment of small direct drive wind turbines with permanent magnet synchronous generator”. In *International Confer-*

ence on Renewable Energies and Power Quality, ICREPQ, volume 8, pages 12–14, 2008.

[96] Carlo L Bottasso, Filippo Campagnolo, and Vlaho Petrović. ”wind tunnel testing of scaled wind turbine models: Beyond aerodynamics”. *Journal of wind engineering and industrial aerodynamics*, 127:11–28, 2014.

[97] MM Hand, DA Simms, LJ Fingersh, DW Jager, JR Cotrell, S Schreck, and SM Larwood. ”unsteady aerodynamics experiment phase vi: wind tunnel test configurations and available data campaigns”. *National Renewable Energy Laboratory, Golden, CO, Report No. NREL/TP-500-29955*, 2001.

[98] Robert Howell, Ning Qin, Jonathan Edwards, and Naveed Durrani. ”wind tunnel and numerical study of a small vertical axis wind turbine”. *Renewable energy*, 35(2):412–422, 2010.

[99] S Masoud Barakati, Mehrdad Kazerani, and J Dwight Aplevich. ”maximum power tracking control for a wind turbine system including a matrix converter”. *IEEE Transactions on Energy Conversion*, 24(3):705–713, 2009.

[100] C Carrillo, AF Obando Montaño, J Cidrás, and E Díaz-Dorado. ”review of power curve modelling for wind turbines”. *Renewable and Sustainable Energy Reviews*, 21:572–581, 2013.

[101] M Lydia, S Suresh Kumar, A Immanuel Selvakumar, and G Edwin Prem Kumar. ”a comprehensive review on wind turbine power curve modeling techniques”. *Renewable and Sustainable Energy Reviews*, 30:452–460, 2014.

[102] Tian-Pau Chang, Feng-Jiao Liu, Hong-Hsi Ko, Shih-Ping Cheng, Li-Chung Sun, and Shye-Chorng Kuo. ”comparative analysis on power curve models of wind turbine generator in estimating capacity factor”. *Energy*, 73:88–95, 2014.

[103] Hong-Woo Kim, Sung-Soo Kim, and Hee-Sang Ko. ”modeling and control of pmsg-based variable-speed wind turbine”. *Electric Power Systems Research*, 80(1):46–52, 2010.

[104] Joonmin Lee and Young-Seok Kim. ”sensorless fuzzy-logic-based maximum power point tracking control for a small-scale wind power generation systems with a switched-mode rectifier”. *IET Renewable Power Generation*, 10(2):194–202, 2016.

[105] Ming Yin, Gengyin Li, Ming Zhou, and Chengyong Zhao. ”modeling of the wind turbine with a permanent magnet synchronous generator for integration”. In *Power Engineering Society General Meeting, 2007. IEEE*, pages 1–6. IEEE, 2007.

[106] Shuhui Li, Timothy A Haskew, Richard P Swatloski, and William Gathings. ”optimal and direct-current vector control of direct-driven pmsg wind turbines”. *IEEE Transactions on power electronics*, 27(5):2325–2337, 2012.

[107] Y Errami, M Ouassaid, and M Maaroufi. ”control of a pmsg based wind energy generation system for power maximization and grid fault conditions”. *Energy Procedia*, 42:220–229, 2013.

[108] Jamal A Baroudi, Venkata Dinavahi, and Andrew M Knight. A review of power converter topologies for wind generators. *Renewable Energy*, 32(14):2369–2385, 2007.

[109] CN Bhende, Shivakant Mishra, and Siva Ganesh Malla. Permanent magnet synchronous generator-based standalone wind energy supply system. *IEEE Transactions on Sustainable Energy*, 2(4):361–373, 2011.

[110] Marcelo Gustavo Molina and Pedro Enrique Mercado. *Modelling and control design of pitch-controlled variable speed wind turbines*. INTECH Open Access Publisher, 2011.

[111] Kabeya Musasa, Michael Njoroge Gitau, and R Bansal. Dynamic analysis of dc-dc converter internal to an offshore wind farm. In *Renewable Power Generation Conference (RPG 2014), 3rd*, pages 1–6. IET, 2014.

[112] Robert W Erickson and Dragan Maksimovic. *Fundamentals of power electronics*. Springer Science & Business Media, 2007.